# FRACTAL DESCRIPTION OF ROUGH SURFACES FOR HAPTIC DISPLAY

A DISSERTATION

SUBMITTED TO THE DEPARTMENT OF MECHANICAL ENGINEERING

AND THE COMMITTEE ON GRADUATE STUDIES

OF STANFORD UNIVERSITY

IN PARTIAL FULFILLMENT OF THE REQUIREMENTS

FOR THE DEGREE OF

DOCTOR OF PHILOSOPHY

Michael Allan Costa

December 2000

© Copyright 2001 by Michael Costa
All Rights Reserved

I certify that I have read this dissertation and that in my opinion it is fully adequate, in scope and quality, as a dissertation for the degree of Doctor of Philosophy.

Mark R. Cutkosky Principal Advisor

I certify that I have read this dissertation and that in my opinion it is fully adequate, in scope and quality, as a dissertation for the degree of Doctor of Philosophy.

Oussama Khatib

I certify that I have read this dissertation and that in my opinion it is fully adequate, in scope and quality, as a dissertation for the degree of Doctor of Philosophy.

John Kenneth Salisbury

Approved for the University Committee on Graduate Studies:

# Abstract

This thesis develops a structure suitable to study the roughness perception of natural rough surfaces rendered on a haptic display system using fractals. A background on traditional methods for describing surface roughness is given. Fractals are used to characterize one-dimensional surface profiles using two parameters, the amplitude coefficient and the fractal dimension. Synthesized fractal profiles are compared to the profiles of actual surfaces. Fractal techniques are extended to two-dimensional surfaces. The Fourier Sampling theorem is applied to solve the fractal amplitude characterization problem for varying sensor resolutions. A framework for an anisotropic characterization of two dimensional fractal Brownian surfaces is developed. A method for anisotropic fractal surface simulation with varying sensor resolutions is given. Synthesized fractal profiles are used to conduct a surface roughness perception experiment using a haptic replay device. The most important factor affecting the perceived roughness of the fractal surfaces was the RMS amplitude of the surface. When comparing surfaces of fractal dimension 1.2-1.35 it was found that the fractal dimension was negatively correlated with perceived roughness.

*In Loving Memory of my Grandparents*

# Acknowledgments

Now, finally at the end of the doctoral process, I can take some time to reflect upon and acknowledge the many people who helped me through my studies. Undoubtedly I will miss a few people and to them I apologize in advance.

I would like to thank my advisor Professor Mark Cutkosky for his guidance and meticulous editing of my dissertation. Next, I am a grateful to Professor Ken Salisbury for not only serving on my reading committee, but for all of the advice and enthusiasm he provided during the last two years of my program. Special thanks are due to Professors Oussama Khatib and Chris Gerdes for reading drafts, asking helpful and insightful questions, and making valuable suggestions. Sean Walker was of invaluable assistance in implementing the haptic display of the two-dimensional surfaces under a very compressed time schedule just before the completion of my dissertation.

Funding for this research was provided in part by the NASA Ames Research Center Honors Co-Op program, the Edward J. Meakin Fellowship at Stanford, and the National Consortium for Graduate Degrees for Minorities in Engineering and Science Inc. (GEM). Additional funding and support was provided by the student affairs section of the School of Engineering with the help of Dr. Noe Lozano.

The people at the Dextrous Manipulation Laboratory have made my time in the lab fun, creative, and intellectually stimulating beyond just engineering. I feel a particular attachment to my generation of Ph.D. students in the DML: Allison “Senior Student” Okamura, Christopher “Chalange?” Richard and Michael “The Repository” Turner. Other people who made it fun in the DML and CDR were Jorge Cham, Sean Bailey, Weston Griffin,

Jonathan Clark, and Beth Pruitt. I also appreciate my unforgettable appearances with Niels Smaby, Ryan Findley, Will Provancher, Moto Hatanaka, Roman Devengenzo, and any other Spice Girls, Smurfs, or Duff Beer Cans that I may have missed.

At NASA I need to thank several people for their support of my development as an engineer and eventually scientist during my summer internships, civil service employment, and finally as a graduate student. I am thankful to Dr. Michael Sims for pointing out the Honors Co-Op program as a means of funding my graduate tuition, and allowing me to participate in it. I owe a great debt to Hans Thomas for being a vigorous defender of my continued participation in the program when others sought to end it. Hans was also an important influence on me as a mentor and friend through our shared experience working on engineering projects, his constant words of encouragement, and his advice. Michael Guerrero, a fine machinist and engineer, cheerfully built (and redesigned) the linear positioner of my experimental apparatus. Dr. Jeremy Frank gladly made long term loans of his books on fractals and had many kind words of encouragement.

I would also like to recognize several of my friends outside of Stanford and NASA who provided support leading up to and during my graduate studies. My friends Dio Tsai and Eddie Guerra who attended portions of high school and U.C. Berkeley with me were an instrumental influence in raising my academic aspirations to a much higher level. They adopted the roles of elder brothers and as trailblazers for which I am lucky and grateful. My long time and closest friend Jose Espinosa, along with his wife Tracy, constructed a social life for me outside of school that was necessary in keeping my sanity. I will not forget their kindness or friendship.

Naturally I must thank my parents who selflessly supported me during my graduate education and my entire life. Their assistance by taking care of a number of mundane, domestic chores freed up time for my pursuits outside of academics. Most comforting was that I always knew with absolute certainty that I had their help should I have had needed it. Finally I would like to recognize every one of my relatives who immigrated to this country so that we could better ourselves.

# Table of Contents

# List of Tables

# List of Figures

# 1 Introduction

We are very adept at picking up objects and identifying their properties by exploring and manipulating them with our hands. By merely grasping an object we can immediately tell if it's made out of metal or not by our sense of temperature. Stroking our finger tips across the object allows us to make judgements about the surface finish - whether it's smooth or rough, slippery or sticky. These types of sensations, observed through the skin's mechanoreceptor nerve endings, such as vibration, adhesion, and temperature, make up our cutaneous sense. Another class of observations can be made based on the forces applied to our limbs. For example we can estimate the mass of an object by holding it in our hand and even judge the rotational inertia by turning it while grasped in our hand. These kinds of observations make up our kinesthetic perception. Combined, our cutaneous and kinesthetic senses form our haptic perception [1].

Although there are many surface properties that affect our haptic perception of an object, it has been suggested that the single most important non-visual cue affecting our perception of a material is the surface roughness [2]. Qualitatively we know that wood, polished metal, and sandpaper all have different surface roughness. We can even use roughness to make further distinctions between like objects, such as two different pieces of sandpaper with different grits, fine and coarse. Most commonly the lateral motion exploratory procedure, in which the fingertips are lightly rubbed over a surface, is used to sense surface roughness [3][4]. However it is sometimes more effective to use tools to explore surface roughness. In interviewing blind field paleontologist Professor G.J. Vermeij, it was found that he uses his fingernail to examine fossil specimens for surface roughness and features while using a hypodermic needle to probe for submillimeter fine features [5]. Using the needle as a fine feature exploration tool has been so successful that his sighted colleagues have begun using the technique. Because the design of haptic interfaces often only allows a single point of contact between the user and the virtual world such as the single

finger thimble of the PHANToM [6] or the hand grip of a force feedback joystick, the needle or stylus method of haptic exploration appears a plausible model of virtual surface interaction to study roughness.

## 1.1 Motivation

Unmanned planetary exploration space programs by NASA have steadily been increasing in scope during the later half of the 1990s. Unmanned orbiting probes mapped the surface with radar. During the summer of 1998 the Sojourner rover of the Pathfinder project rolled a few meters across Mars and began sending images and spectroscopy data back to geologists on earth. Now a two rover mission is planned for 2003. One of the main goals of these missions has been to study the Martian geology. Automated devices do not possess the sophistication to synthesize the complex pattern of information inherent in geological materials to conduct the science by themselves [7]. "Field study...absolutely requires human geologists to be involved intimately" [7].

Of course it is not practical to send a geologist on all surface missions to Mars. Remotely operated vehicles appear to remain a fixture of upcoming Martian missions for some time to come. All explorations occur through telepresence, a "mediated presence" of the remote environment through the robotic vehicle [8]. The ultimate telepresent system would closely approximate the experience for the scientist as if exploring one’s immediate environment [8]. The ability of planetary scientists to conduct geology through virtual environments created by rovers wandering through remote terrain have been tested in mock up Mars missions in the deserts of California, Arizona, Peru and most recently Nevada. Currently the primary sensors used by remote geologists are high-resolution cameras, augmented with some spectrometer and chemical sensors. The haptic experience is completely absent in previous and upcoming virtual environments used for exploring Mars. However field geologists use haptic sensations to help conduct their studies. The feel of a hammer striking a rock, the feel of the ground underfoot, and the grittiness felt between fingertips to differentiate between silt or clay, are all part of the exploration process [8].

One possible method of haptically interacting with the geometric data of the virtual environment is to model a single point of contact like a stylus. Vermeij’s stylus tool helps him identify fine fossil features on the order of 1 mm and below. As an expert in paleon-

tology he knows what these features can signify in a fossils. He has described an example in which he corrected an erroneous fossil classification by sighted colleagues based on the color they observed of a specimen of sea shell. With the stylus tool Vermeij observed the presence of tiny teeth-like features which constituted the salient classification feature of the fossil [5]. A virtual stylus tool could similarly be used to explore the surface of a rock. This leads to the question: what kinds of things could we potentially learn from the surface roughness of a rock from a geological standpoint?

### 1.1.1 Geological Considerations of Rock Texture

A rock's surface appearance is referred to as its texture [9]. Specifically the characteristics determining rock texture are grain size, grain shape, grain orientation, and the relative proportion of grains and matrix material [10]. In rock engineering, texture has been shown to be a useful tool for predicting mechanical performance, such as crack propagation [11], drillability, and cuttability [10]. Available textural data will influence the selection of equipment in rock engineering [10]. For planetary geology, rock texture yields insight into the origins of a rock.

One of the two properties used to classify igneous rocks is their texture (the other being their mineral content). Igneous rocks are formed either underground or at the surface when molten rock cools and crystallizes. Depending on the amount of time taken for the rock to cool crystals can grow to sizes visible to the unaided eye. These igneous rock textures containing visible grains are classified as phaneritic textures. Rocks with crystals barely or not visible to the eye are classified as having aphanitic textures. Rocks that have visible grains surrounded by an aphanitic matrix are designated as having a porphyritic texture [9].

Rocks that slowly cool underground have phaneritic textures, such as plutonic rocks that form from magma intruding into preexisting solid rocks. Phaneritic rocks include granites, diorites, and extremely course-grained pegmatites. Grain growth in phaneritic rocks will depend on pressure as well as time spent cooling. Extrusive rocks form from lava flowing onto the surface of the earth and rapidly cooling. These volcanic rocks have little time for crystals to form or grow, resulting in aphantic textures. Basalts have aphanitic textures. If a volcanic rock cools so rapidly that no crystals form the resulting texture is described as

glassy. Obsidian and pumice are two different types of volcanic glasses [9]. Although pumice is a glass it can be differentiated from obsidian by its tiny cavities formed by bubbling, highly gaseous magma.

Sedimentary rocks form from accumulated sediment, fragments of rock that have been transported by wind, water, or ice, or precipitating out of solution in water. Texture in sediments is determined by the size, shape, and arrangement of the transported particles. Most sediments are the product of erosion of preexisting rocks. Sediment grain size is determined by the parent rock being eroded along with the nature and energy of the transport medium. Coarse-grained granites will produce larger grains than eroded aphanitic rocks. Sediments could be broken down by a glacier, worn-down by white water, or remain unchanged in mudflows. Grain shape will also be affected by the transport medium. Irregular grains will lose their angularity and become rounded in abrasive media such as swiftly flowing rivers. The farther a particle is carried, the more rounded it will become. Another phenomenon associated with the distance of transported particles is sorting. As sediment is carried, particles requiring greater energy to be moved get left behind. Well sorted sediments, such as those created by wind, will have a narrow range of sizes. In glaciers and flooding rivers sedimentary deposits will be poorly sorted [9].

Loose sedimentary particles are classified by their particle size. The smallest particles, those below 2mm, make up mud, sub classified into clay, silt, and sand, while larger particles make up gravel, consisting of granules, pebbles, cobbles, and boulders. Sedimentary rocks formed from lithification of loose particles are classified by their particle sizes. Finer grained rocks include mudstones, such as shale, siltstone and sandstone, while gravels form conglomerates and breccias [9].

Texture is used in geology to classify various rocks and add insight into the formation of the rocks. In igneous rocks, texture indicates cooling time and cooling mechanism. Since sedimentary textures are determined by the arrangement, shape, and size of deposited particles, these properties can be used to indicate sediment classification. As the grain shape indicates transport mechanism and distance, sedimentary texture could potentially be used for deductive geology. In the next section the texture characteristics that will hopefully yield geological information will be quantified in terms of surface metrology metrics.

### 1.1.2 Quantifying Roughness and its Haptic Perception

At this point it appears that roughness could be useful to study from a geological standpoint, and that the single point of contact stylus method could work with current haptic devices as a model for interaction with virtual surfaces. Even with this motivation the problem needs to be further defined. How can surface roughness be measured and how can it be applied to roughness perception?

First is the problem of quantifying the surface roughness of a rock. Metrologists have had difficulties defining surface roughness [42], so it's no surprise that pyshcophysicists have had problems as well [1]. Psychophysicists have been studying roughness perception with human subjects interacting with gratings or other defined surfaces [72][73][74]. This is clearly not the same as interacting with a natural surface such as that of a rock. Defined surfaces are easily quantifiable using statistical measures from surface metrology. For quantifying what appears to be the random surface of a rock this thesis turns to fractals. With the fractal characterization in place the second part of the problem can be investigated: how to apply a fractal characterization of roughness to a perception experiment.

## 1.2 Thesis Outline

This thesis develops a structure suitable to study the roughness perception of natural surfaces rendered on a haptic display system using fractals. The chapters are organized to provide a background on traditional methods of describing surface roughness, to use fractals to characterize and synthesize profiles of rough surfaces, to extend the fractal techniques to anisotropic surfaces, and finally to conduct a surface roughness perception experiment on a haptic replay device.

Chapter two reviews traditional methods of analyzing roughness taken from the field of surface metrology. For the most part this involves statistical analysis of two dimensional surface profiles. Limitations and complications using these mathematical tools are discussed.

Chapter three explores fractal methods to characterize the surface roughness of materials using the fractal dimension and amplitude coefficient. Fractal versus standard

surface metrology techniques are compared. Using measured parameters new realistic surfaces are simulated. The surface metrics of the simulated surfaces are then compared to the metrics of the actual surfaces.

In chapter four the fractal techniques for describing surface roughness are extended for height profiles of a two-dimensional surface. A brief review of surface metrology statistical tools is given. The capabilities and limits of using fractal methods with structure tensors to characterize isotropic and anisotropic surfaces are discussed. The sampling theorem is applied to enable a fractal characterization regardless of the resolution of the measuring instrument. Finally a general fractal characterization and generation of anisotropic surfaces is given.

Chapter five describes a roughness perception experiment utilizing synthesized fractal surface profiles displayed on a haptic interface. Subjects used a force feedback joystick to explore virtual surface profiles and report which of the profiles they felt was rougher. The most important factor affecting the perceived roughness of the fractal profiles was the RMS amplitude of the surface, although in some cases the fractal dimension did have a small effect.

Chapter six summarizes the thesis and contributions. It also suggests future research areas utilizing fractals for telepresent geology and haptics.

## 1.3 Contributions

The main contributions of this thesis are

- Developing an anisotropic characterization of two-dimensional fractal Brownian surfaces that extends the previous idea of fractal dimension as a function of direction to include an amplitude coefficient as a function of direction.
- Applying the Fourier sampling theorem to solve the fractal amplitude characterization problem for varying sensor resolutions.
- Using a fractal surface characterization and synthesized fractal surfaces to study roughness perception with a haptic device.

It is hoped that a reader of this thesis will take away an alternative framework for studying the haptic perception of rough surfaces. Instead of using artificial, deterministic surfaces for pyschophysical perception studies, fractal surfaces can be used to better reflect

naturally occurring roughness. Since it is difficult to manufacture a large set of these types of fractal surfaces, the flexibility of a haptic replay device can be used to display a large range of synthesized fractal surfaces. The method of fractal characterization presented also gives an advantage over traditional metrology metrics: a scale independent characterization of surfaces.

# 2 Surface Metrology Review

Studying the roughness perception of natural rough surfaces such as rocks rendered on a haptic display system requires the ability to characterize the surface roughness. With a set of metrics to describe a rough surface we can attempt to generate random surfaces based on the real surface profiles. We begin in this chapter with a review of traditional methods of surface metrology for one-dimensional profiles. Limitations and complications using these mathematical tools are discussed.

## 2.1 Statistical Measures

Surface metrology methods have been employed extensively in manufacturing to describe the surfaces for fabricated objects. Other fields such as cartography, hydrodynamics, aircraft engineering, highway engineering and bioengineering have also employed these methods [14]. We now review some of the more common metrics used to describe two-dimensional surface profiles in an attempt to apply them to the description of roughness properties of natural surfaces.

### 2.1.1 Amplitude Probability Density Function

The Amplitude Probability Density Function (APDF) is used describe the height information of a profile $z(x)$. The APDF is the probability that a profile ordinate is within a height interval of $z$ and $z+\delta z$. The APDF can then be used to compute other amplitude statistics, such as the mean departure from the mean reference line and the root mean square deviation relative to the mean line. Digitally the APDF is constructed by creating a histogram of $n$ height intervals and dividing the number of ordinates in each interval by the total number of ordinates. In Principles and Applications of Tribology, Bhushan recommends using 15-50 height intervals for general random data, trading off between accuracy and resolution [45]. In this thesis histograms are constructed with 50 height intervals spanning the minimum and maximum heights of the profile. An example of an APDF is given in figure 2-1.

**Figure 2-1.** Amplitude Probability Density Function for a Concrete Profile

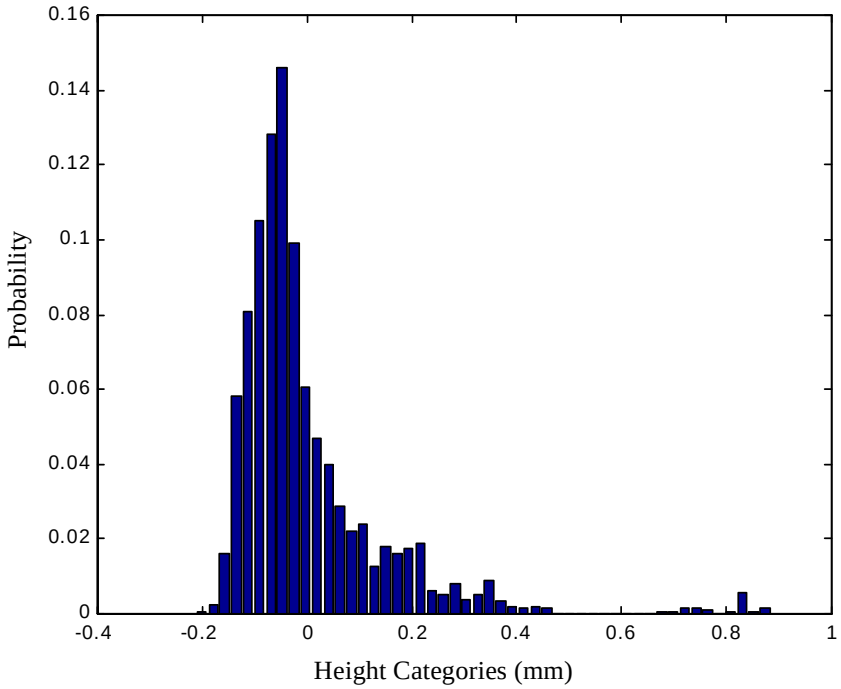


## 2.1.2 Amplitude Parameters

Amplitude measures one of the most widely used ways to describe the roughness of a surface. With a single value these parameters quantify the amplitude of the profile ordinates from a reference line. Other parameters quantify the shape of the distribution of the heights of an APDF.

### 2.1.2.1 $R_a$, The Mean Departure from the Reference Line

One of the most frequently used amplitude measures in surface metrology is $R_a$, the mean departure of the profile from the mean reference line. In continuous form $R_a$ is defined as

$$R_a = \frac{1}{L}\int_0^L |z|\,dx \tag{2.1}$$

where $f(x)$ is the profile and $L$ is the length of the profile [42]. In discrete form we use the APDF to compute $R_a$

$$R_a = 2\left(\bar{z}\sum_{\substack{i=l \\ z_i<\bar{z}}}^{N} p_i - \sum_{\substack{i=l \\ z_i<\bar{z}}} p_i(\Delta z_i)\right) \tag{2.2}$$

where $p_i$ is the probability density at the *i*th level of the APDF and $\Delta z_i$ is the height of the *i*th level of the APDF [42].

#### 2.1.2.2 $R_q$, The Root Mean Square Deviation from the Mean Line

A second amplitude measure that we use is $R_q$, the root mean square deviation from the mean line. In continuous form $R_q$ is defined as

$$R_q = \frac{1}{L}\int_0^L z^2 dx \tag{2.3}$$

[42].

While $R_a$ and $R_q$ are useful in measuring the amplitude of the profile, we attempt to describe the shape of the waveform by computing two other metrics, skew and kurtosis. These parameters are derived from the third and fourth central moments of the continuous APDF and the profile.

#### 2.1.2.3 *Sk*, Skew

Skew is a measure of symmetry of the height distribution of the profile, with a zero value of skew indicating a symmetrical distribution. Examples of probability density functions of positive and negative skewness, and a symmetrical skew of 0 are shown in figure 2-2.

**Figure 2-2.** Probability Density Functions with Different Skewness

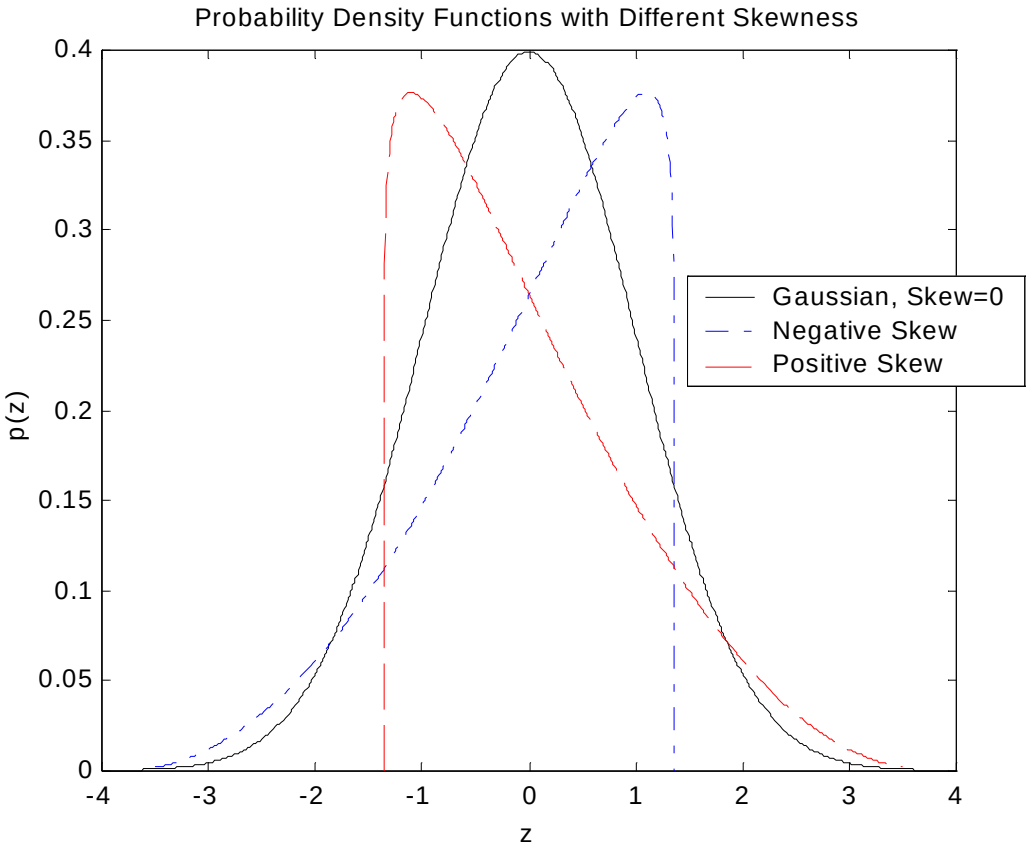


Skew is defined as

$$Sk = \frac{1}{\sigma^3}\int_{-\infty}^{\infty}(z-\bar{z})^3 p(z)dz \tag{2.4}$$

where $p(z)$ is the continuous amplitude probability density function [12]. In discrete form the skew is

$$sk = \left[\frac{1}{m}\sum_{i=1}^{m}(z_i)^3 - \frac{3}{m^2}\sum z_i\sum(z_i)^3 + \frac{2}{m^3}(\sum z_i)^3\right] \Big/ \left[\frac{1}{m}\sum(z_i)^2 - \left(\frac{1}{m}\sum z_i\right)^2\right]^{3/2} \tag{2.5}$$

[12].

### 2.1.2.4 *K*, Kurtosis

Kurtosis is a measure of peakedness of the height distribution, with increasing kurtosis indicating increasing pointedness, and decreasing kurtosis indicating increasing blunt-

ness Examples of probability density functions with different values of kurtosis are shown in figure 2-3. Skew and kurtosis can be used to check if a distribution is Gaussian. A symmetrical Gaussian distribution will have a zero skew and a kurtosis of 3 [45].

**Figure 2-3.** Probability Density Functions with Different Kurtosis

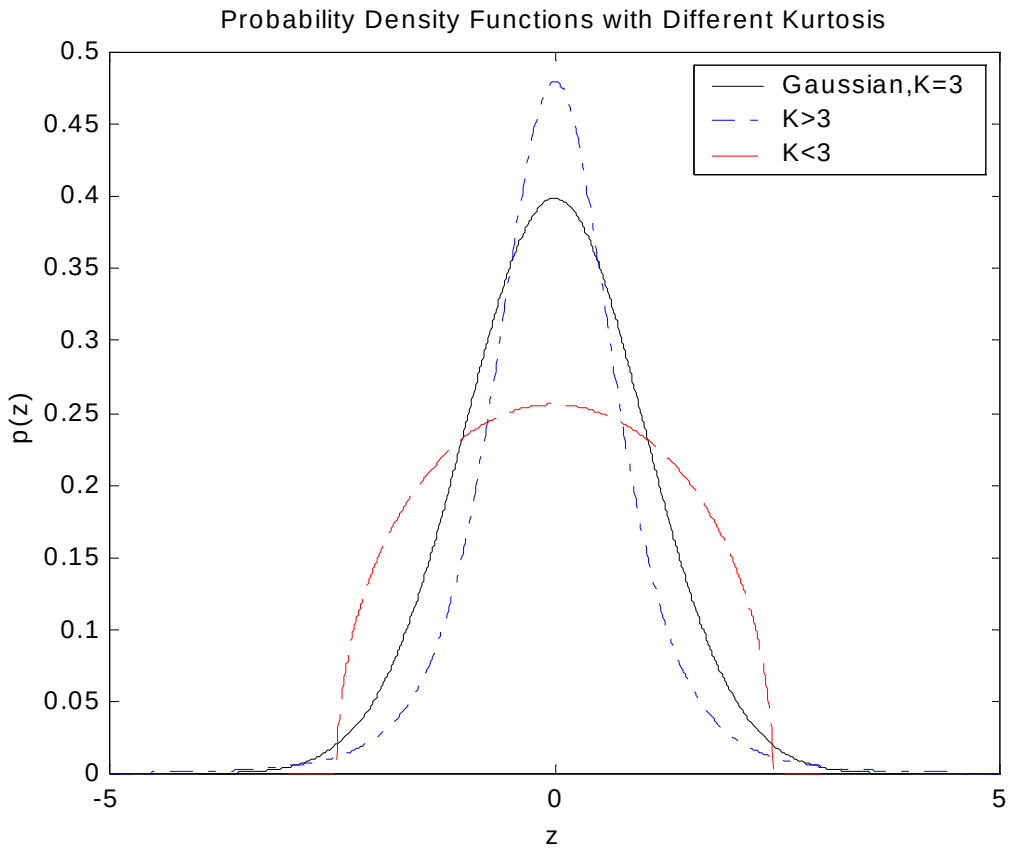


In continuous form the kurtosis is defined as

$$K = \frac{1}{\sigma^4}\int_{-\infty}^{\infty}(z-\bar{z})^4 p(z)dz - 3 \tag{2.6}$$

[42]. In discrete form the kurtosis is

$$K = \frac{\left[\frac{1}{m}\sum_{i=1}^{m}(z_i)^4 - \frac{4}{m^4}\sum z_i\sum(z_i)^3 + \frac{6}{m^3}(\sum z_i)^2\sum(z_i)^2 - \frac{3}{m^4}(\sum z_i)^4 - 3\right]}{\left[\frac{1}{m}\sum(z_i)^2 - \left(\frac{1}{m}\sum z_i\right)^2\right]^2} \tag{2.7}$$

[42].

In terms of a surface profile, increasing kurtosis for a symmetric distribution signifies an increased amount of ordinates near the mean value (figure 2-4). Profiles with a negative skewness have larger number of height ordinates above the mean value (figure 2-4). The functions in figure 2-4 were synthesized with a heuristic algorithm utilizing a random number generator to illustrate profiles with different skew and kurtosis distributions.

**Figure 2-4.** Simulated Profiles Demonstrating Skew and Kurtosis

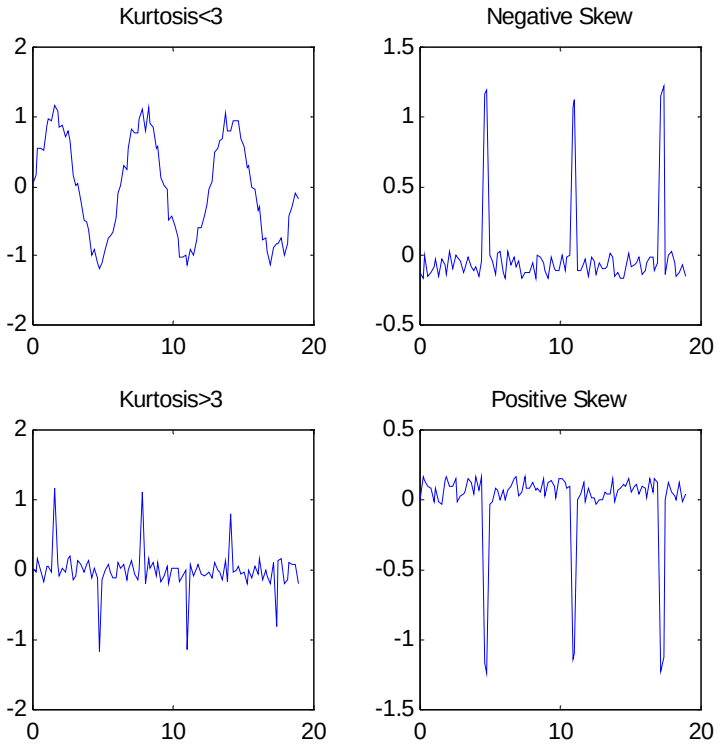


## 2.1.3 Spacing Parameters

While the previous parameters have tried to describe amplitude and shape of peaks in the profile, other techniques try to measure the spacing between the peaks. The autocorrelation function (ACF) of the profile is used to compute two of these spacing parameters, the root mean square (RMS) wavelength and the peak density above the mean value. The ACF, $A(\tau)$, is the expected value of the products of two heights a distance $\tau$ apart and can be found from

$$A(\tau) = \lim_{L \to \infty} \frac{1}{L} \int_{-L/2}^{L/2} z(x)z(x+\tau)dx \tag{2.8}$$

The RMS wavelength, $\lambda_{RMS}$, is the RMS distance between peaks and is found from

$$\lambda_{RMS} = 2\pi\frac{\sigma}{\sigma'} \tag{2.9}$$

[42] where $\sigma$ is the standard deviation of the profile and $\sigma'$ is computed from the second derivative of the ACF at the origin

$$\sigma'^2 = -\frac{d^2}{d\tau^2}A(0) \tag{2.10}$$

[42].

The peak density above the mean line, $p_p$, is the expected number of peaks per unit length. Since all of our profiles have the mean subtracted out, $p_p$ is the number of peaks above 0. The second and fourth derivatives of the ACF evaluated at $\tau$=0 and the variance are used to compute $p_p$ [42]

$$p_p = \frac{1}{4\pi}\left[\left(\frac{A^{iv}(0)}{-A''(0)}\right)^{1/2} + \left(\frac{A''(0)}{\sigma^2}\right)^{1/2}\right] \tag{2.11}$$

However the equations for the peak density make the assumption that the profile is Gaussian and that the ACF is differentiable at $\tau$=0. For rock surfaces the ACF is generally not differentiable at $\tau$=0, so we revert to the peak counting method of Whitehouse [42]. The average peak count is simply the number of peaks divided by the sample length. One of the most used definitions of a peak is the three-point definition [42]. This method defines a peak as any point between two lower points. Other peak definitions exist including using four or more ordinates to define a peak, using a height discriminator to set a minimum difference between points before registering a peak, and using an amplitude band to count peak crossings [42]. The numerous definitions unfortunately leads to conflicting measured peak densities by different researchers, even for the same data [42]. I feel that this problem illustrates a recurring theme in traditional surface metrology; too many ways of attacking

the same problem leading to conflicting answers. In this thesis the three-point definition is used because of its simplicity and wide use.

For fractal surfaces the derivatives at the origin of the ACF are undefined. Anticipating that the surfaces will exhibit fractal properties we explore fractal methods of describing roughness in chapter 3.

### 2.1.4 Surfaces Indistinguishable to Statistical Parameters

One problem with descriptive amplitude statistics is that it is relatively easy to find two different surfaces that have the same statistics. In figure 2-5 two square surfaces with the same amplitude but different spatial frequencies of .1 and 1 Hz are shown. The statistical parameters for the surfaces are given in table 2-1. The mean departure, RMS amplitude, skew and kurtosis are the same for each surface. Of course, the ACF related measures will be different.

**Table 2-1.** Metric Comparison of Square Wave Surfaces

| Surface | $R_a$ | $R_q$ | Skew | Kurtosis |
|---|---|---|---|---|
| Surface .1 Hz | 0.4900 | 0.4900 | -.0240 | -47.01 |
| Surface 1 Hz | 0.4900 | 0.4900 | -.0240 | -47.01 |

However, peak density estimation using the three-point counting method also runs into difficulty. Because of the broad plateaus of the square waves no single point is between two lower points, causing no peaks to be counted. For either surface the algorithm fails to generate a non-zero result. This illustrates the definition-dependent nature of some of the statistics.

As discussed in the next section, complications with amplitude statistics are associated with the definition of the gross geometry and surface features. These geometry factors affect the calculated values of the parameters and must be removed

**Figure 2-5.** Two Surfaces with Equivalent Amplitude Parameters

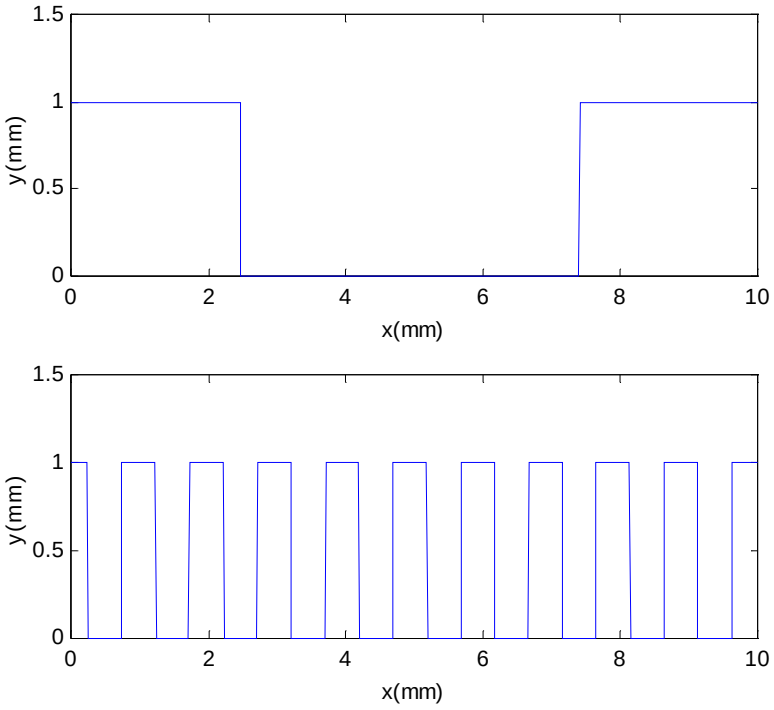


# 2.2 Errors of Form

## 2.2.1 Removing Gross Geometry

In surface metrology engineering surfaces have three components, surface roughness, waviness, and form [42]. Each component considers height variations in the surface of increasing wavelength respectively. Exact definition of the difference in wavelength between roughness and waviness is left ambiguous in the literature, as it is application dependent [45] or changes from manufacturing process to process [42]. Complicating the matter is the controversy surrounding whether or not waviness should be included with roughness as a part of the surface texture, and separating waviness from the form of the piece being analyzed [42]. One definition used for form geometry is that it consists of spatial components with a wavelength 1/3 or ¼ of the sample length or greater [42]. The sample length and the sample resolution will also affect the roughness parameters [45]. We use the definition of surface roughness as the variations in height of the surface relative to a reference plane [45]. Defining the reference line determines the mean height, tilt, and curvature which are subtracted from the height data before calculating the roughness parameters [45]. This sepa-

rates the roughness from the form of the object. For example when a flat sample is placed such that it is not normal to the sensor, the surface profile generated will be sloped, gradually increasing or decreasing. A curved surface such as a ball will have a surface roughness, but its overall curvature is not considered to be a part of the roughness. These gross geometry effects must be removed from the profile before computing any surface metrics.

For a manufactured object the form is known from the design. Using a least-squares fit to a parameterization of the form geometry (line, circle, etc.) establishes the reference line. The form geometry of a rock is not well defined. While we choose samples that are nominally flat over the sample length, there is still going to be some tilt that needs to be removed.

For a rock we can define form geometry as any slants due to misalignment of the sample, or curvature or waviness inherent to the sample, that can be removed with a second order polynomial fit to the data. This is accomplished by fitting a polynomial of the form

$$Y(x) = a_0 + a_1 x + a_2 x^2 \tag{2.12}$$

to the profile where the coefficients of the equation are computed using a least squares fit. The fitted curve is computed and subtracted from the profile, flattening it out. After the fit has been subtracted from the profile, the mean of the ordinates is computed and subtracted from the ordinates to give the profile a zero mean. For the work in this thesis it was determined empirically that a quadratic worked well for the rock samples used. This scheme can effectively match a ¼ wavelength sine wave, the spatial definition of form components suggested by Whitehouse [42]. Some examples of removing slant and curvature are given in figure 2-6 of a 63 mm long concrete profile sampled with a spatial resolution .0097mm/ sample.

**Figure 2-6.** Original Data and Data with Tilt Removed for a Profile of Concrete

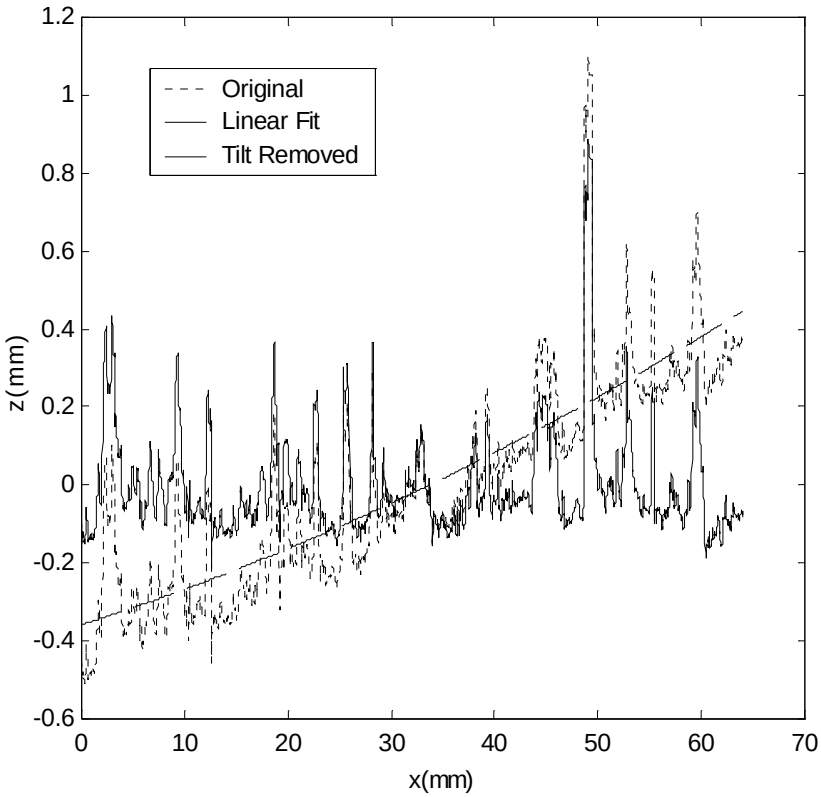


## 2.2.2 Removing features

When computing the statistical parameters of roughness the gross geometry effects of waviness and form were excluded because they do not comprise the texture of the object. Similarly surface features need to be identified and removed before computing roughness parameters. Like the definition of waviness and form, the definition of a feature is somewhat arbitrary and application dependent. For the application of this thesis a feature is a bump, ridge or hole that can be individually detected. When these features become so numerous and small that they cannot be perceived individually they then become part of the texture. An example of removing features from a concrete sample, a conglomerate of pebbles and a matrix of sand and cement, is given to illustrate the difficulties in defining what a feature is.

In figure 2-7 the top profile of the concrete contains a large feature located between 26 and 31 mm along the 45 mm sample. While fitting a polynomial works to remove gross geometry effects, it is difficult to use it to selectively remove features without distorting the

rest of the profile. Instead we use a heuristic algorithm to identify and remove such features. For the case of the concrete the following conservative algorithm was found to be effective in removing distinct bumps and valleys that are not representative of the overall texture of the sample.

The profile is filtered with a low- pass, phase-corrected, Butterworth filter [67] with a corner spatial frequency of 0.15 cycles/mm (or about 1/5 the frequency content of the sample data). The filtered profile is shown against the original profile in the top plot of figure 2-7. The low pass profile is subtracted from the original profile to leave the higher frequency information shown in the second plot. The $R_q$ value of the high frequency profile is computed. The algorithm then searches the low pass profile for ordinates with magnitudes over 2.5*$R_q$. This value has been empirically determined to work well with concrete samples in identifying features. A continuous collection of ordinates over this amount is considered a feature. The identified feature is finally extended by a safety margin of thirty percent of its original length when removing points. The margin is necessary because otherwise the ordinates below 2.5*Rq that are still a part of the feature would be left behind. The 30% percent margin insures that the entire feature is removed. Feature selection by this algorithm is shown in the bottom profile of figure 2-7.

The amount of arbitrary definitions used in the heuristic algorithm illustrates the application dependent nature of identifying a feature. The features in the concrete were large holes and the algorithm was developed to find them. If the thinner holes were just as deep as the large holes they would have been identified as a feature when they would have been perceived as part of the texture. The algorithm would have had to be changed for this scenario, and in all likelihood would have to be changed for a different material. This example also illustrates the difficulties in using statistical parameters along with arbitrary definitions of geometry and features to characterize surface roughness. In the next section other difficulties are briefly discussed that indicate that a simpler, more robust method of surface characterization is needed.

**Figure 2-7.** 44.4 mm long concrete profile sampled with a spatial resolution .0099mm/sample.

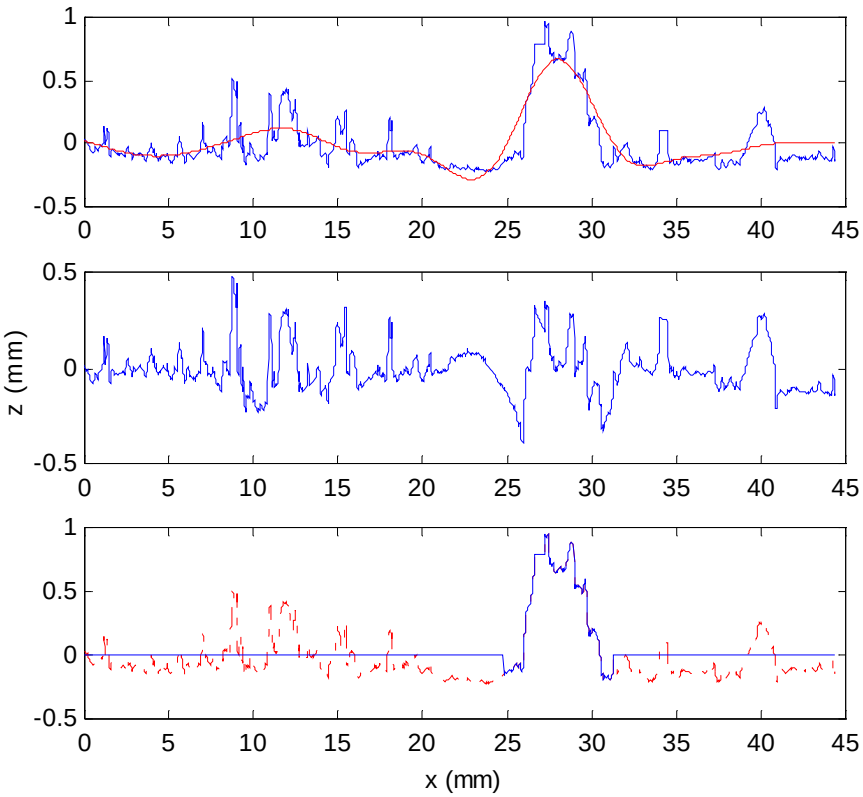


## 2.3 Application Difficulties

The biggest difficulty in using statistical surface metrology parameters is implementing them to be measurement invariant. Many of the parameters are at least partly dependent on arbitrary definitions. The values of parameters will change depending on what constitutes object geometry as opposed to surface roughness and how the two are separated. Peaks can be defined in numerous ways leading to different values for the same surface [14][42]. Metrologists using different measuring instruments will also calculate different statistical roughness parameters. While the surface roughness is an intrinsic property, the actual measured roughness is not. The measured surface roughness is a function of the bandwidth of the measuring instrument [45]. Furthermore the length of the sample measured will change the value of amplitude statistics as well. It has been shown that the variance of the heights increases proportional to the sampling length squared [14]

$$\sigma \propto L^{1/2} \tag{2.13}$$

Poon and Bhushan report that roughness parameters initially increase with $L$ before reaching a constant value [15]. Multiple definitions for the desired scan length have been suggested [42][16][17].

What we begin to realize with these inconsistencies is that roughness is application dependent. Roughness for one application is waviness for another [45]. In addition to the measurement inconsistencies, the diverse set of disciplines that the applications for surface roughness covers has led to the development of multiple yet similar roughness metrics [14]. Whitehouse has termed this a "parameter rash" [43]. Fractals are examined in the next chapter in search of a simplified roughness characterization that is invariant to measurement devices and setup. For a current survey of a variety of surface metrology techniques the author of this thesis recommends the article "Quantitative Characterization of Surface Texture" [44].

# 3 Fractal Methods

In this chapter we explore fractal methods to characterize the surface roughness of rocks such that we can realistically simulate new surfaces based on measured parameters. We compare the use of standard surface metrology techniques and fractal methods to analyze various surface samples. Simulated surfaces are generated from measured parameters. The surface metrics of the simulated surfaces are then compared to the metrics of real surfaces. The relationship between the fractal parameterization and a surface metrology amplitude statistic is explored. This relationship is used to create simulated surfaces with metrics that closely approximate the parameters of the original surface.

## 3.1 Fractal Methods

### 3.1.1 Fractal Dimension

Fractals have been used to describe irregular shapes that do not lend themselves to description by Euclidean geometry. Natural structures such as mountains, coastlines, clouds and snowflakes, in addition to recursive, self-similar structures (figure 3-1) such as the Von Koch snowflake curve [23] are examples of shapes that exhibit a fractal nature. Each of these objects has a non-integer fractal dimension, 1.4, 2.3, etc., measuring how much space it occupies [24]. The most significant digit, such as the 2 of 2.3, represents the Euclidean dimension. For example a straight line has a topological dimension of one, and a square has a dimension of two. The second part of the fractal dimension, the fractional part varying from .0 to .999..., is called the fractal increment [24]. The higher the dimension, the more space the curve occupies. All of the profile curves we analyze fall between one and two.

Because fractal geometry has been used to describe natural phenomena [49], we explored it as a possible tool to describe and synthesize rock surfaces. Several attempts have been made to use the fractal dimension to characterize the roughness of rock surfaces [25][26]. We use two methods to measure the fractal dimension. The first method measures

the compass dimension of a surface profile. The second method characterizes the surface with two parameters, the fractal dimension and an amplitude coefficient.

**Figure 3-1.** Recursive Fractal Structure, Von Koch Snowflake Variant [12]

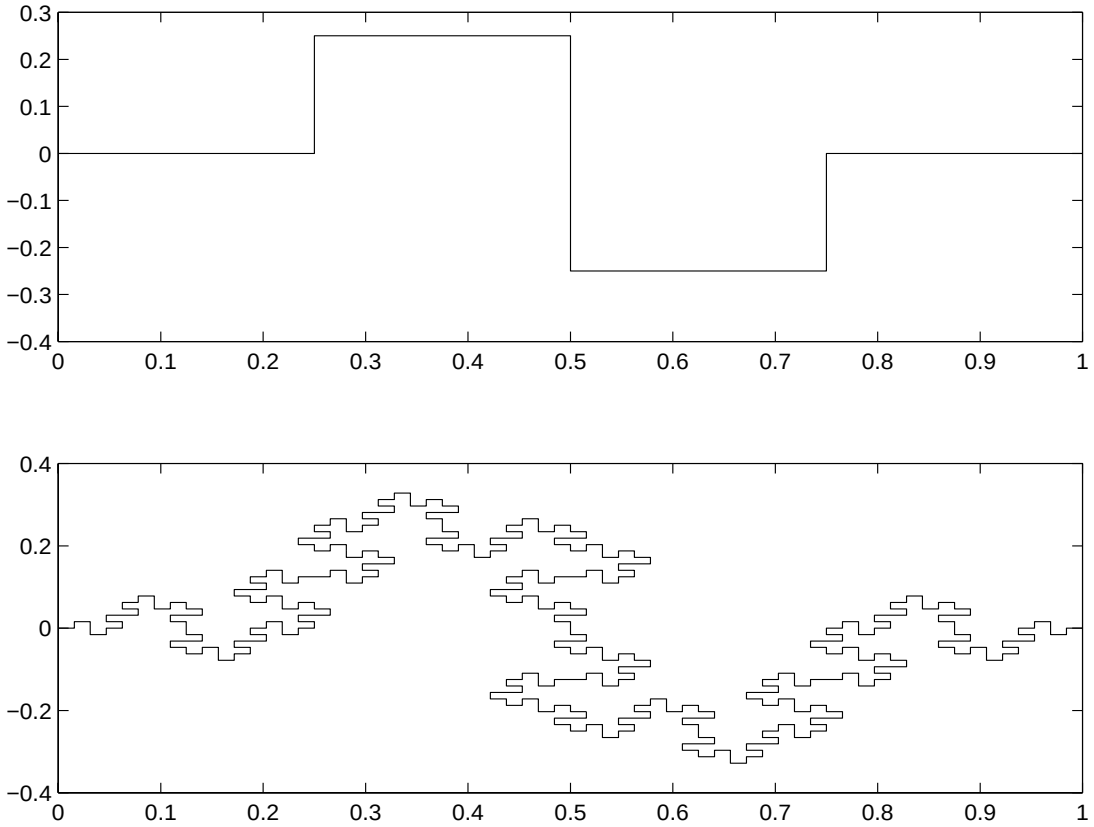


### 3.1.2 Measuring Fractal Dimension

One way to measure the fractal dimension of a curve is to measure its compass dimension. A common example illustrating the compass dimension is measuring the length of a coastline with a ruler. The distance measured will depend on the size of the ruler used. If a person walks along a coastline measuring the length with a meter stick he will measure a certain distance. If the measurement is done again with a smaller ruler the distance will be greater. One can imagine using smaller rulers to measure more details of the coast. The compass dimension relates the number of rulers used, $N$, to the ruler size, $r$ [49].

$$D = \frac{\log N}{\log(1/r)} \tag{3.1}$$

**Figure 3-2.** Measuring the fractal compass dimension for the Von Koch Snowflake Variant of Figure 3-1 on page 23 by chord fitting. The linear relationship when plotting number of chords vs. chord size on log-log scale is characteristic of fractals.

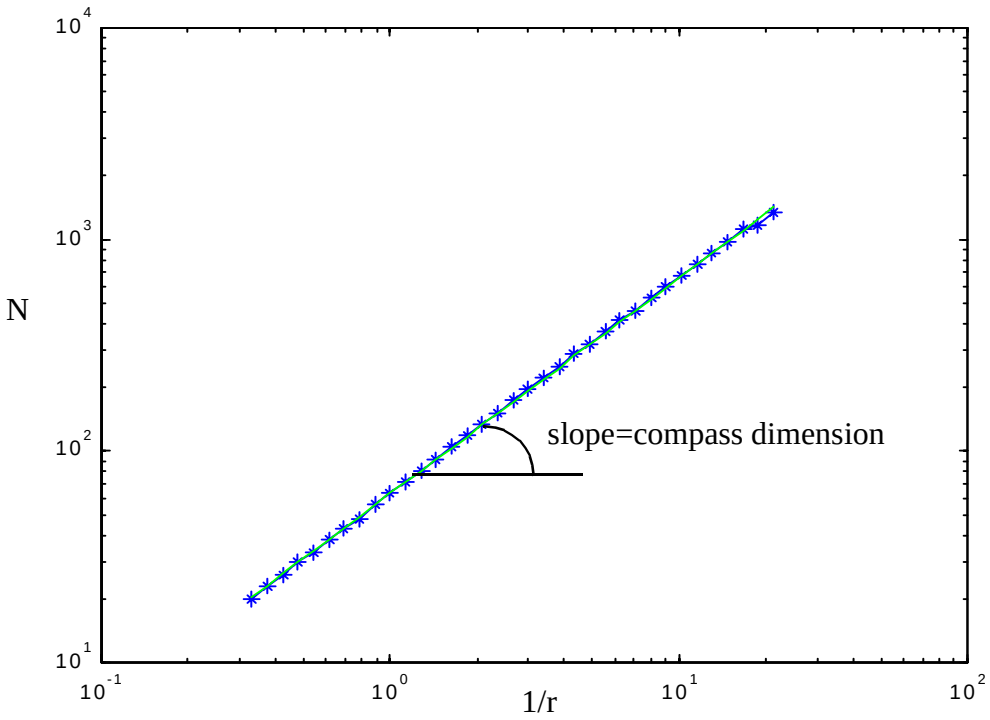


The procedure we use to measure the compass dimension is to first select a range of sizes of the chords that will be fit over the profile. Then, beginning with the first ordinate, the Euclidean distance to the next ordinate is computed. If the chord length is not exceeded we move onto the next point until it is. The first point exceeded is now the new origin point where the next chord is fitted. Shelberg, Moellering, and Lam use an algorithm that interpolates a new point between the two ordinates to match the chord length [27]. In the present work, interpolating points did not affect the dimension significantly and therefore this was not done.

This fitting process is repeated until chords have been fit over the entire profile. The number of chords is recorded. The process is repeated until all the chord lengths have been used. The number of chords *N* is plotted against the chord size *r* on logarithmic axes (figure 3-2). The graph of this log-linear relationship is called a Richardson plot [51]. We then fit a line to the plot using a least squares fit. The slope of the fitted line is the compass dimension.

The algorithm for selecting the chord lengths is based on the method reported by Shelberg [27] and used by Longley [28]. The Euclidean distance between each coordinate is computed and averaged to give an average chord length of $r$. The new chords are computed from $r_i=2k_ir$, where $k_i$ are 35 equally spaced points between 1 and 10. The points are adjusted to be spaced between 2 and 9, or even 2 and 8 if the logarithmic plot of $N$ versus $r$ plot is not linear, indicating that the profile is not fractal over the scales chosen. The values of $k_i$ are adjusted to give a linear plot over the largest range of scales possible. We found that plot would be become nonlinear for scales near the resolution of the sensor, and for scales at the same magnitude as the profile length. The same effect has been reported in previous work [29][46].

Measuring the spectral exponent β of the profile is the second method we employ to measure the fractal dimension. Random noises with spectral densities inversely proportional to frequency are commonly found in nature and take the form [12]

$$P(f) \propto \frac{1}{f^{\beta}} \tag{3.2}$$

When β=0 the slope is zero, all frequencies are represented in equal amounts, and white noise is generated. If a profile was generated from this spectral density by using the inverse Fourier transform the points in the trace would be completely uncorrelated. For β=2 the spectral density represents Brownian motion. This is the same type of Brownian motion discovered by botanist R. Brown in 1827. He observed that the motion of particles suspended in fluid is irregular and erratic [12]. If the motion of one of these particles was graphed out over time in one dimension, the spectral density computed from the motion would yield β=2.

For 1<β<3, the noise is called fractal Brownian motion (fBm). The traces made by these noises are fractal, and we can measure the fractal dimension from the spectral density [12]. By plotting the log of the spectral density versus the log of the frequency and fitting a line to the resulting plot, we can measure β from the slope of the fitted line (figure 3-3). Although noises vary in time, our curves vary in space. For our application this means our spectral densities are computed as a function of spatial frequency instead of time frequency.

Once we have measured β we can compute the fractal dimension from [12]

$$D = \frac{(5 - \beta)}{2} \tag{3.3}$$

Our β measurement is only taken from the linear portion of the plot. At these scales the profile is considered to be exhibiting fractal behavior. The other points are discarded before making the fit. In figure 3-3 the PSD drops sharply off at the frequency of the sampling length, .05 samples/mm. The linear fit also excludes points above the spatial resolution of the sensor, 15.62 samples/mm.

The spectral method of finding the fractal dimension has the advantage of being faster to compute than the compass dimension technique. However the power spectrum method of finding the fractal dimension has a larger variance than the compass method [26].

**Figure 3-3.** $1/f^{\beta}$ Noise of Concrete Profile 20mm long. A line can be fit to the range of frequencies for which the profile exhibits fractal behavior.

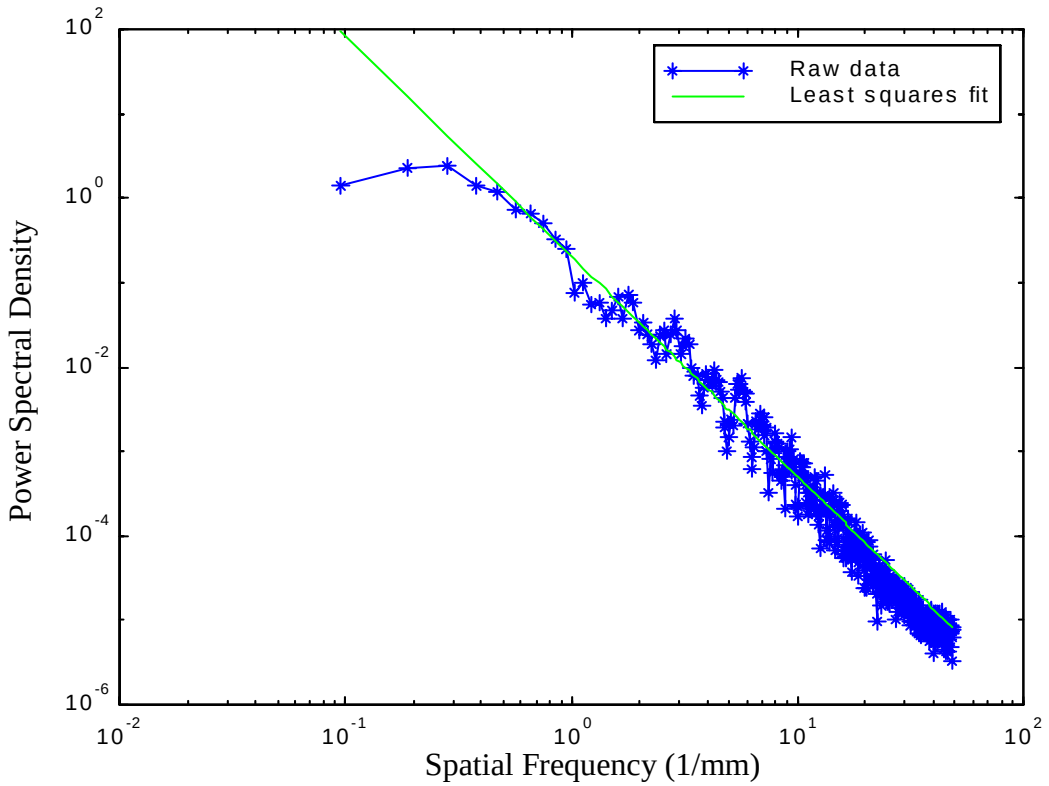


While the fractal dimension is a measure of the frequency content of the profile, it doesn't indicate the height magnitudes of the profile. A self similar object, such as a fractal,

appears similar or even identical to itself regardless of magnification scale [12]. At different magnification scales a profile exhibiting fractal properties will have the same fractal dimension. However with increasing magnification scales the scan length decreases and with it the measured height variance decreases [13]. One dimension value can be characteristic of several different fractal Brownian motion profiles with different average height amplitudes. A second parameter is needed to characterize the surface.

### 3.1.3 Amplitude Coefficient

In addition to the fractal dimension *D*, Ganti and Bhushan measure a scale independent amplitude coefficient *C* that relates the amplitude of the frequency contents. They report that *C* increases monotonically with the variance of surface heights and also report increasing surfacing friction with increasing *C* [13]. The amplitude coefficient is the second parameter measured from the profile and is used to simulate a fractal surface.

The structure function has been used in studying surface roughness as an alternative to the correlation function [21]. Structure functions are able to show functional changes more clearly than ACF [14]. For functions exhibiting fractal Brownian motion the structure function has a linear relationship with length [65]. The amplitude coefficient is measured from the structure function [13]

$$S(\tau) = C\eta^{2D-3}\tau^{4-2D} \tag{3.4}$$

where $\tau$ is an increment of length and $\eta$ is the lateral resolution of the profiling instrument. When computing the structure function $\tau$ varies from the lateral spacing between points to the length of the sample being examined. The structure function is the expected mean square difference in height over a distance $\tau$ [45].

$$S(\tau) = \lim_{L \to \infty} \frac{1}{L} \int_0^L [z(x) - z(x+\tau)]^2 \, dx \tag{3.5}$$

In practice the structure function was computed from the profile data by circular convolution. For a profile of *N* points the calculation is [13]

$$S_j = \frac{1}{N}\sum_{k=1}^{N}(z_{k+j} - z_k)^2 \qquad (3.6)$$
$$z_{N+j} = z_j$$

After computing the structure function the log of *S* is plotted versus the log of τ (figure 3-4). A line is fit to the linear portion of the plot by a least-squares approximation. Using equation 3.4 the amplitude coefficient can be computed from

$$C = \frac{m}{(\eta^{2D-3}(4-2D))} \qquad (3.7)$$

where *m* is the slope of the fitted line.

**Figure 3-4.** Structure Function for a concrete sample 20mm long. A line can be fit to the linear portion of the plot. The measured slope can then be related to the amplitude coefficient C. The plateau portion of the plot continues on until τ=20mm, but is not displayed.

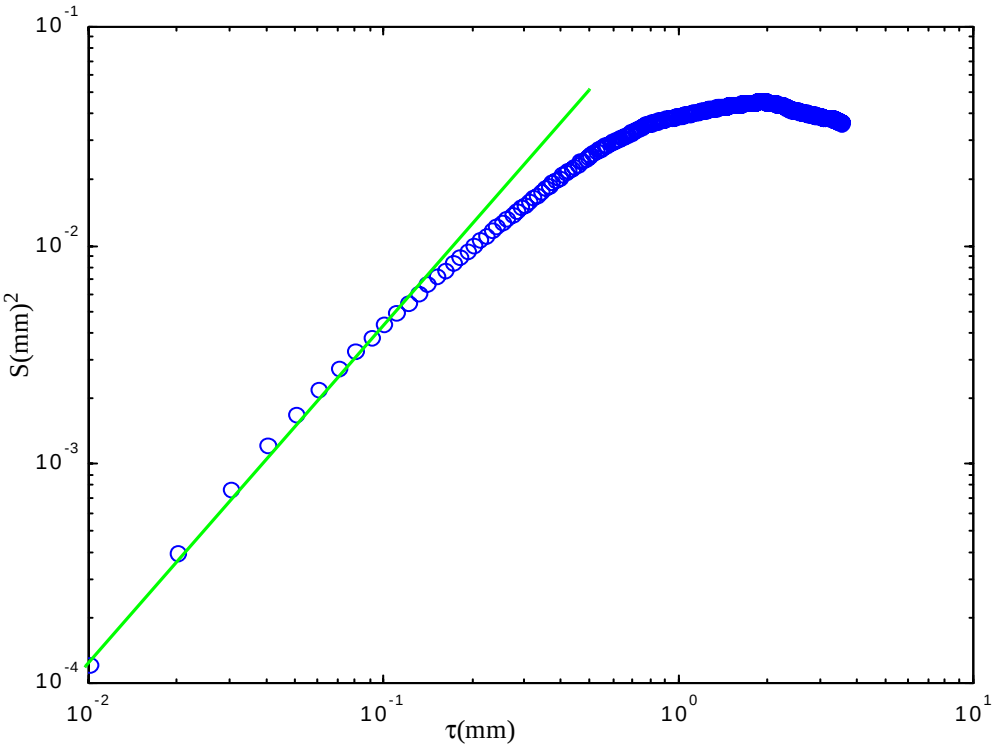

## 3.2 Synthesizing a Surface: Fractal Brownian Motion using Fourier Filtering

One of our goals is to be able to conduct a psychophysical roughness experiment with a haptic replay device using realistic synthesized surfaces. An experiment with synthesized surfaces has the advantage of not requiring the collection of multiple profiles over a range of different surface roughness metrics. Synthesized surfaces could be made to the desired range of surface metrics. Fractal geometry has been used in computer graphics to generate mountainous landscapes, plants, and water surfaces [24]. These objects are generated to appear natural on a computer screen without a quantitative comparison to their real counterparts. Using the measured fractal parameters of actual surfaces we can try to generate our own synthetic surfaces and see how they compare to real surfaces using both fractal and traditional surface metrology metrics. Our first step is to find a fractal algorithm to synthesize surfaces with.

The first algorithm we tried was based on the "Fractal motion using Fourier filtering method" described in The Science of Fractal Images [12]. The Fourier Filtering method works by imposing the spectral condition of fractal Brownian motion, $P(f)\alpha 1/f^{\beta}$, onto the coefficients of the discrete Fourier transform. However this condition uses only the fractal dimension. This does not allow adjusting of the amplitudes of the generated surfaces.

### 3.2.1 Synthesizing a Surface with a Fractal Dimension and an Amplitude Coefficient

Ganti uses a similar $1/f^{\beta}$ power spectral density function to generate fractal surfaces but also includes an amplitude parameter $C$ that scales the amplitudes of frequencies [13]

$$
\begin{aligned}
P(f_k) &= \frac{C_1 K}{(2\pi k f_0)^{5-2D}} \\
C_1 &= C\eta^{2D-3} \\
K &= \frac{\Gamma(\beta)\sin[\pi(2-D)]}{2\pi} \\
f_0 &= \frac{1}{L}
\end{aligned}
\tag{3.8}
$$

The amplitude coefficient $C$ is related to the variance of the heights by [13]

$$S(\tau) = \sigma^2(x - x_0) = C\eta^{2D-3}\tau^{4-2D} \tag{3.9}$$

where $R_q$ is equivalent to the variance $\sigma$ [42]. This enables us to synthesize a surface with any desired root mean square amplitude.

To synthesize a surface the conditions of equation 3.8 are imposed onto the coefficients of the discrete Fourier transform [12][13]

$$X(t) = \sum_{k=0}^{N-1} H_k e^{2\pi i k t} \tag{3.10}$$

The real and imaginary parts of the Fourier coefficients $H_k$ are computed from

$$\begin{aligned} ReH_k &= random\_sign * rand * \left(\sqrt{\frac{C_1 K}{L(2\pi)^{5-2D}}}\right) \\ ImH_k &= random\_sign * \left(\sqrt{\frac{C_1 K}{L(2\pi)^{5-2D}} - (ReH_k)^2}\right) \\ k &= 0, 1, \ldots N/2 \\ ReH_{N-k} &= ImH_k \\ ImH_{N-k} &= ReH_k \\ k &= N/2, N/2+1, \ldots N-1 \end{aligned} \tag{3.11}$$

[13] for a desired profile of $N$ points, where *random_sign* is randomly ±1, and *rand* is a random Gaussian number from 0 to 1. We then form $H_k$'using the complex conjugate operator *

$$H'_k = \frac{1}{\sqrt{2}}(H_k + (H_{N-k})^*) \tag{3.12}$$

The conditions of the power law are imposed onto $H_k$'by

$$
\begin{aligned}
H'_k &= \sqrt{\frac{1}{[(k+1)f_0]^{5-2D}}}H'_k \\
&\quad 0 \le k \le \frac{N}{2} \\
H'_k &= \sqrt{\frac{1}{[(k+1-N/2)f_0]^{5-2D}}}H'_k \\
&\quad \frac{N}{2} \le k \le N-1
\end{aligned}
\tag{3.13}
$$

where $f$ is the fundamental frequency, $1/L$, the inverse of the desired length of the profile. We then compute our synthesized function, $X(t)$, using our random coefficients and the discrete inverse Fourier transform [10]

$$
X(t) = \sum_{k=1}^{N/2} (ReH'_k \cos(kt) + ImH'_k \sin(kt)) \tag{3.14}
$$

One problem with using this method is that the generated surface repeats itself every $x=2\pi n$ intervals. To circumnavigate this problem we divide the surface we would like to generate into 5.12 mm fragments of 512 equally spaced points, generating a new set of Fourier coefficient pairs for each fragment. The newly generated fragment has a constant added to it so that it is attached to end of the last fragment. This process continues until the new surface is complete.

The original algorithm calls for $N$ Fourier coefficient pairs to compute $N$ points of a surface. With our segmenting algorithm we are able to use fewer coefficients to compute each point. This leads to large computational savings in taking the inverse Fourier transform. If we compute a 3072 point surface we need 512 Fourier coefficient pairs. When we compute each point using the inverse Fourier transform (equation 3.14) we compute 512 pairs of sine and cosine functions. By breaking up the surface into six, 512 point surfaces, we can compute each point using only 512 coefficient pairs, and only 512 pairs of sine and cosine functions instead of 3072 pairs of functions.

### 3.2.2 Modeling Fractal Surfaces with a White Noise - Transfer Function Model - An Alternative

In vehicle dynamics transfer function models with a white noise input have been used to model the input disturbances due to the roughness of roads [35]. Thomas represented the power spectral density of an average road as proportional to $1/f^{\beta}$, with $\beta=2$. [35]. A stochastic process can be realized from a white noise sequence operated on by a transfer function [36]. As can be seen from figure 3-3 the PSD has the linear portion that is fractal, but flattens out for lower frequencies. A transfer function with a magnitude response can be made to model both the flat spot and the linear fractal portion to give a more complete model of the measured PSD. The transfer function coefficients could be measured off the actual PSD. New profiles with the same behavior could be synthesized by operating the transfer function on a white noise sequence of random values. It seems to have the advantage over the fractal characterization in that it also models the roll off at lower frequencies.

However this model is not easily developed into a workable form for two dimensional surfaces with anisotropic behavior as described in chapter four. As such it is not further developed in this thesis but rather left here as a suggestion to alternatively model one-dimensional profiles.

## 3.3 Surface Characterization Experiment Description

This experiment was conducted to explore the performance of various roughness metrics and fractal characterizations of surfaces, and how synthesized surfaces compare to actual surfaces that they are based on. Profiles of concrete were collected and used to examine surface metrics and fractal characterizations. Various types of sandpaper that were qualitatively different but had the same grit rating were also compared to see how their metrics differed. New profiles were synthesized based on the measured properties of painter's sandpaper and compared to the original profiles.

### 3.3.1 Profile Sensing

Before surface profiles could be collected for examination, different sensing devices were tried in order to find the most practical method of profile sensing. Three different sensors were used to take profiles of a known surface: a micro-machined stylus with strain sensitive cantilever previously developed for biomedical research [31], a commercially available

laser displacement sensor, and an ordinary phonograph cartridge stylus that is usually used to play records. The output of a stereo phonograph stylus is a two-channel velocity signal that can be added and integrated to produce a profile [32]. Phonograph styli employed in this fashion have been used to measure displacements with resolutions comparable to atomic force microscopes, but with a much larger dynamic range [30]. However in that work the phonograph stylus was deflected with a sine wave input of constant frequency, and not actually used for surface profiling. The signal that was measured was the velocity signal of the phono cartridge and was not integrated to recover any profile shape.

**Figure 3-5.** Profiles From Different Sensors, Micro-machined cantilever, laser displacement sensor and phonograph stylus

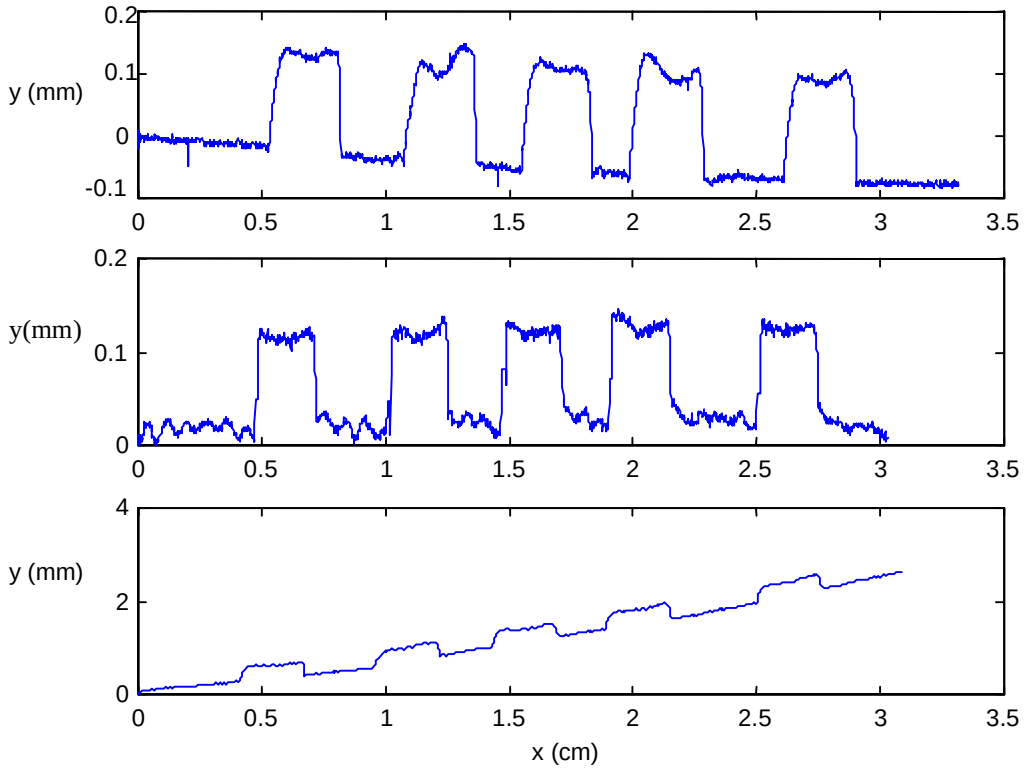


The test surface was composed of five copper strips approximately .09 mm thick with adhesive backing laid onto a circuit board. In figure 3-5 we compare profiles of test surface taken by each of the three sensors [32]. While we were able to use the phono cartridge to capture the shape of the copper strips on the test surface by integrating its velocity signal, a consistent integration error would indicate a slant in the test surface. While this sensor was the most economical, it was unusable because the integration error made it

impossible to distinguish DC component features in the profile. It is possible to remove the DC curvature *if* the gross geometry of the surface is known a priori. However as the application of this thesis is for the irregular surfaces of rocks, the gross geometry will usually be more complicated than for flat surfaces. This makes it more difficult to remove DC drift accurately.

The micro-machined force probe, while providing high resolution, low noise profiles, failed catastrophically under slight loads far too easily to be of practical use. The probe required a computer controlled actuator with the ability to servo with sub-millimeter precision to keep the cantilever in contact with the surface without exerting so much force that it off. The cantilever had an approximate working range of 2mm before catastrophic failure. Numerous micro-probes also broke by inadvertent touches or merely dropping the sensor. The easiest sensor to use, while still providing usable profiles, was the laser displacement sensor.

### 3.3.2 Experimental Setup

Surface height profiles were collected with an Omron Z4M-N30V reflective laser displacement sensor. The sensor is able to measure the distance of an emitted laser spot with a resolution of 4μm. Moving a sample across the front of the sensor generates its height profile. All of the height profiles collected were one-dimensional. The resolution is limited by internal electrical noise of the device. Spatial resolution of the sensor is determined by its spot size of 64μm [33]. Using the Nyquist sampling criterion, the maximum spatial frequency we can measure with this sensor is 7.81 cycles/mm. Profiles were spatially filtered with a phase corrected Butterworth filter with a corner frequency of 7.81 cycles/mm. Twenty millimeter sections of data were selected from the sample profiles for analysis.

A motorized linear stage moved the sample in front of displacement sensor at a fixed velocity. The position of the stage was read with an optical encoder with a resolution of 2.37e-3mm/tick. The velocity of the stage and the sampling of the height profile were controlled by an MS-DOS computer operating at a sampling frequency of 4.5 kHz. A spatial sampling resolution of .008mm to .01mm was achieved with this setup. Photos of the

linear stage, laser sensor, and a sandpaper sample in position to be profiled are given in figure 3-6.

### 3.3.3 Measurement Procedure Summary

A summary of the surface measurement procedure is given in figure 3-7. The procedure describes the process of computing surface metrics, both fractal and statistical, after a surface profile has been collected.

**Figure 3-6.** Profiling Equipment Setup Photos

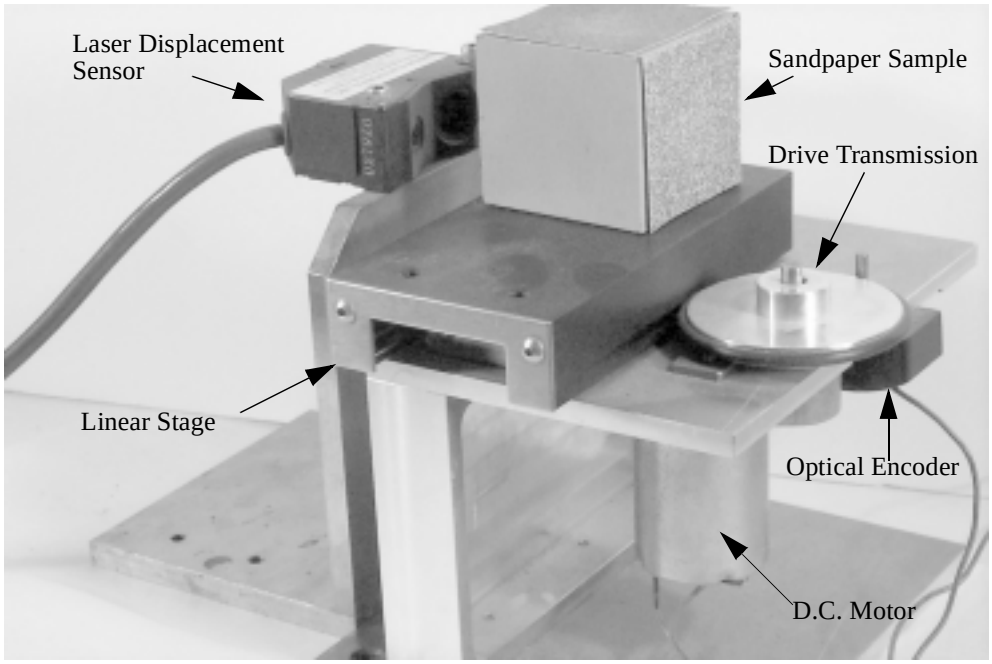


Reverse Angle

**Figure 3-7.** Procedural Flowchart

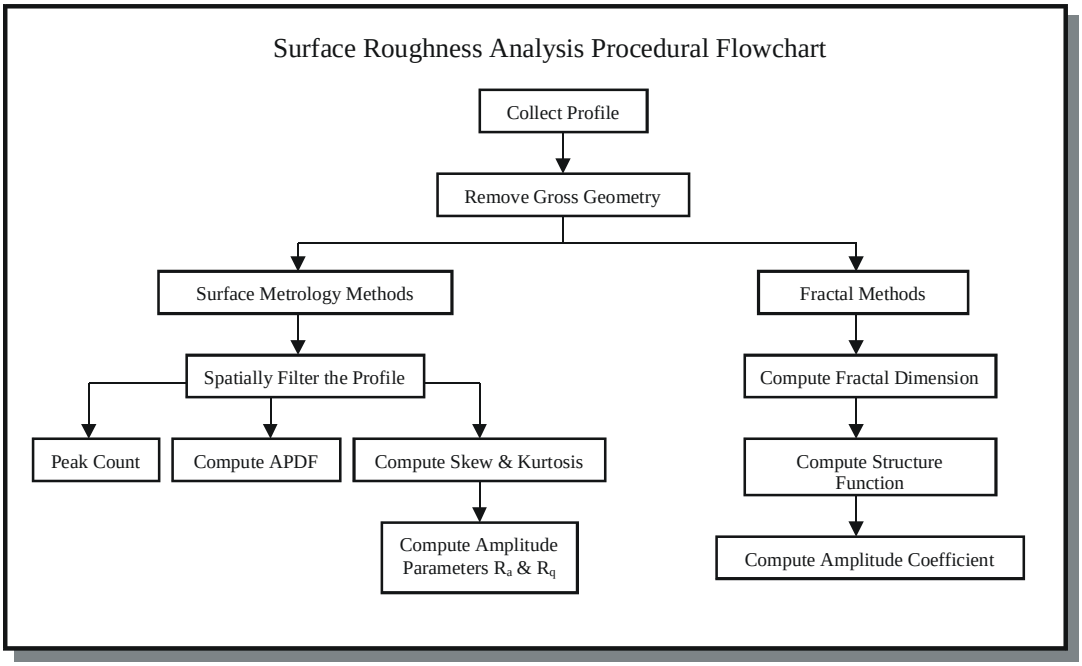


# 3.4 Experiment Results

## 3.4.1 Utilizing Surface Metrics

Profiles of a concrete block were taken in five different areas. Typical concrete profiles are given in figure 3-8. From the profiles 20 mm sample lengths were selected. This involved selecting lengths that are absent of features. In the third profile a large feature is located between 26 and 31 mm. Instead of trying to fit a linear equation to the feature, the length chosen to compute the surface metrics excluded this feature. In section 2.2.2 a heuristic algorithm for selecting features was described. In the second profile at approximately x=24 mm, a large surface variation can be seen. This was considered to be part of the surface texture as opposed to a feature because its width is narrower than the spatial definition we use for form geometry: one fourth of the distance of the sample length.

**Figure 3-8.** Concrete Profiles measured with the apparatus shown in figure 3-6.

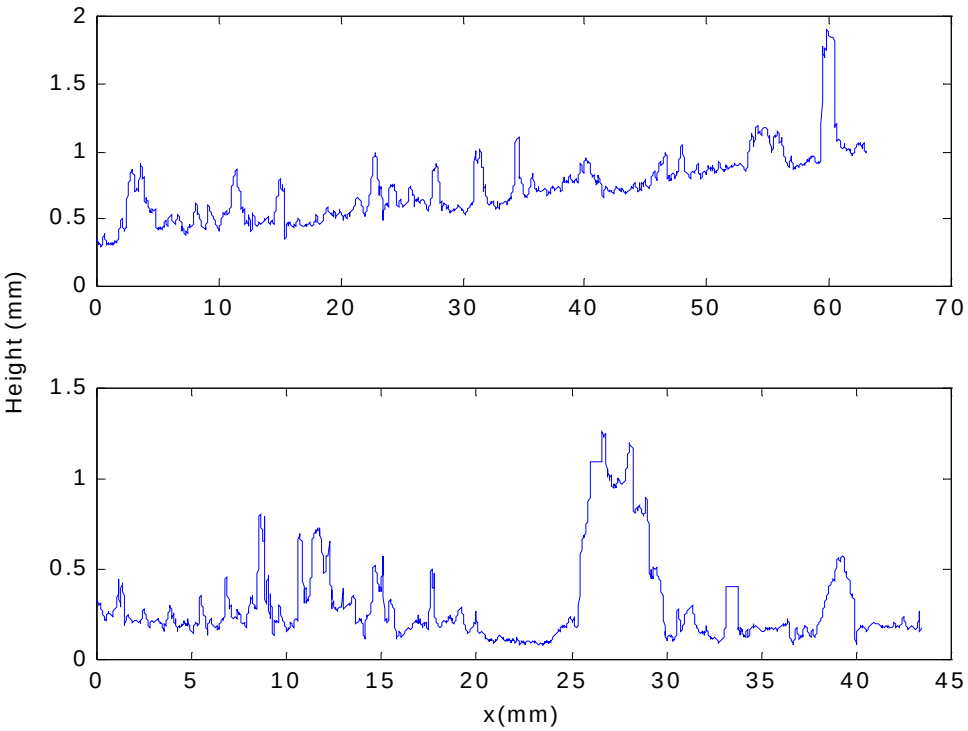


The measured surface metrics of the concrete block are summarized in table 3-1. The amplitude parameters, $R_a$, the average deviation, and $R_q$, the RMS deviation, are both measured from a mean reference line of zero. The standard deviation of the kurtosis is of the same order of magnitude as its mean, demonstrating the difficulty of measuring it consistently. Although the Kurtosis is difficult to measure, our experimental value is far below three indicating that the profile does not have a Gaussian height distribution.

**Table 3-1.** Concrete Block Surface Metrics

| | Skew | Kurtosis | Ra(mm) | Rq(mm) | PD (Pks/mm) | Compass Dimension | Spectral Dimension | Amplitude Coefficient |
|---|---|---|---|---|---|---|---|---|
| Mean | 1.331 | -2.27e4 | .087 | .111 | 3.97 | 1.038 | 1.163 | .023 |
| Std | .072 | 1.24e4 | .012 | .016 | 0.155 | .016 | .078 | .015 |

The frequency content of the profile can be examined by looking a plot of its power spectral density. A comparison of the concrete's PSD to a PSD of painter’s sandpaper is given in figure 3-9. While we can use the PSD to examine under what scales the profiles exhibit the linear behavior characteristic of fractals, differentiating between the two by

mere examination can be more challenging. The fractal dimension and amplitude coefficient quantifies the differences between the two plots.

The mean compass dimension was consistently smaller than the mean spectral measurement of the fractal dimension. We found this to be the case for a synthesized von Koch fractal of known dimension as well. Low values of the fractal dimension calculated by the compass method have been noted previously [25]. However the compass dimension has a much smaller standard deviation than the spectral dimension.

**Figure 3-9.** PSD of Concrete and Painter's Sandpaper. A line can be fit for frequencies which the sample exhibits fractal behavior.

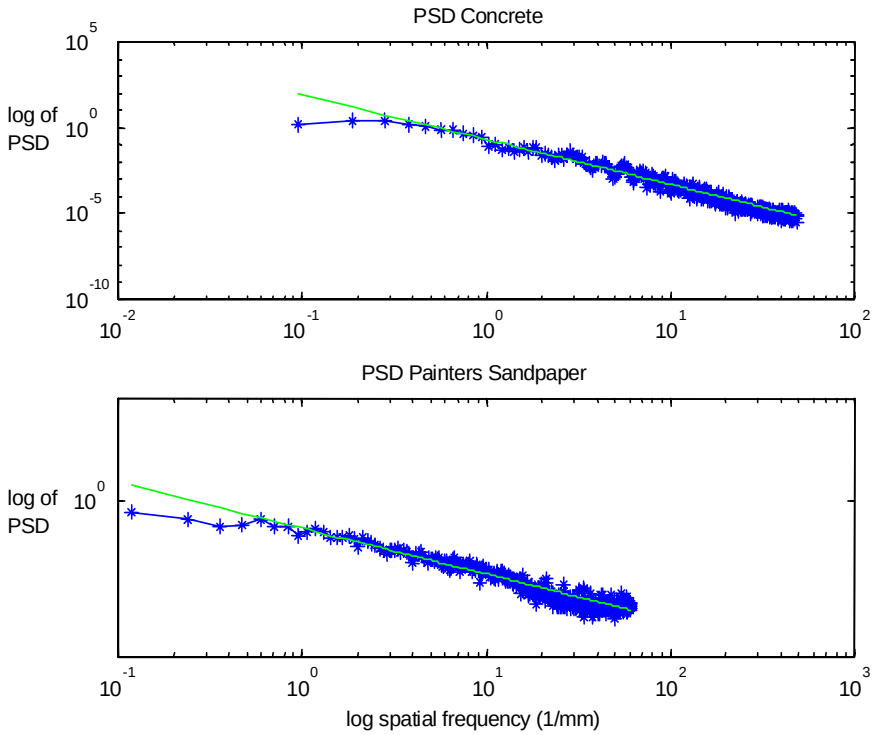


Now we have set of parameters that describe four things about a profile, the shape of the height distribution, the amplitude parameters, the peak density, and the Fractal parameters. Of the distribution parameters, kurtosis seems the least valuable because it is hard to measure, but it can indicate if the profile has a Gaussian distribution. The fractal parameters are a method of describing the PSD. The amplitude and peak density parameters describe the profile in physically intuitive terms. We can now use all of these parameters to try and describe the profiles of different types of sandpaper.

**Figure 3-10.** Sandpaper Profiles for 10 mm long samples measured with laser displacement sensor. with a resolution of .008 mm/sample. The profiles were filtered with a 19$^{th}$ order Butterworth low pass filter with a corner spatial frequency of 7.2 (1/mm).

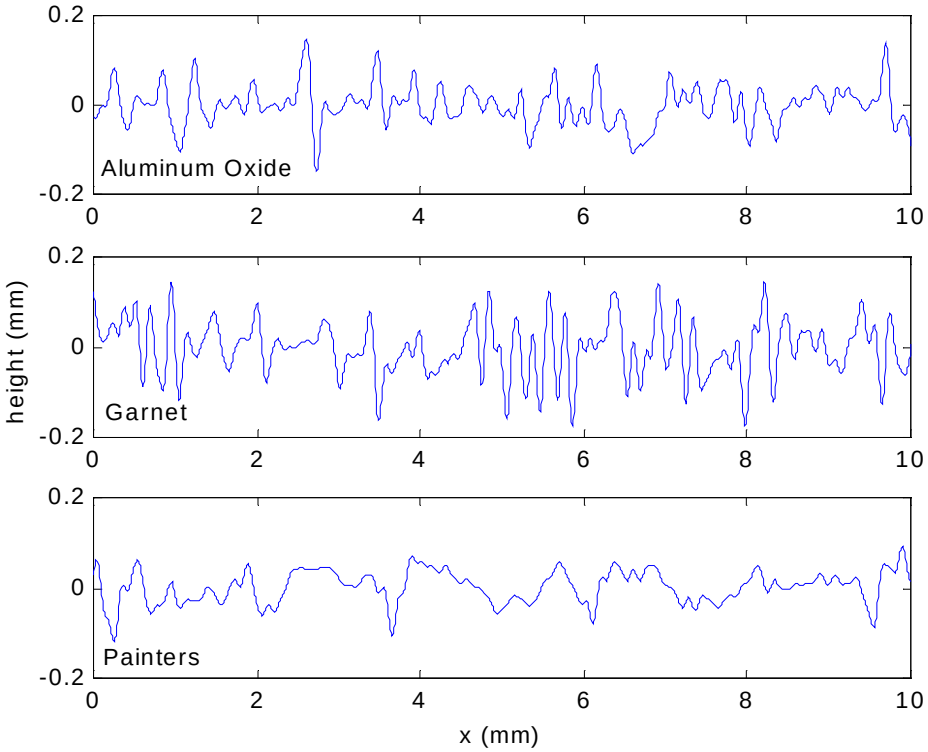


One hundred and sixty grit aluminum oxide and garnet sandpaper, along with painter's 100 grit sandpaper, were profiled (figure 3-10) and had their surface metrics computed[1]. The tabulated results are presented in table 3-2. At the same grit rating the amplitude parameters $R_a$ and $R_q$ successively decrease between garnet, aluminum oxide, and painter's sandpaper. As expected, the amplitude parameters decrease with increasing grit rating for all samples.

1. Garnet sandpaper is qualitatively sharpest and fastest cutting; painter's sandpaper is the least sharp.

**Table 3-2.** Sand Paper Comparisons

| Sample | Skew | Kurtosis | Ra(mm) | Rq(mm) | PD (Pks/ mm) | Compass Dimension | Spectral Dimension | Amplitude Coefficient |
|---|---|---|---|---|---|---|---|---|
| Al-Ox 60 | .183 | -7.25e4 | .063 | .081 | 1.83 | 1.122 | 1.333 | .150 |
| Garnet 60 | -.296 | -2.77e4 | .079 | .103 | 2.187 | 1.151 | 1.388 | .427 |
| Al-Ox 100 | .151 | -7.34e5 | .034 | .045 | 1.441 | 1.07 | 1.127 | .035 |
| Garnet 100 | .131 | -2.20e5 | .046 | .062 | 2.153 | 1.122 | 1.174 | .099 |
| Painter's 100 | -.619 | -2.0e6 | .028 | .036 | .312 | 1.01 | 1.129 | .005 |

There is also a difference between the fractal dimension measurements of the samples with the same grit. Using the compass dimension, the fractal dimension decreases between garnet, aluminum oxide and painter's sandpaper, and then decreases for decreasing grit. The spectral fractal dimension does nearly the same, with the exception that the fractal dimension of 100 grit painter's sandpaper is slightly larger than aluminum oxide.

Examining the height distribution parameter kurtosis indicates that none of the different types of sandpaper have a Gaussian height distribution. The skew of the different sandpapers shows that aluminum oxide sandpaper has a greater skew than the garnet sandpaper at each grit rating.

Originally the aluminum oxide and garnet sandpaper profiles contained large noise spikes that caused unusually large spectral fractal dimension measurements as compared to the painter's sandpaper. The spikes were probably caused by spurious reflections of a combination of the grit adhesive and the odd shiny grit on the aluminum oxide and garnet sandpaper. The dull painter's sandpaper had no such spikes. Krylon® photographic dulling spray was used on the sandpaper to eliminate these reflections. It was also used on the painter's sandpaper to test the effect of the spray on the amplitude parameters. The $R_q$ and $R_a$ values were less than 1.1% and 2.5% smaller than the untreated sandpaper. While the spray ameliorated the spectral fractal dimension measurement problem, it had little effect on the other parameters.

### 3.4.2 Examining Synthesized Fractal Surfaces

We used the Ganti's method of Fourier filtering [13] to synthesize surfaces using the fractal dimension and amplitude coefficient measured from a profile of 100 grit painter's sandpa-

per (figure 3-11). The surface metrics of the measured surface and the generated surfaces are presented in table 3-3. When simulated with the measured fractal dimension amplitude coefficient the synthesized amplitude parameters $R_q$ and $R_a$ are smaller than the measured amplitude parameters by 2.6 and 2.9 times respectively. Since we can relate $R_q$ to the amplitude coefficient $C$ by equation 3.9, we verify if our amplitude coefficient has been underestimated by our measurement technique. The predicted value of $C$ for the measured $R_q$ is .0062, nearly the same as the measured value. We synthesized the surface again using $C$=.12 to achieve a surface with an $R_q$ value closer to the measured surface.

The peak density metric was greatly dependent on the resolution we chose for generating our fractal, decreasing with decreasing fractal resolution. Whether or not this would influence a user's perception of two haptically displayed surfaces with the same fractal and amplitude properties but with different resolutions could be measured by the peak density. The surface we generated with the larger amplitude coefficient of .12 was generated at the same spatial resolution as the measured original profile. Its peak density was 83% of the measured surface peak density value. The smaller value of the peak density could be attributed to the smaller $R_q$ value of the generated surface. The surface simulated with $C$=.0063 failed to generate peaks large enough to be counted by our algorithm.

**Table 3-3.** Sand Paper and Synthesized Surface Comparisons. Note that the synthesized surface using the measured amplitude coefficient of the sandpaper had much smaller amplitude parameters than the actual sample.

| Profile | Skew | Kurtosis | Ra(mm) | Rq(mm) | PD (Pks/mm) | Spectral Dimension | Amplitude Coefficient |
|---|---|---|---|---|---|---|---|
| Painter's Sand Paper | -.874 | -1.396e6 | .0285 | .0386 | .4999 | 1.166 | .0063 |
| Simulated C=.0063 | .0663 | -9.996e7 | 0.110 | .0132 | 0 | 1.1543 | 3.967e-5 |
| Simulated C=.12 | .1560 | -1.532e6 | .0293 | .0374 | .4167 | 1.254 | .0012 |

**Figure 3-11.** Actual versus Synthesized Profiles. The profiles are respectively, Painter's 100 grit sandpaper, fractal simulation with parameters set to D=1.166, C=.0063, and fractal simulation with parameters set to D=1.166, C=.12. The surface metrics of these profiles correspond to each of the three rows in table 3-3.

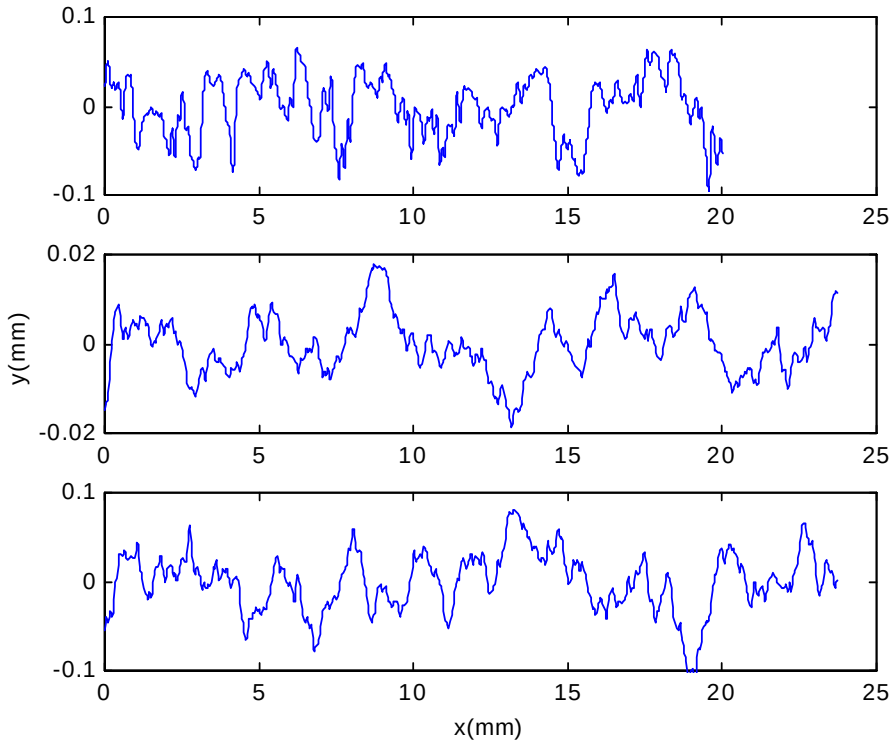


### 3.4.3 Experiment Accomplishments and Applications

Methods of surface roughness metrology were reviewed. Synthesizing new surfaces was accomplished by characterizing surfaces by two properties relating to their power spectral density functions: the fractal dimension, which relates to the power of the frequency contents of the profile, and the amplitude coefficient, which describes the amplitude of all frequencies. The amplitude coefficient measured by the structure function was able to predict the measured RMS amplitude of the profile.

Surfaces were compared using amplitude parameters, and a two-parameter fractal characterization. These parameters were used to compare sandpaper of the same grit rating but made of different materials. It was found that the amplitude parameters of aluminum oxide and painter's sandpaper were smaller than those of the sharper garnet sandpaper of the same grit classification, while the amplitude parameters over all decreased with increasing grit. Fractal dimension *D* of aluminum oxide sandpaper and painter's sandpaper was

smaller than for garnet sandpaper of the same grit. As the grit increased the fractal dimension decreased, illustrating decreasing fractal dimension for smoother surfaces.

Synthetic surfaces were generated from the measured fractal parameters of painter's sandpaper using a modified Fourier filtering method. The resulting profile while having a larger fractal dimension than the actual surface had amplitude parameters $R_a$ and $R_q$ approximately 34% and 38% of the measured values. We found that the structure function method of measuring the amplitude coefficient could predict the actual $R_q$ value. A synthesized surface using the measured fractal dimension and an increased amplitude coefficient was used to create a surface with amplitudes approaching the measured $R_q$. Although generated with a larger amplitude coefficient, this synthesized surface approached the original measured profile in terms of amplitude parameters and peak density.

We are able to use two parameters to synthesize new surfaces, the fractal dimension, *D* and the amplitude coefficient, *C*. The value of the amplitude coefficient is adjusted to generate a fractal surface with a desired RMS amplitude, $R_q$. In chapter 5 we describe a psychophysical roughness perception experiment that utilizes fractal surfaces synthesized by this method and displays them on a haptic replay device. Before we do that, chapter 4 extends the fractal techniques from two dimensional profiles to the three dimensional case of surfaces.

# 4 Two-Dimensional Fractal Surfaces

In this chapter surface roughness is described for the two-dimensional case. Analogs of the statistical roughness parameters for one-dimensional profiles are reviewed for two-dimensional surfaces. Other surface metrology methods that consider anisotropic surfaces using spectral and correlation techniques are examined. The capabilities and limits of using fractal methods with structure tensors to characterize isotropic and anisotropic surfaces are discussed. Finally the sampling theorem is applied to enable fractal characterization and generation of anisotropic surfaces.

## 4.1 Two-Dimensional Surface Metrology Methods

In chapter 2 methods from the field of surface metrology were described to characterize one-dimensional surface profiles. Statistical parameters were computed to describe the mean and RMS amplitude of the profile as a measure of its roughness. Additionally the shape of the height distribution of the profile was described by the skew and kurtosis parameters. In this section extensions to computing these parameters from two dimensional surface height data are reviewed. The statistical parameters presented for both one- and two-dimensional data contain the underlying assumption that the measured surface is isotropic. Quantifying the degree of surface isotropy is done by using the autocorrelation and power spectral density functions of the surface.

### 4.1.1 Removing Gross Geometry

In the one-dimensional profile case the surface roughness was separated from the form of the object before computing any roughness amplitude parameters. This was accomplished by fitting a second order polynomial to the profile to remove slant, curvature or waviness; along with setting the mean level of the profile to zero. Similarly for a two dimensional sur-

face the trends and form geometry of the surface are removed by fitting a least-squares mean or datum plane

$$f(x,y) = a + bx + cy \tag{4.1}$$

to the surface data, $z(x,y)$ before any amplitude statistics are computed [14][18]. A higher order polynomial may be used the fit the form but is usually not required [14]. The statistical roughness parameters are computed from the residual surface, $\eta(x,y)$ formed by subtracting the least-squares from the original surface [18]

$$\eta(x,y) = z(x,y) - f(x,y) \tag{4.2}$$

### 4.1.2 Statistical Parameters for 2-Dimensional Surfaces

Several 1-D profile metrics such as the root mean square amplitude, skew, and kurtosis, have 2-D surface definitions to describe the amplitude and distribution of the surface height data. To distinguish between 1-D profile and 2-D surface parameters we follow the naming convention that has variables beginning with the capital letter 'S' variables denoting 2-D surface parameters as opposed to variables using captial 'R' for 1-D measurements [19].

Amplitude parameters are widely used to describe the magnitudes of the departures of profiles and surfaces from a reference line or plane. For a surface the RMS deviation from the datum plane, $S_q$ is given in continuous form as [14]

$$S_q = \sqrt{\frac{1}{A}\int_A \eta^2(x,y)\,dx\,dy} \tag{4.3}$$

integrated over a surface area $A$. The discrete form of $S_q$ can be computed from [18]

$$S_q = \sqrt{\frac{1}{MN}\sum_{j=1}^{N}\sum_{i=1}^{M}\eta^2(x_i,y_j)} \tag{4.4}$$

where $M$ and $N$ bound the ordinates in the $x$ and $y$ directions. While insensitive to the sampling intervals, this metric is sensitive to the size of the sampling area [18], similar to how 1-D amplitude metrics are sensitive to the sampling length. In non-stationary processes the variance of the amplitudes increase with scan length [20][22][34].

Symmetry of the distribution of the surface height ordinates is measured by the skew parameter. The discrete form of skew for a surface is [18]

$$S_{sk} = \frac{1}{MNS_q^3} \sum_{j=1}^{N} \sum_{i=1}^{M} \eta^3(x_i, y_j) \tag{4.5}$$

Kurtosis measures the peakedness or bluntness of the surface height distribution. The discrete form for kurtosis of a surface is [18]

$$S_{ku} = \frac{1}{MNS_q^4} \sum_{j=1}^{N} \sum_{i=1}^{M} \eta^4(x_i, y_j) \tag{4.6}$$

The way in which the surface profile skew and kurtosis describe the shape of a height distribution is identical to profile skew and kurtosis. Again, a Gaussian height distribution will have a skew of 0 and kurtosis of 3. Examples of how skew and kurtosis affect height distributions are given in chapter 2 (figure 2-2 and figure 2-3). These parameters assume that surface is isotropic in that there is no distuinguishment of the location of any height ordinate, and that there is only one value of the metric for a scanned surface.

Describing the spatial properties of surfaces typically begins with peak counting. For one-dimensional profiles the peak density is a common spatial parameter to begin with. The two-dimensional surface parameter analog is the summit density, computed in units of *peaks/mm*$^2$ [18]

$$S_{ds} = \frac{n_s}{(M-1)(N-1)\Delta x \Delta y} \tag{4.7}$$

where $n_s$ is the number of summits and valleys, and $\Delta x \Delta y$ is the product of the interelement spacing in the $x$ and $y$ directions. However, like peak density, the summit density value is dependent on the definition of a summit [18]. Unfortunately there are numerous summit definitions, varying from the highest point lying within four or eight nearest neighbors [37], the highest point within a small zone [38], and contour-based summit detection [39]. This spatial property isn't able to characterize the degree of isotropy of the surface.

### 4.1.3 Spectral and Correlation Methods for Anisotropic Surfaces

The parameters discussed in section 4.1.2 give no insight about whether or not the surface properties change with direction. Numerous surfaces exhibit anisotropic behavior. For surfaces manufactured with a cutting tool anisotropy arises from the pattern of marks left by tool. In surface metrology the lay of the surface measures the direction of the predominate pattern left by the manufacturing process. In geology, materials formed by sedimentary layering is an example of surface anisotropy. The presence and degree of anisotropy can be examined with the autocorrelation and power spectral density functions of the surface.

The autocorrelation function is frequently used to analyze observational data with random characteristics [41]. In surface metrology the autocorrelation function can be used to compute the texture aspect ratio of a surface $S_{tr}$ which indicates the degree of anisotropy of a surface [40]. The areal or area autocorrelation function is the expected value of the product of two points a distance $\tau$ apart [42]. Computing the area autocorrelation, AACF, can be done by first computing the area auto covariance function

$$ACVF(\tau_x,\tau_y) = \frac{1}{(L_x-\tau_x)(L_y-\tau_y)} \int_0^{(L_x-\tau_x)} \int_0^{(L_y-\tau_y)} z(x,y)z(x+\tau_x,y+\tau_y)dxdy \qquad (4.8)$$

The computation of the AACF is completed by normalizing with the value of the ACVF at the origin, which is also the variance of the surface [14]

$$AACF(\tau_x,\tau_y) = \frac{ACVF(\tau_x,\tau_y)}{ACVF(0,0)} \qquad (4.9)$$

An example of an AACF of an isotropic surface is given in Figure 4-1 on page 49. At the origin the AACF has a value of 1, and decays to 0 with increasing distance. Depending on the direction away from the origin the AACF will decrease with varying speeds. By examining the decay distances to 0.2 in various directions the degree of anisotropy can be measured. The texture aspect ratio of a surface $S_{tr}$ is

$$0 < S_{tr} = \frac{d_f}{d_s} \leq 1 \qquad (4.10)$$

where $d_f$ is the fastest decay distance to 0.2 on the normalized AACF, $d_s$ is the slowest decay distance to 0.2 on the normalized AACF. The decay distance of 0.2 has been selected by convention in the surface metrology field. For values of $S_{tr}$ approaching one the surface displays stronger isotropy while values approaching zero indicate anisotropic behavior, In surface metrology $S_{tr}$=0.5 is considered the cutoff between a surface being isotropic and anisotropic [18].

**Figure 4-1.** Areal Auto Correlation Function of a Fractal Isotropic Surface

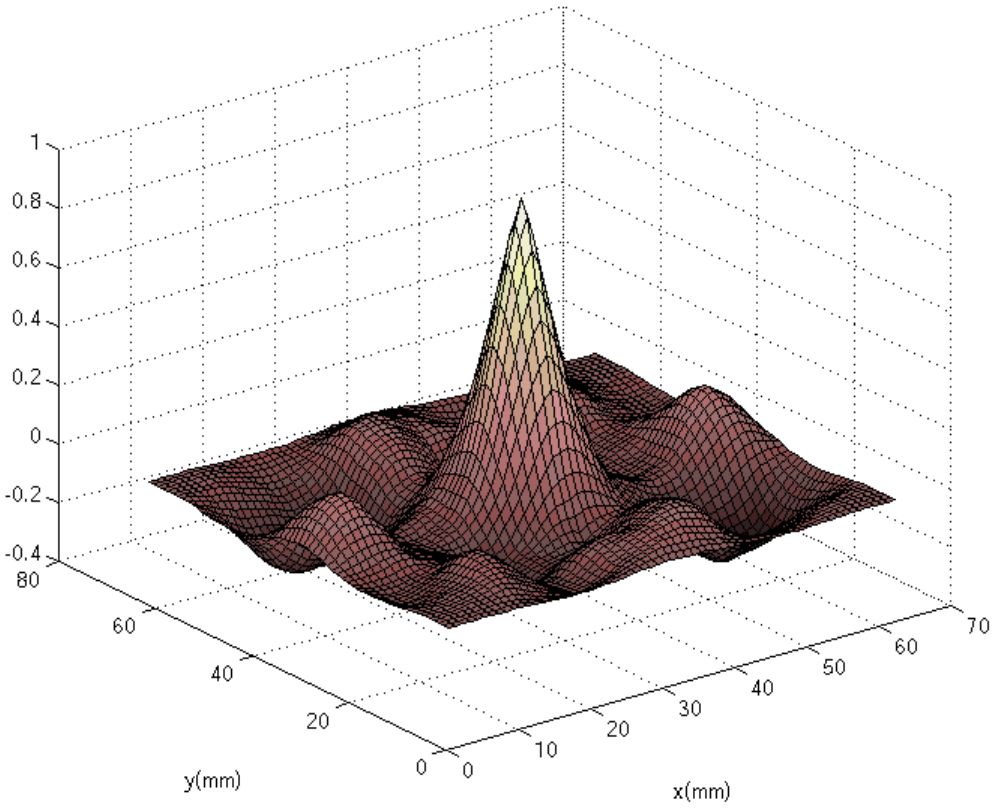


In surface metrology surfaces frequently have a prominent texture left by the manufacturing processes. The angle of the pattern is called the lay direction of the surface. The direction of the texture pattern can be measured using the areal power spectral density (APSD). The APSD can be computed from the discrete two dimensional Fourier transform [41]

$$\Im(\mu,\nu) = M^{-1}N^{-1}\sum_{\sigma=0}^{M-1}\sum_{\tau=0}^{N-1} f(\sigma,\tau)e^{-i2\pi(\mu\sigma/M+\nu\tau/N)} \tag{4.11}$$

and then squaring the magnitude of the complex Fourier pair to find power spectral density

$$P(\mu,\nu) = |\Im(\mu,\nu)|^2 \tag{4.12}$$

An example of a power spectral density function of a surface is given in figure 4-2. In this particular figure the APSD is displayed as an image intensity map instead of the 3-dimensional isometric view used for the AACF in figure 4-1. Both methods are used for display in surface metrology. Because of the high value of the APSD at its center and steep dropoff it was found easier to examine the APSD with an image intensity map.

**Figure 4-2.** Areal Power Spectral Density Function of a Fractal Isotropic Surface

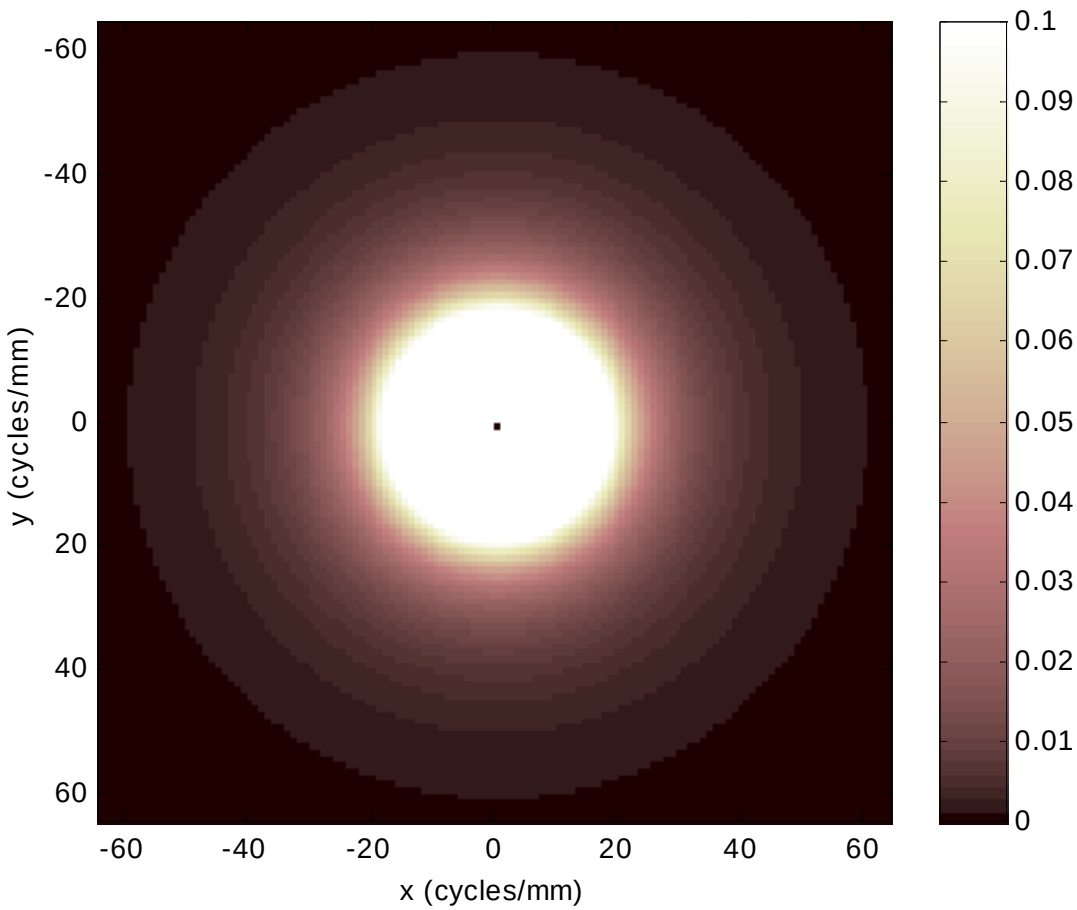

The texture direction of a surface or lay direction, $S_{td}$ is defined as the angle where the maximum power occurs in the APSD [18]. This assumes that the texture aspect ratio indicates anisotropy and is less than 0.5.

Using $S_{tr}$ and $S_{td}$ to analyze geological materials isn't necessarily appropriate because they are not formed by machining processes. They may not have anisotropic behavior due to texture patterns in one direction resulting from machining operations. However the idea of using spectral methods to examine for anisotropic behavior is a start. Later in this chapter we will use the APSD for characterizing surfaces as fractals and generating new surfaces with anisotropic behavior.

This section does not provide an exhaustive set of parameters available to describe surfaces. Additional metrics used to characterize surfaces can be found as a part of the proposed "Birmingham 14" set of metrics [14]. Numerous other parameters can be found in the Handbook of Surface Metrology [42]. However the increasing catalogue of metrics has lead to what Whitehouse coined as "parameter rash" [43]. So far, the parameters dealing with anisotropic properties have simplified the behavior to one angular direction. Instead of using fourteen or even five parameters to describe a surface we again turn to fractal methods to simply the surface characterization while enabling description and synthesis of multi-angular anisotropy.

## 4.2 Fractal Methods

In chapter three fractal methods for describing one-dimensional profiles of rough surfaces were discussed. Multi-dimensional fractal analysis has been used for classification of medical images [47], studying outlines of particles such as sediments [48], and satellite texture analysis [55]. For the application of this thesis, real surfaces, two-dimensional fractals will have to be used for both analysis and synthesis. Sythesized fractal terrains have been used in movies since the early eighties with great success beginning with the classic computer generated Genesis scene in *Star Trek II: The Wrath of Kahn* [12]. However almost all fractal mountain terrains in computer graphics are homogeneous and isotropic [24]. For analyzing real surfaces anisotropic surfaces must be considered to describe and synthesize two-dimensional surfaces with fractals.

### 4.2.1 Measuring the Fractal Dimension of Surfaces

Many of techniques used to measure the fractal dimension of profiles, such as the compass divider method, Minkowski coverings, and spectral methods, can be applied to measuring the fractal dimension of a surface with some modification. The common introductory fractal dimension problem of measuring the length of the British coastline and the land frontier of Portugal illustrates the compass divider method [49]. As discussed in chapter 2 the total distances of boundary profiles are measured by fitting lines of various lengths to the profile. The distance measured changes with each measuring length scale used. Plotting the measured distance versus the measuring length scale on a log-log scale creates the Richardson Plot of the boundary profile [51]. If the profiles are fractal a straight line will be plotted whose slope can be related to the fractal dimension. This can be applied to surfaces as well by intersecting a horizontal plane with the surface to create boundary profile, called the zeroset [46]. While the fractal dimension of the zeroset will be computed to be between one and two, $1 \le D < 2$, Mandlebrot speculated that the surface fractal dimension will be exactly the dimension of the intersection plus one, $D$+1. This has been found to be true for some uniform, isotropic surfaces [46]. Because of these restrictions we do not use this method; however this does illustrate the idea that one profile can be used to measure the fractal dimension of am isotropic surface.

Analogous to the divider method, triangular tiling of the surface also uses a Richardson plot to compute the fractal dimension [52]. The area of the surface is computed by fitting the surface with equilateral triangles of one size. This computation is repeated multiple times for various triangle sizes. A log-log plot of the surface area estimated by the triangles versus triangle edge size then produces a Richardson plot for the surface. Adding two to the slope gives the fractal dimension of the surface. Another covering scheme is the Minkowski Comforter, which uses spheres to sweep out a volume over surface [46]. Also searching for linear relationships graphed over a log-log scale is the Hurst Plot, which separates height differences at various spacings in the data [53]. Although this method is only useful for isotropic surfaces Russ has modified its use into the Hurst Orientation Transform to measure the directionality of surface anisotropy [46].

#### 4.2.1.1 Measuring Fractal Dimension with Power Spectral Density Functions

The two-dimensional Fourier transform has found applications in image analysis, television display, radar, and analysis of other two-dimensional data sets. In chapter two the power spectrum of a one dimensional fractal Brownian motion profile was given as proportional to $1/f^{\beta}$. The fractal dimension of a profile was quickly determined by computing the power spectral density and relating the slope $\beta$ to the fractal dimension. It is possible to make extensions to higher dimensional self-affine fBm processes. The power spectrum for a fBm surface is [12][54]

$$P(\boldsymbol{k}) \propto \frac{1}{\|\boldsymbol{k}\|^{\beta+1}} \tag{4.13}$$

where $\boldsymbol{k}$ is the vector spatial frequency and $\|k\|$ is the euclidean distance. The fractal dimension can be related to $\beta$ by

$$D = E + \frac{3-\beta}{2} \tag{4.14}$$

where $E$ is the euclidean dimension [12]. By substituting equation 4.14 into equation 4.13 and setting $E$=2, the power spectrum for a fractal surface can be expressed in terms of its fractal dimension

$$P(\boldsymbol{k}) \propto \frac{1}{\|\boldsymbol{k}\|^{8-2D}} \tag{4.15}$$

This proportionality relationship will be the basis used to model rough surfaces. Now we will use it to measure the fractal dimension over a surface. The procedure begins by computing the two-dimensional Fourier transform of the height data $z(x,y)$, using equation 4.11 and then forming the two-dimensional power spectral density function by taking the magnitude of the Fourier transform (equation 4.12.). A power spectral density function is shown in figure 4-2. The radial magnitude lines originating from the center of the APSD combine the information for all profiles in the same corresponding direction. Sampling the APSD along each of these radial lines is equivalent to sampling profiles in different directions from the original height data [50]. The fractal dimension is computed from each of

the radial lines in a similar fashion as described in chapter two. A radial line is selected at an angle from the APSD (see figure 4-3).

**Figure 4-3.** APSD and Power Spectral Density Along Radial Line.

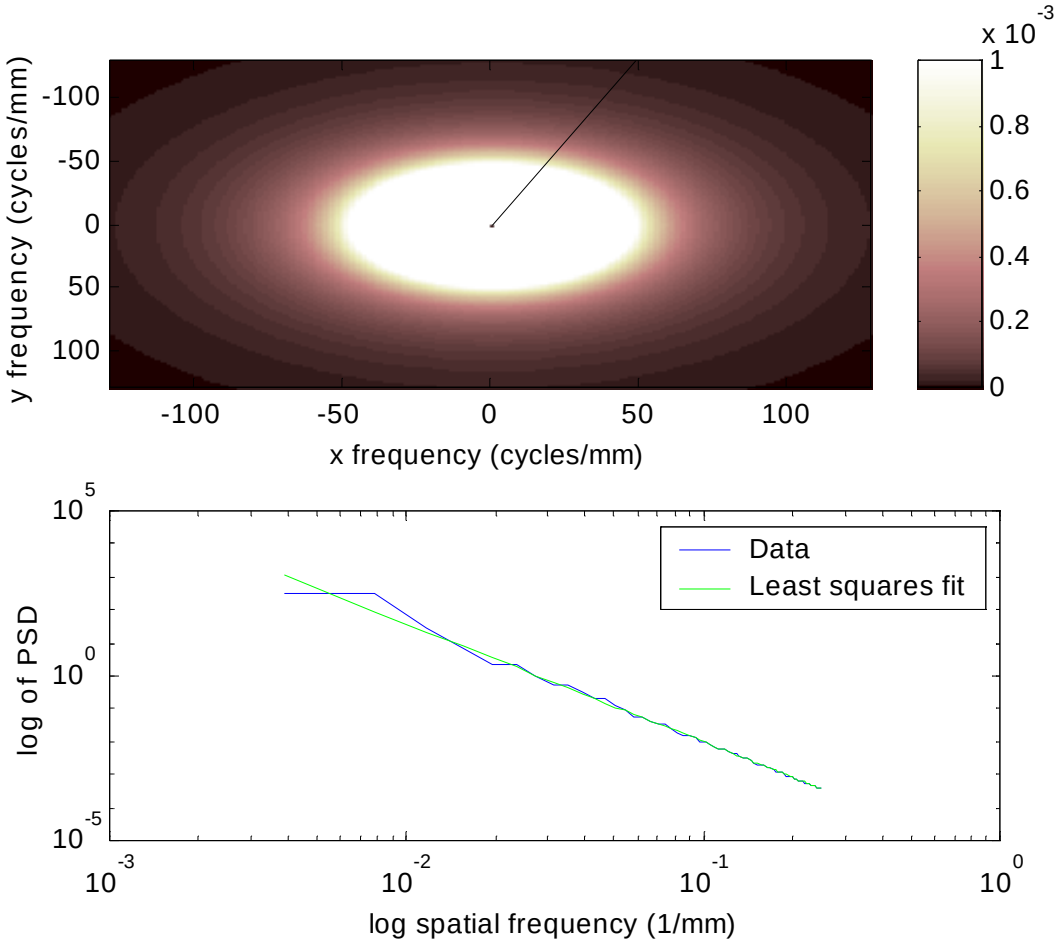


The APSD magnitudes at an angle $\theta$ are selected by forming a one-dimensional frequency magnitude matrix *r*, and then computing the frequency coordinates $f_x = r\cos\theta$ and $f_y = r\sin\theta$. The power spectral density in the direction $\theta$ is the collection of magnitudes at those coordinates. A least squares line is fitted to the spectral power magnitudes over a log-log scale. By ignoring the first few Fourier coefficients near the center of the APSD that contains the low frequency information, any structual information for the entire surface data is skipped [50]. The slope of the fitted line is related to the fractal dimension from equation 4.15 by

$$D = \frac{8 - slope}{2} \tag{4.16}$$

This is the fractal dimension for that angle. The angle is varied to build up a collection of fractal dimensions along each radial line. Because the APSD is symmetric the angle only needs to be varied from $0 \geq \theta \geq \pi$ . The size of the APSD limits how many radial lines can be selected. By plotting each of the fractal dimensions on polar coordinates the directionality of the fractal dimension can be examined. This type of plot is called a rose plot [46]. An isotropic rose plot is given in figure 4-4, contrasted with an anisotropic surface rose plot in figure 4-5.

**Figure 4-4.** Rose Plot of Fractal Dimension of Isotropic Surface

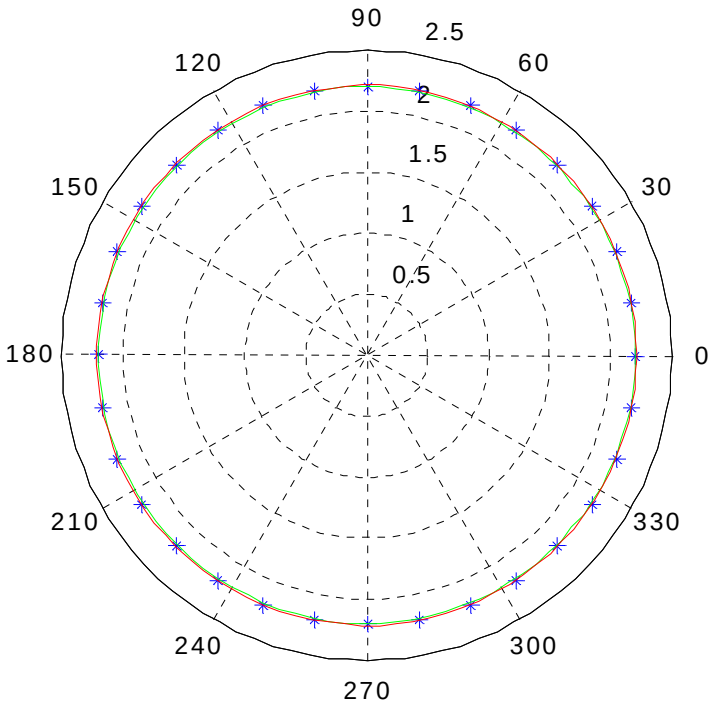

**Figure 4-5.** Rose Plot of Fractal Dimension of Anisotropic Surface.

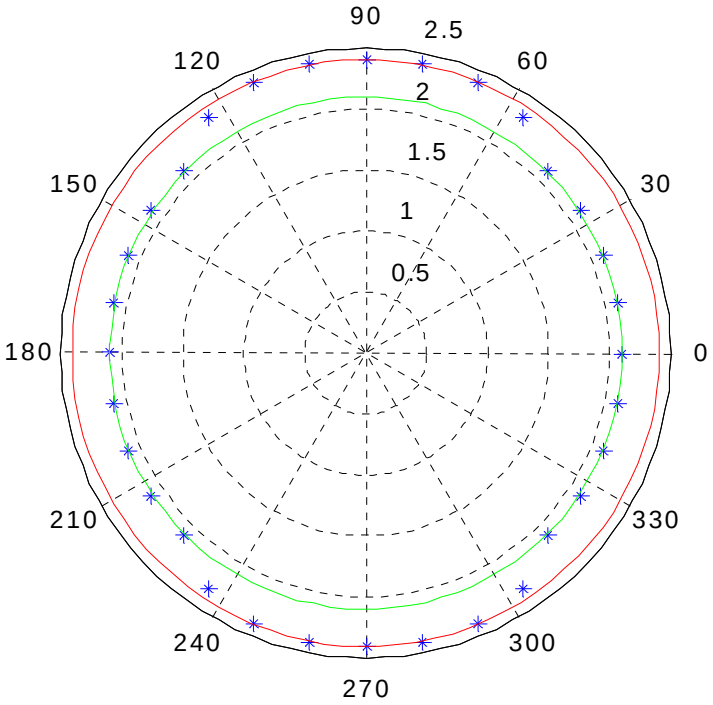


In addition to computing the APSD magnitudes the phase space should also be calculated. While the two-dimensional phase space is not used to find the fractal dimension it should be checked to ensure randomness, a necessary property for the surface to be fractal [46]. The phase angle is found by dividing the imaginary part of the Fourier coefficient by the real part, and then taking the arctangent of the quotient [56].

$$\phi(\mu, \nu) = \operatorname{atan}\left(\frac{Im(F(\mu, \nu))}{Re(F(\mu, \nu))}\right) \tag{4.17}$$

A random phase space for an isotropic fractal is shown in figure 4-6.

**Figure 4-6.** Phase Space of Isotropic Surface

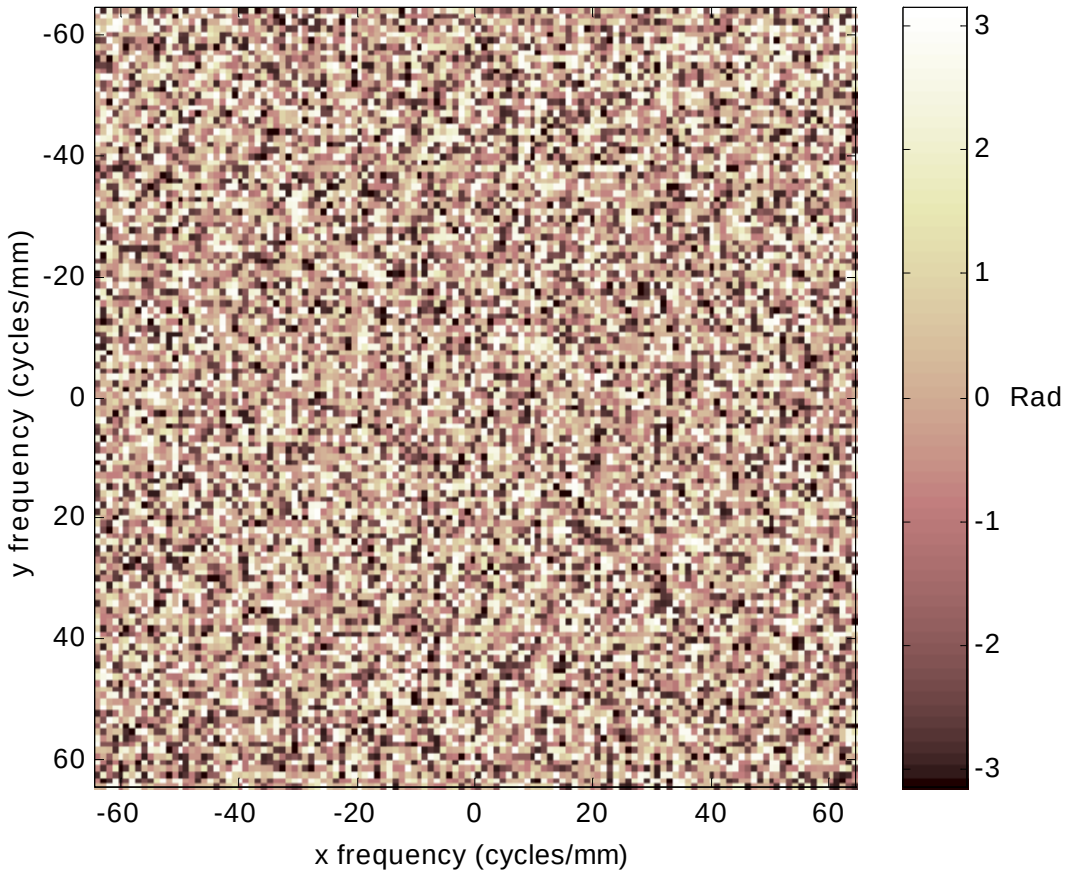


## 4.2.2 Characterizing Surfaces Review

A number of research papers have used the Weierstrass-Mandlebrot function as a fractal characterization of engineering surfaces [34][59][60]. Similar to fractal Brownian motion $1/f^{\beta}$ noises, the Weierstrass-Mandlebrot function has a power spectrum that is inversely proportional to the frequency raised to a constant. The continuous power spectrum of the W-M function for a profile is approximated by [58]

$$P(\omega) = \frac{A^{2(D-1)}}{2\ln\gamma}\frac{1}{\omega^{(5-2D)}} \tag{4.18}$$

where $A$ is an amplitude coefficient and $\gamma$ is the inverse of the sample length and must be greater than one. This power spectral relationship has also been extended to two-dimensional surfaces [59]

$$P(\omega) = \frac{A^2}{16(\ln\gamma)^2 \|\omega\|^{\beta+1}} \tag{4.19}$$

Using this function the fractal dimension *D* and the amplitude coefficient *A* provide a two-parameter, scale invariant characterization of an isotropic surface. However for the profile case described by equation 4.18, Ganti and Bhushan noted that when they changed the lateral resolution of the sensor that there was also a lateral shift in the power spectrum, although the slope was preserved. While the new power spectrum gave the same fractal dimension, a different amplitude parameter *A* was computed, thus demonstrating that *D* is unique and independent of the sensor resolution, while the change in *A* is not explained by the W-M function [13]. Because different sensors are employed in surface metrology for different applications the instrument resolution needs to be taken into account to measure scale invariant fractal parameters that characterize the surface. Otherwise a fractal characterization is no better than using the statistical parameters that vary with sample length and instrument resolution.

To get around the scale invariance problem in the one-dimensional profile case Ganti and Bhushan used structure functions to compute an amplitude coefficient independent of the sensor resolution used to measure the surface. This was discussed in chapter 2. We attempt to extend using structure functions to the two dimensional surface case.

## 4.3 Structure Functions

Structure functions have been used in the study of optics [63], stratified media [62], fluid mechanics for turbulent flow [61], random process analysis [64][65][66]. They have also found some use in surface metrology as an alternative to the correlation function [20]. Some benefits of structure function are its stability, that it does not require high pass filtering before computation, and its ability to show functional changes more clearly than the auto correlation function [14].

One previous work with surface metrology and structure functions used a two dimensional structure function to compute fractal parameters as a function of angle to investigate anisotropy due to the lay of the surface left by machining. In this work the struc-

ture function was very sensitive to any trends in the surface, so it required the form error of the surface to be removed by mean plane, and if necessary, further polynomial fitting [68].

### 4.3.1 Relating Structure Functions to Fractal Parameters

The structure function was discussed in chapter 2 in conjunction with computing the amplitude coefficient of the fractal characterization of a profile. In that chapter the fractal dimension was computed from the power spectral density. The fractal dimension and the sensor resolution were used with the structure function to compute an amplitude coefficient. The surface was then characterized by the spectral density relationship using the fractal dimension and amplitude coefficient (equation 3.8). In two dimensions for a locally isotropic field, the structure function has the same form as the profile structure function [65]

$$D(\boldsymbol{r}) = C|\boldsymbol{r}|^{m} \tag{4.20}$$

where $C$ is a constant and $m$ can be related to the fractal dimension. A similar relationship between the profile spectral density and structure function also exists for the field structure function and spectral density [65]

$$P(\omega) = A\omega^{-m-1} \tag{4.21}$$

where

$$A = \frac{2^{m} m\Gamma(1+m/2)}{\Gamma(1-m/2)} C \tag{4.22}$$

Although equations 4.20 through 4.22 were developed for locally isotropic fields, we will use these relationships to attempt to use structure functions to characterize an anisotropic fractal surface. The procedure is to compute the fractal dimension as a function of direction using the spectral density, compute the structure function, and similar to the Rose plot for fractal dimension, compute the amplitude coefficient as a function of direction. Like the amplitude coefficient for a profile, the dependence between the amplitude coefficient and the sensor resolution in the structure function will need to be found.

### 4.3.2 Computing the Structure Function For Surfaces

In field form the structure function is the expectation value of the difference squared between a function and its value at the origin [64]

$$D(\mathbf{r}) = E[(f(\mathbf{r}) - f(0))^2], \quad \mathbf{r} \in \mathbf{R}^2 \tag{4.23}$$

For computing the discrete form of the structure function of a field we turn to circular convolution again [13]

$$D(i,j) = \frac{1}{N^2} \sum_{y=0}^{N} \sum_{x=0}^{N} (z_{x+i,\, y+j} - z_{x,\, y})^2 \tag{4.24}$$

$$z_{N+i,\, N+j} = z_{i,\, j},\ i = 0, 2 \ldots N,\ j = 0, 2 \ldots N$$

for a square field of size $N$+1 where the points are equally spaced in the x and y directions.

### 4.3.3 Examples of Structure Functions

Figure 4-7 shows the structure function of the isotropic surface represented by the APSD in figure 4-3. Unsurprisingly the structure function appears isotropic in all directions near the center.

**Figure 4-7.** Structure Function Isotropic Surface

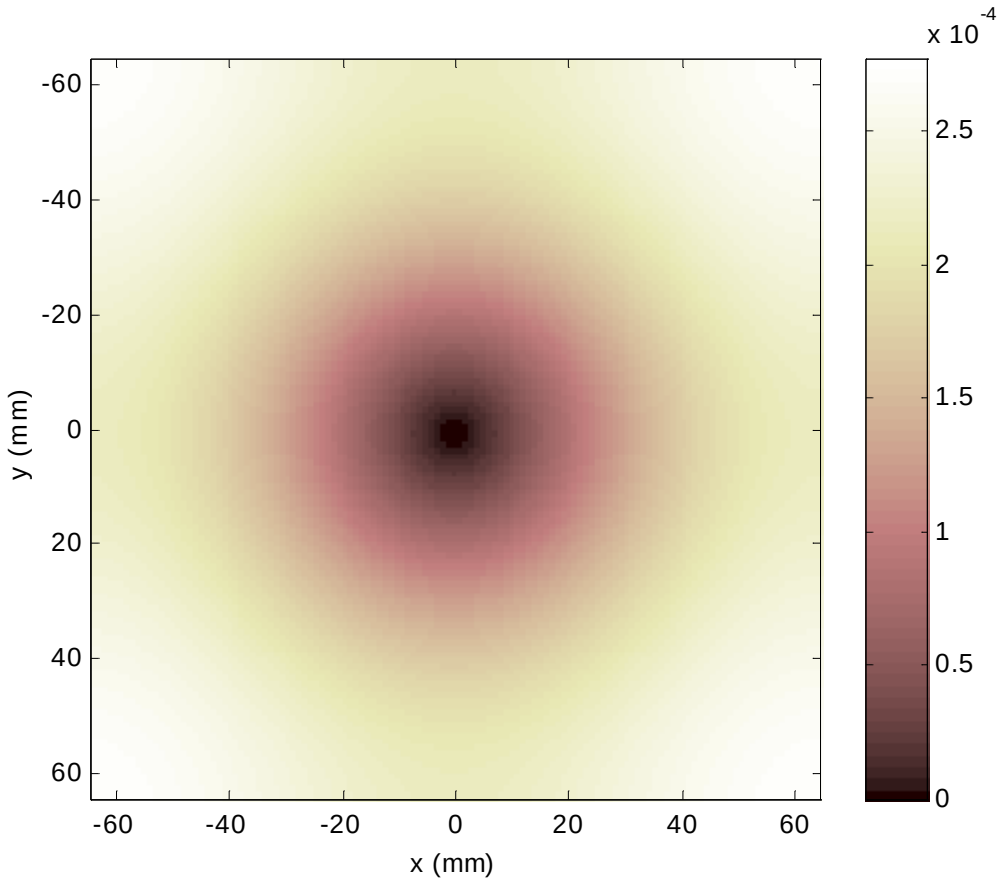


Now the structure function of an anisotropic surface is taken. An anisotropic surface is generated so that the fractal dimension changes from 2.1 to 2.4 at $\theta = \pm 45°$ and a constant amplitude coefficient (generating surfaces is covered in section 4.4). The APSD of the surface is given in figure 4-8.

**Figure 4-8.** Anisotropic APSD

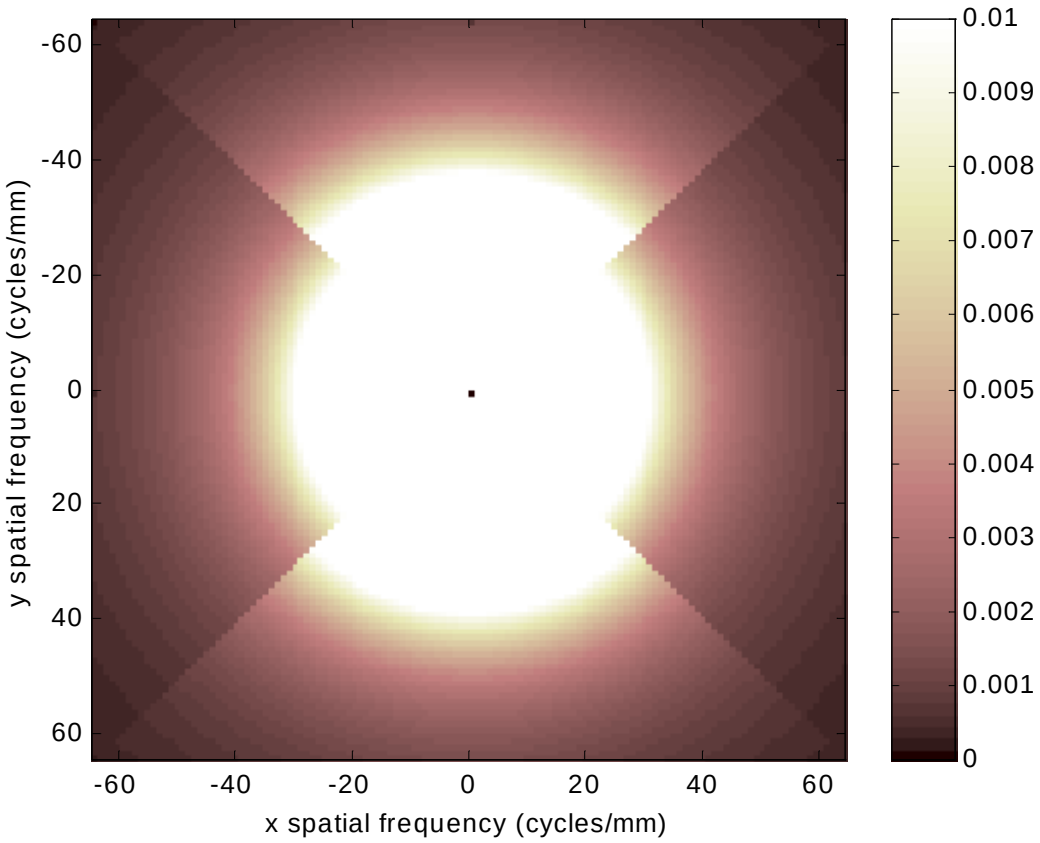


The structure function for this surface is given in figure 4-9. Looking at figure 4-9 illustrates some serious problems in trying to use structure functions on anisotropic surfaces. Instead of the distinct edge where the fractal dimension changes, the structure function is distorted. This poses a great difficulty in that it is uncertain whether there is one or more changes in the surfaces properties at any given angle. We have to remember that structure functions were developed for isotropic fields, and now we see the problem in using them on anisotropic surfaces. We abandon this method for characterizing anisotropic fractal surfaces.

**Figure 4-9.** Structure Function of an Anisotropic Surface

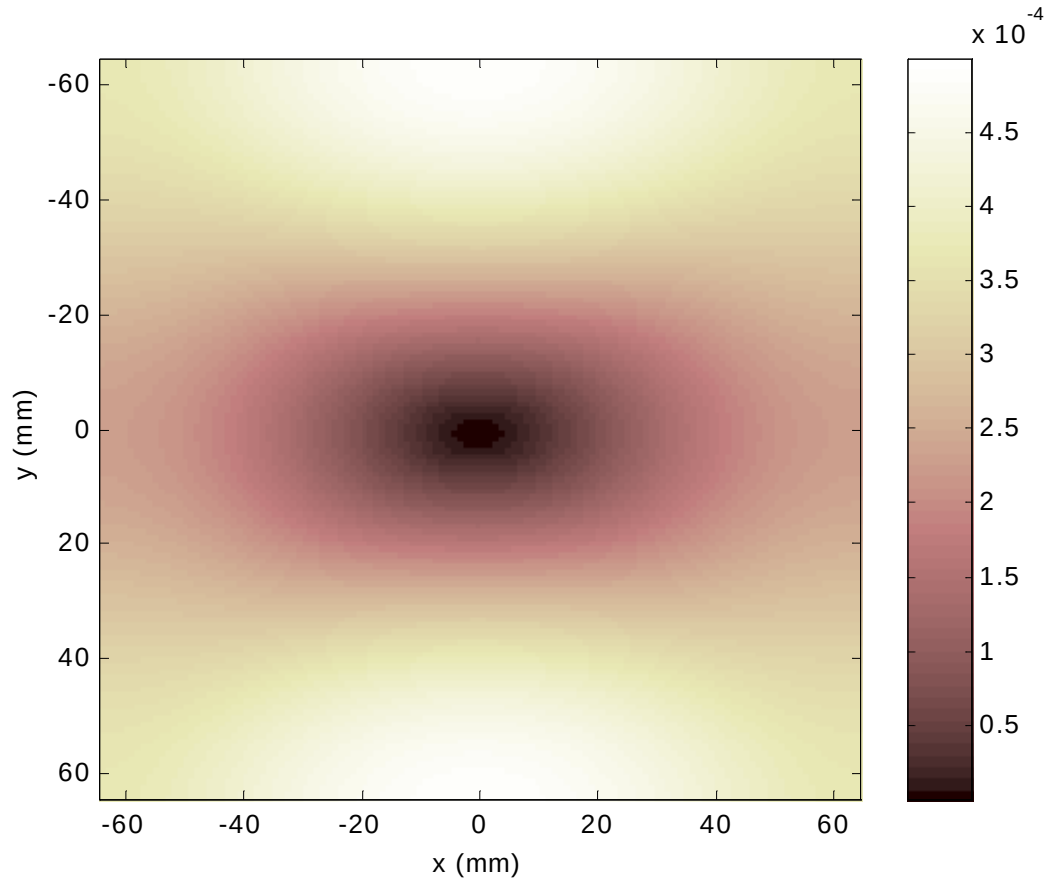


# 4.4 Sythesizing Fractal Surfaces

In this section we examine generating fractal surfaces with a power law, explore problems with remeasuring the amplitude coefficient of a resampled surface (simulating decreasing sensor resolution), and then apply the sampling theorem to reformulate our fractal relationship. Finally we propose a full anisotropic characterization of a fractal surface that takes into account the sensor resolution.

## 4.4.1 Generating Isotropic Fractal Surfaces

The procedure for generating a two-dimensional surface with fractal Brownian motion $1/f^{\beta}$ behavior is similar to the procedure for generating fBm profiles in chapter three. A fractal power spectral density law that describes the surface is chosen. The real and imaginary parts of a Fourier coefficient are generated such that the phase is random. The coefficient is then made to obey the power law. Finally the two-dimensional inverse Fourier

transform is used to transform the array of coefficients into a surface. We illustrate this process with an isotropic surface based on equation 4.15. The equation is multiplied by a constant *C* to describe the power spectrum of an isotropic fractal surface with constant fractal dimension and constant amplitude coefficient

$$P(\boldsymbol{k}) = \frac{C}{\|\boldsymbol{k}\|^{8-2D}} \tag{4.25}$$

The magnitudes of the Fourier coefficients are defined as the power spectral density [41]

$$\left|A_{(i,k)}\right|^2 = P(\boldsymbol{k}) \tag{4.26}$$

where *A* is the complex matrix of the Fourier coefficients with indices *i* and *k*. Our Fourier matrix *A* is a square matrix of size *N*. The matrix is divided into four quadrants, I, II, III, and IV, that calculating the coefficients is organized around. The naming of the quadrants is somewhat confusing as they do not follow the traditional counter-clockwise ordering. This is because the Fourier transform matrix does not have the DC component of the spectrum in the center of the matrix. It is much easier to visualize the Fourier power spectrum with the DC component in the middle of the spectrum. In all previous figures of the two-dimensional power spectral densities the DC component of the spectrum has been shifted to the center of the spectrum. After computing *A* we use the Matlab® command FFTSHIFT(X) to swap the first and third quadrants and the second and fourth quadrants of the matrix before computing the power spectrum [67]. Unshifted and shifted power spectra are compared in figure 4-10. The quadrant names we use correspond to the quadrants of the shifted power spectrum in the usual counter clockwise orientation beginning with quadrant I in the uppermost right hand corner. The naming convention is illustrated in figure 4-11.

**Figure 4-10.** Unshifted And Shifted Power Spectrums

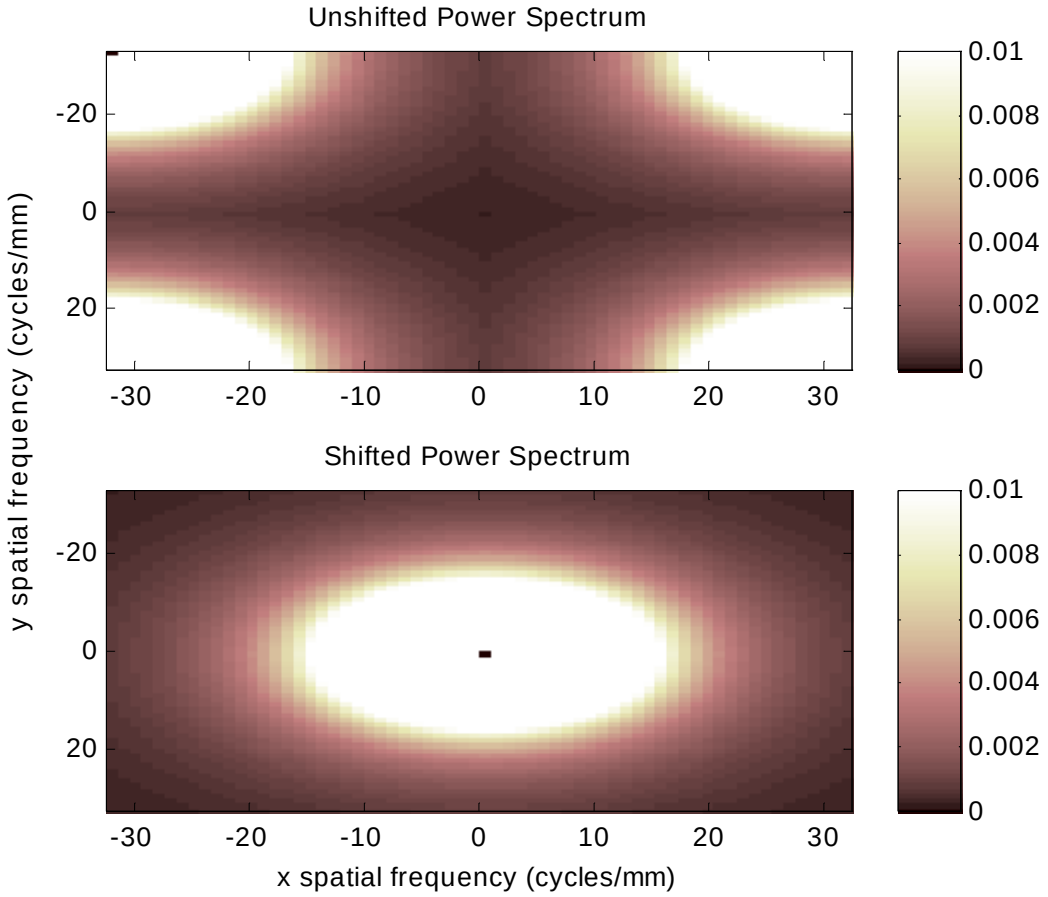

**Figure 4-11.** Quadrant Mapping

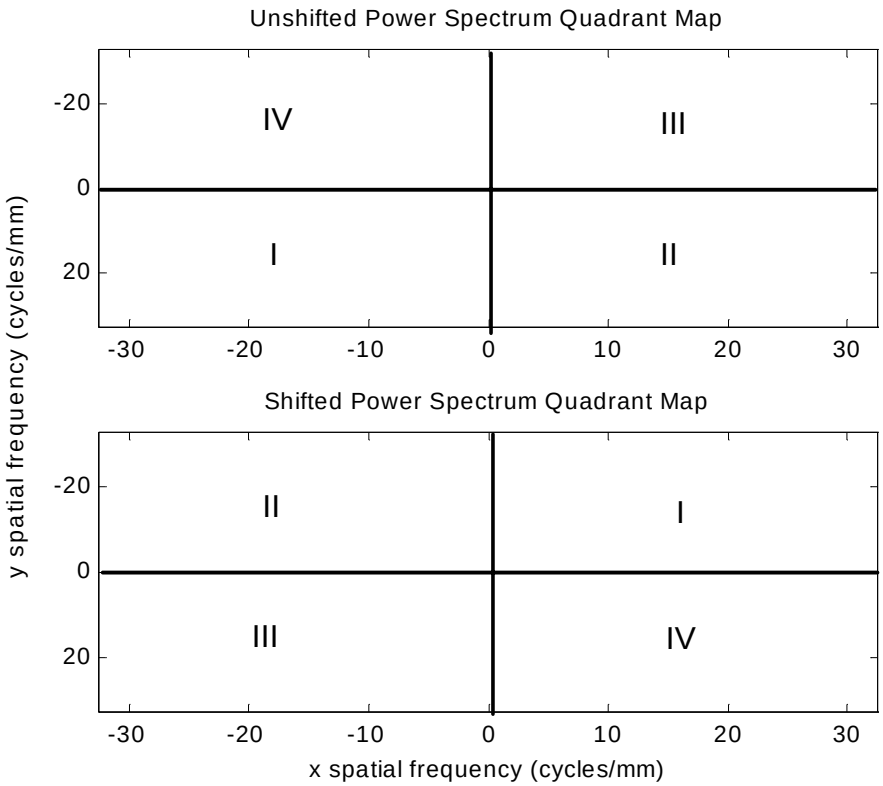


Assignment of the Fourier matrix terms begins with defining the real and imaginary parts of the quadrant IV coefficients

$$ReA_{(i,k)} = random\_sign * rand * (\sqrt{C}) \tag{4.27}$$

$$ImA_{(i,k)} = random\_sign * rand * \sqrt{C - (ReA_{(i,k)})^2}$$

$$i=1,2,...N/2. \quad k=1,2,...N/2$$

where *random_sign* is a random positive or negative sign, and *rand* is a random number from 0 to 1. This gives a magnitude of $C$ for the coefficient at $i$, $k$, while giving a random phase angle. The complex coefficient is formed by adding the real and imaginary parts

$$A_{(i,k)} = ReA_{(i,k)} + j(ImA_{(i,k)}) \tag{4.28}$$

The coefficient is finally completed by substituting equation 4.25 into equation 4.26, taking the square root to solve for the Fourier coefficient $A_{(i,k)}$, and evaluating the expression at the $i$, $k$ coordinates

$$A_{(i,k)} = A_{(i,k)} \sqrt{\frac{1}{\left[\frac{1}{L}\sqrt{i^2 + k^2}\right]^{(8-2D)}}} \tag{4.29}$$

In equation 4.29 we have explicitly substituted the discrete scaled frequency for the frequency vector **k** with the magnitude of the coordinates *i*,*k* scaled by the distance of the side of the sample, *L*.

As the power spectral density is symmetric, the quadrant II magnitudes are equal to the quadrant IV magnitudes. The coefficients are formed from the complex conjugate of the quadrant IV coefficients.

$$A_{(i0,k0)} = (A_{(i,k)})^* \tag{4.30}$$

where $i0=N-i$, and $k0=N-k$.

To find the coefficients of the quadrants I and III the procedure outlined in equations of 4.25 through 4.30 is used again, this time assigning the coordinates as

$$\begin{aligned} &i = 1, 2 \ldots N/2 - 1, \; k = 1, 2 \ldots N/2 - 1 \\ &A_{(i,N-k)} = A_{(i,k)} \\ &A_{(N-i,k)} = (A_{(i,k)})^* \end{aligned} \tag{4.31}$$

At the origin $i=0$, $k=0$ equation 4.29 will to tend to $\infty$. For this case we set $A_{(0,0)}=0$. This simply eliminates the DC component of the spectrum.

Once all the Fourier coefficients are determined the surface can be computed by using the discrete inverse Fourier transform [57]

$$z(x, y) = \frac{1}{MN} \sum_{k=0}^{M-1} \sum_{l=0}^{N-1} A(k, l) e^{(jxk2\pi)/M} e^{(jyl2\pi)/N} \tag{4.32}$$

The surfaces generated for this research were computed in Matlab® using the fast inverse Fourier transform in two dimensions, IFFT2 [67]. An isotropic surface of fractal dimension $D=2.2$ and amplitude coefficient $C=.01$ is synthesized by this method is shown in figure 4-12.

**Figure 4-12.** Synthesized Isotropic Surface, D=2.2, C=.01

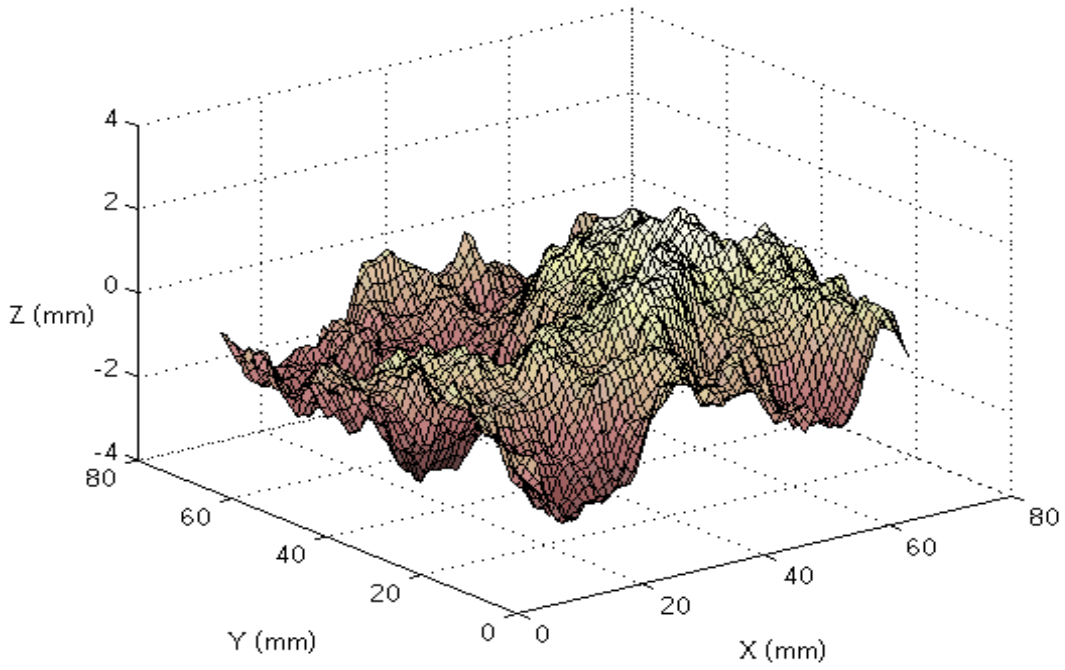


## 4.4.2 Sampling Theorem

Previously in Section 4.2.2 we described the shifting power spectrum when different sensors are used to sample the surface. This creates a problem when trying to do a fractal characterization. While the fractal dimension *D* is constant because the slope of the spectrum is preserved, its shifting changes the measured amplitude coefficient. Russ notes this problem in Fractal Surfaces, referencing a graph of two power spectra from elevation profiles collected by two different sensors by Majumdar and Bhushan [46]. The spectra are displaced by several orders of magnitude on the power axis, while the fractal dimensions measured are within .05 of each other. Russ described the spectra displacement in the graph as unexpected and unexplained. The sensors used to take the elevation profiles had two different resolutions of 1 μm for the optical interferometer, and 1 nm for the scanning tunneling microscope [69]. We hypothesize that differing sensor resolution can account for the power spectra shifting. In our simulations of surfaces we notice the same shifting problem after sampling generated surfaces to a lower resolution. We can solve this problem by taking into account the sensor resolution by applying the sampling theorem for Fourier transforms.

Functions that are sampled experience a reduction in their Fourier coefficients by a factor of $1/\Delta w$, where $\Delta w$ is the spacing between sampled points [70]. For a one-dimensional sequence of sampled points $f(k)$, the sampling theorem is [70]

$$A(j) = \frac{1}{\Delta w}\left(\frac{1}{N}\right)\sum_{k=0}^{N-1} f(k)e^{-2\pi ikj/N}$$
$$A(j) = \frac{1}{\Delta w}\Im[f(k)] \tag{4.33}$$

where $\Im$ is the Fourier transform operator and $N$ is the number of points. Previously our surface was modeled on the fractal Brownian motion power relationship for the profile case (equation 4.13)

$$\{\Im[f(k)]\}^2 = \frac{C}{\omega^{5-2D}} \tag{4.34}$$

By substituting equations 4.34 and 4.33 into the one-dimensional relationship between power and spectral density

$$P = A(j)^2 \tag{4.35}$$

we get the fBm power relationship for sampled one-dimensional functions

$$P = A(j)^2 = \frac{1}{\Delta w^2}\frac{C}{\omega^{5-2D}} \tag{4.36}$$

The work in this thesis toward a two-dimensional fractal characterization that took sensor resolution into account began with structure functions. The structure functions did not work with anisotropic surfaces so another way to explain power spectra shifting was needed. To address this we can apply the sampling theorem for the two-dimensional case to find an analogous relationship to equation 4.36. The two-dimensional sampling theorem takes the form [71]

$$A(i,k) = \frac{1}{\Delta w}\frac{1}{\Delta q}\Im[f(i,k)] \tag{4.37}$$

where $\Delta w$ and $\Delta q$ are the sample spacings in the orthogonal x and y directions, respectively. By substituting equation 4.37 into equation 4.26 we find fBm power relationship for a surface

$$P(\boldsymbol{k}) = |A(\boldsymbol{k})|^2 = \frac{1}{\Delta w^2}\frac{1}{\Delta q^2}\frac{C}{\|\boldsymbol{k}\|^{8-2D}} \tag{4.38}$$

In the simulations, surfaces are always square with the same number of ordinates on a side, and sampled with the same spacing $\Delta w$ in both x and y directions. With this simplification equation 4.38 becomes

$$P(\boldsymbol{k}) = \frac{1}{\Delta w^4}\frac{C}{\|\boldsymbol{k}\|^{8-2D}} \tag{4.39}$$

We simulate isotropic surfaces using the spectral methods described in section 4.4.1 to check that equation 4.39 will predict the same amplitude coefficient for a surface sampled at various resolutions. A surface of 1024 by 1024 points was generated using equation 4.39 as the fBm power law at a spatial resolution of 1 mm/sample. This surface was then sampled at lower resolutions of 2 mm/sample and 4 mm/sample to simulate being sampled by different sensor resolutions. Examples of the original and resampled surfaces are given in figure 4-13. Only small sections of surface samples are shown as the higher density plots are difficult to view printed. The fractal dimension was computed as previously described in section 4.2.1.1. After finding the fractal dimension for a particular radial direction in the APSD, we perform one additional computation to find *C*. The intercept $\Omega$ of the radial slice of the APSD shown (figure 4-3) is measured and used to compute *C* from equation 4.39

$$C = (10^{\Omega}) \cdot (\Delta w^4) \tag{4.40}$$

For a simulated isotropic surface generated with fractal dimension D=2.2, C=1 and a spatial resolution of 1mm/sample, the measured amplitude coefficients for the resampled surfaces of 2mm/sample and 4mm/sample were $C_2$=.995±.073 and $C_4$=1.02±.11 respectively. The measured amplitude coefficient of the original surface $C_o$, had a mean value of 1.007 and standard deviation of ±.006 over all 16 directions. Compared as a percentage of $C_o$ the amplitude coefficients of the resampled surfaces were $C_2$=(98.1%±7.1%)$C_o$, and

$C_4$=(102%±10.9%)$C_o$. Repeating the process for an isotropic surface generated with D=2.2 and C=.01 we find relative values for the resampled surfaces of $C_2$=(102%±8.1%)$C_o$, and $C_4$=(108%±9.7%)$C_o$. The amplitude coefficients for the second case are plotted in polar coordinates in figure 4-14.

**Figure 4-13.** Original and Sampled Surfaces. All dimensions in mm.

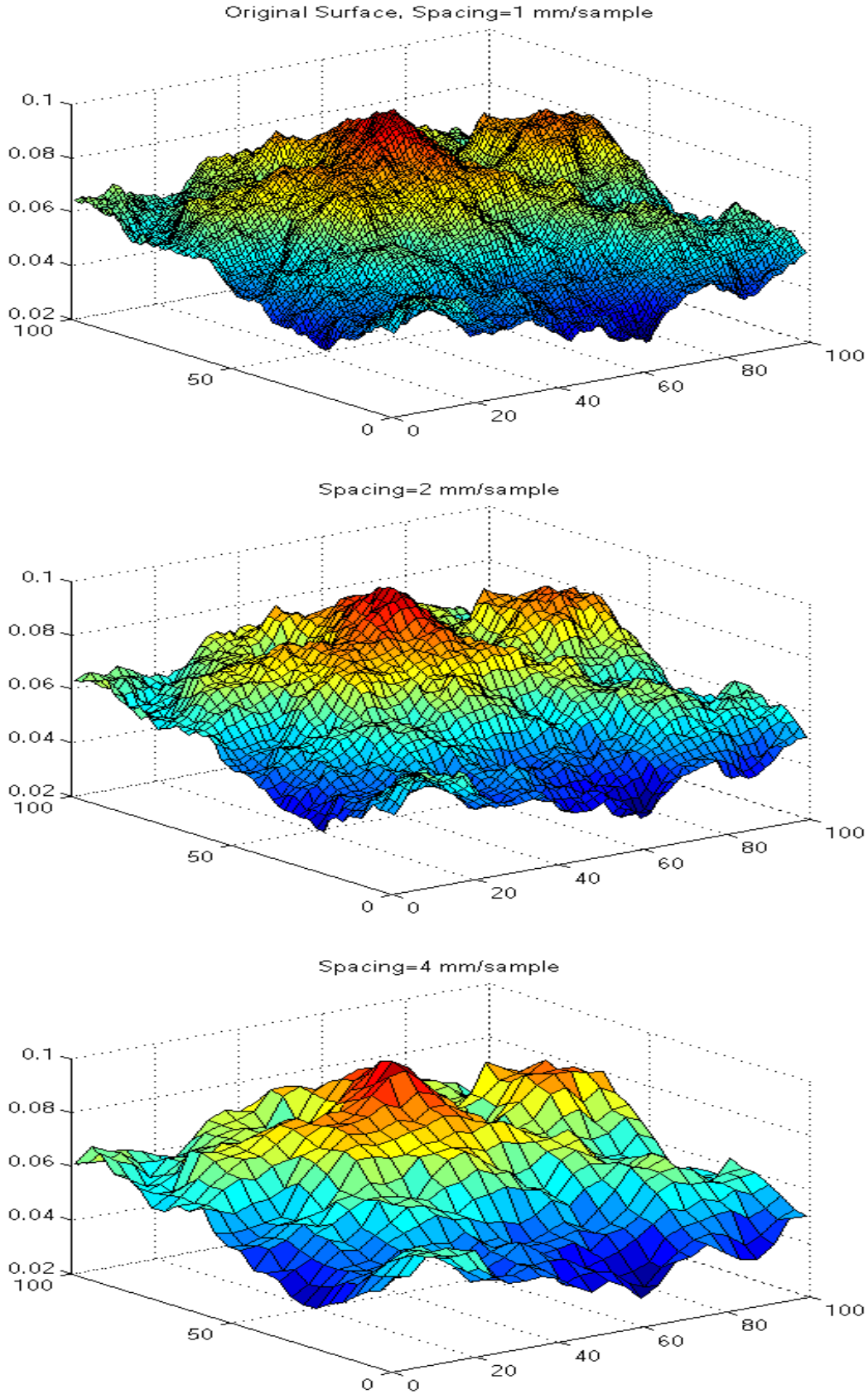

**Figure 4-14.** Amplitude Coefficients of Original and Sampled Surfaces

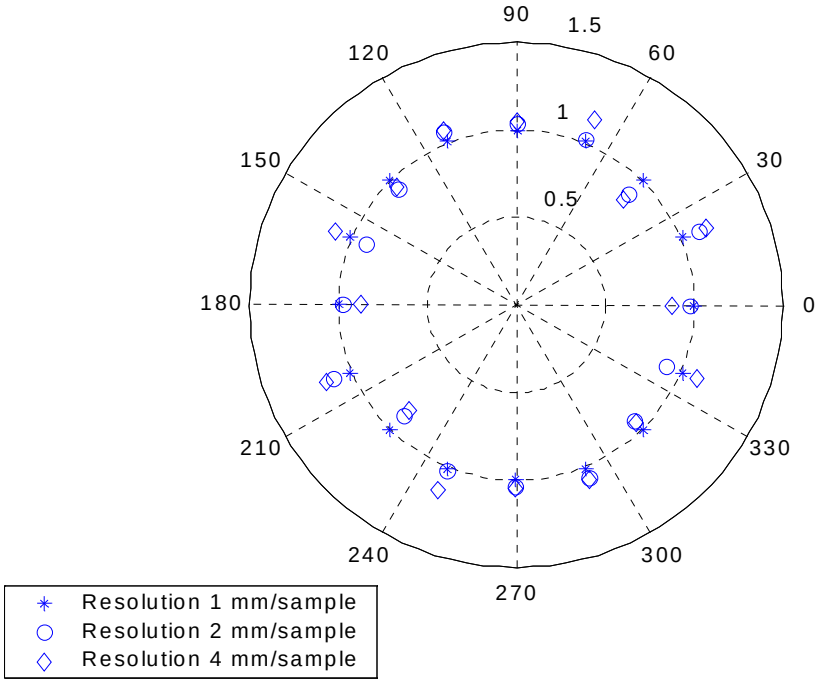


## 4.4.3 Fractal Description of Anisotropic Surfaces

At this point we try to put everything in this chapter together to describe fractal anisotropic surfaces with parameters that are invariant with the sampling resolution. We illustrated measuring the fractal dimension as a function of angle for both isotropic and anisotropic surfaces (figure 4-4 and figure 4-5). The process for generating a two-dimensional isotropic fractal Brownian motion surface based on a power law was discussed in section 4.4.1. In section 4.4.2 altering the power law in equation 4.25 to take into account shifting power spectrums from changing sampling resolutions kept measured fractal parameters constant and enabled us to measure the amplitude coefficient. We add one more idea alluded to but not explicitly stated in the previous section that is needed to complete the characterization.

In figure 4-14 the amplitude coefficient *C* is plotted as a function of angle in polar coordinates for an isotropic surface. Similar to how the fractal dimension *D* was measured and visualized in figure 4-5 for the anisotropic surface, we can also measure anisotropic values of *C* and plot them on a Rose plot as a function of angle. We integrate this with the other concepts to characterize an anisotropic fractal surface. A surface is characterized by taking its two-dimensional Fourier transform and computing the two fractal parameters as

a function of angle, $C(\theta)$ and $D(\theta)$, and using the sampling theorem to correct for power spectral shifting due to different sampling resolutions. Once $C$ and $D$ are characterized as a function of angle we can systhesize new surfaces with the same directional fractal properties as the original measured surface or define new fractal properties for the surface.

#### 4.4.3.1 Synthesizing Anisotropic Fractal Surfaces

With our approach to characterizing anisotropic surfaces stated, we can now apply it to fractal surface synthesis. The procedures to generate Fourier coefficients based on a power law and invert them to form a surface were described in section 4.4.1. Our power function of equation 4.38 is now made capable of describing anisotropic surfaces by replacing the $C$ and $D$ constants with amplitude and fractal dimension functions of angle, $C(\theta)$ and $D(\theta)$

$$P(\boldsymbol{k}) = \frac{1}{\Delta w^2 \Delta q^2} \frac{C(\theta)}{\|\boldsymbol{k}\|^{8-2D(\theta)}} \tag{4.41}$$

Each time we form a coefficient its frequency coordinates are used to compute $\theta$. Then $C$ and $D$ is found for that direction. For the surfaces the we systhesize we have set the sampling resolutions to be the same in both directions, which simplifies the power law of equation 4.41 to

$$P(\boldsymbol{k}) = \frac{1}{\Delta w^4} \frac{C(\theta)}{\|\boldsymbol{k}\|^{8-2D(\theta)}} \tag{4.42}$$

As an example we take a look at a surface generated with a severe anisotropy. A surface was generated so that its power function had a narrow band with fractal a dimension of 2.25 and amplitude coefficient of .1, while the rest of the spectra has a fractal dimension of 2.4 and amplitude coefficient of .008. The APSD is shown in figure 4-15. The surface generated is shown in figure 4-16. The longer wavelengths tend of the lower fractal dimension anisotropy can be viewed along the $y$ axis. The higher dimension, but lower amplitude surface roughness is spread out all over the surface in almost all directions as expected. This surface roughness can be seen in the close-up of the plateau of the surface in figure 4-17.

**Figure 4-15.** APSD of Anisotropic Surface

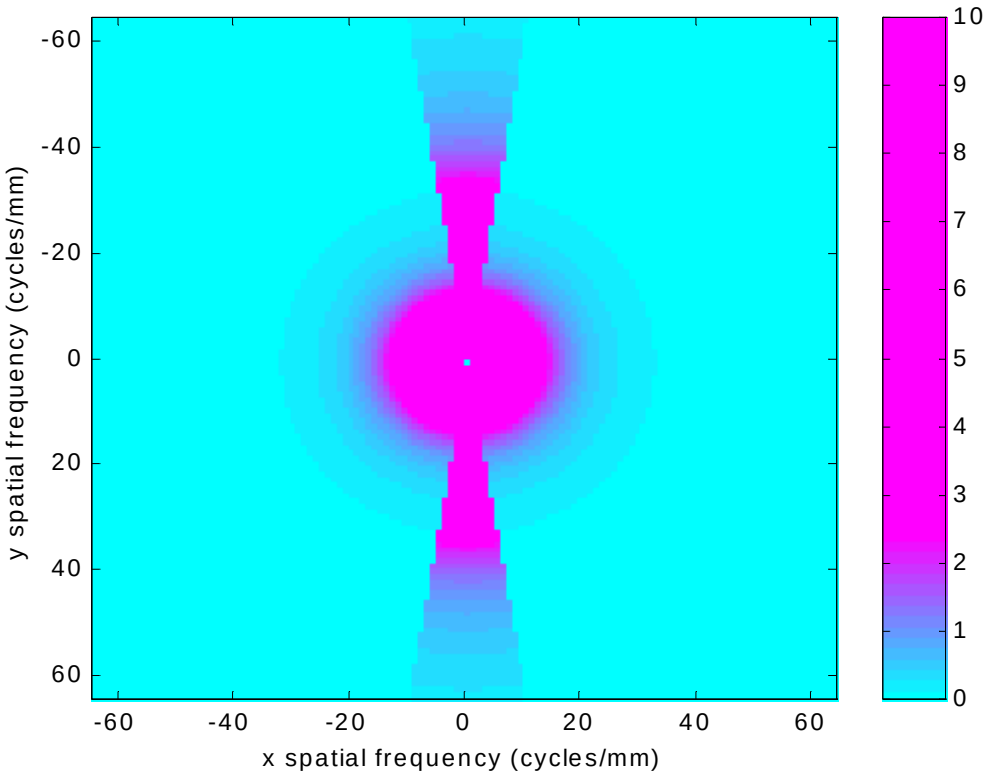


**Figure 4-16.** Very Anisotropic Surface

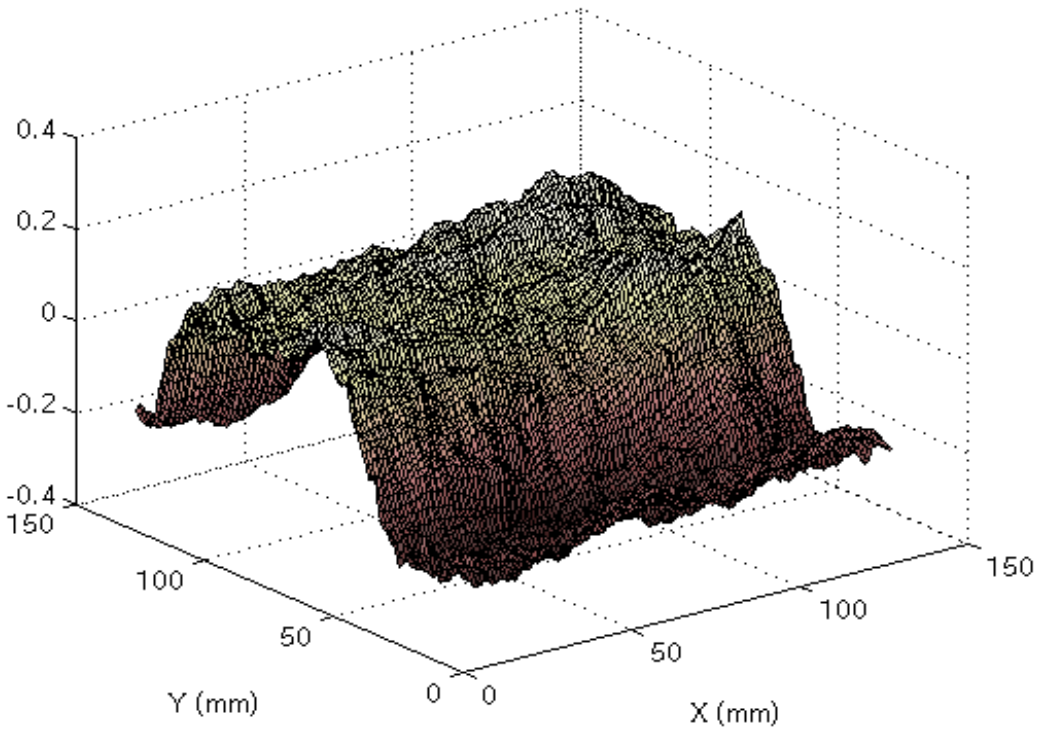

**Figure 4-17.** Close up section of figure 4-16

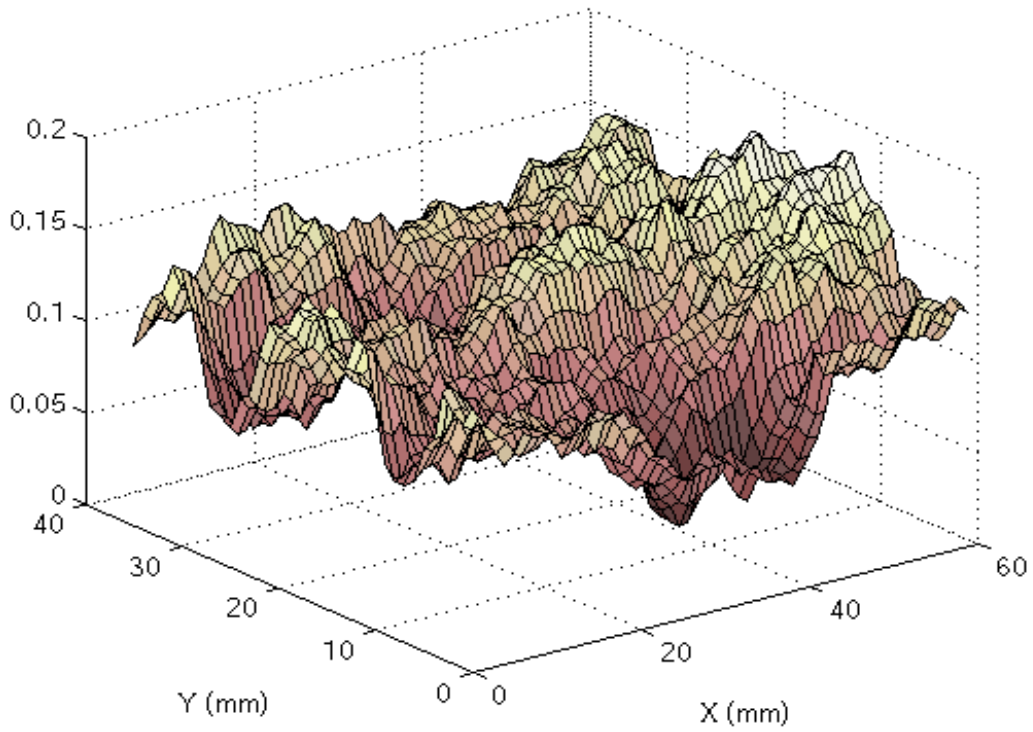


We simulated anisotropic surfaces using the spectral methods described in section 4.4.1 to check that equation 4.39 will predict the same amplitude coefficient for a surface sampled at various resolutions. A surface of 1024 by 1024 points was generated using equation 4.42 as the fBm power law at a spatial resolution of 1 mm/sample. The fractal dimension and amplitude coefficient functions were defined as

$$\begin{aligned} D &= 2.4, 0 \le \theta \le \pi/4, 0 \le \theta \le -\pi/4 \\ D &= 2.1, \pi/4 < \theta < \pi/2, -\pi/4 < \theta < -\pi/2 \\ C &= 0.04, 0 \le \theta \le \pi/4, 0 \le \theta \le -\pi/4 \\ C &= 0.01, \pi/4 < \theta < \pi/2, -\pi/4 < \theta < -\pi/2 \end{aligned} \tag{4.43}$$

This surface was then sampled at a lower resolution of 2 mm/sample. Compared as a percentage of the original surface amplitude coefficients $C_o$, the amplitude coefficients of the resampled surface was $C_2$=(99.2%±9.4%)$C_o$. The amplitude coefficients for the original are plotted in polar coordinates in figure 4-18. The measured fractal dimension of the resampled surface compared as a percentage of the original is $D_2$=(99.8%±.6%)$D_o$. The vari-

ation of the resampled surface dimension is much smaller than the variation of the amplitude coefficient.

**Figure 4-18.** Rose Plots of $C_o$ for Anisotropic Surface.

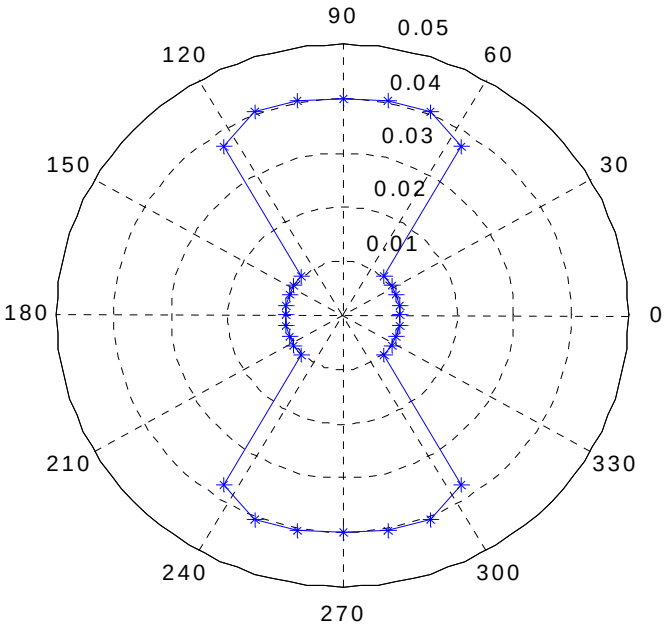


# 4.5 Haptic Display of Synthetic, Fractal, Two-Dimensional, Surfaces

Once the surfaces are generated it would be instructive to haptically display them on a force feedback device. Particularly it would be interesting to see if anisotropic behavior of surfaces can be detected through touch. Preliminary experimentation with haptically displaying synthetic, fractal, two-dimensional surfaces on a three degree of freedom force feedback device was completed.

## 4.5.1 Haptic Display Setup Description

The surfaces were haptically displayed using a PHANToM Desktop® from SensAble Technologies (see figure 4-19). The device can display forces in three directions to the user at its pen end-effector. A dual 900 MHz Pentium processor computer operating Windows 2000 was used to control the PHANToM. A visual representation of the surface and the

user's proxy point was shown on the monitor. A servo loop of 1 KHz was achieved with this setup.

Interaction forces displayed to the user was computed by the Ghost v3.1 software API. A triangle mesh of the fractal surface height maps had to be formed to render the surfaces with Ghost. The computer setup described running Ghost could render surfaces of 128 points by 128 points. Surfaces with more points would overwhelm and stop operation of the system.

**Figure 4-19.** PHANToM® setup

### 4.5.2 Qualitative Results

Compared to the dynamic contact model used in chapter five, the surfaces felt rubbery when rendered using the Ghost API. The surface spacing resolution at 0.078mm was also somewhat low, but could not be avoided because of the computational constraints of the setup. Still the surfaces could be explored and felt textured. This was adequate to conduct preliminary explorations with detecting surface anisotropies.

Fractal surfaces of dimension 2.2 with a narrow, 1/16π wide anisotropy in the APSD were synthesized (see figure 4-20). The anisotropy had an amplitude coefficient of 5 compared to the rest of the surface at 0.2. The surfaces were fit with a fourth order polynomial surface to remove the low frequency form. The surface amplitudes had maximum

undulations of ±5mm. When haptically displayed, the anisotropic behavior of the surfaces was felt pronouncedly when exploring in the direction of the anisotropy. In other directions the surface was far less rough, while in the perpendicular direction to the anisotropy it was far smoother.

**Figure 4-20.** APSD of Anisotropic Surface Displayed

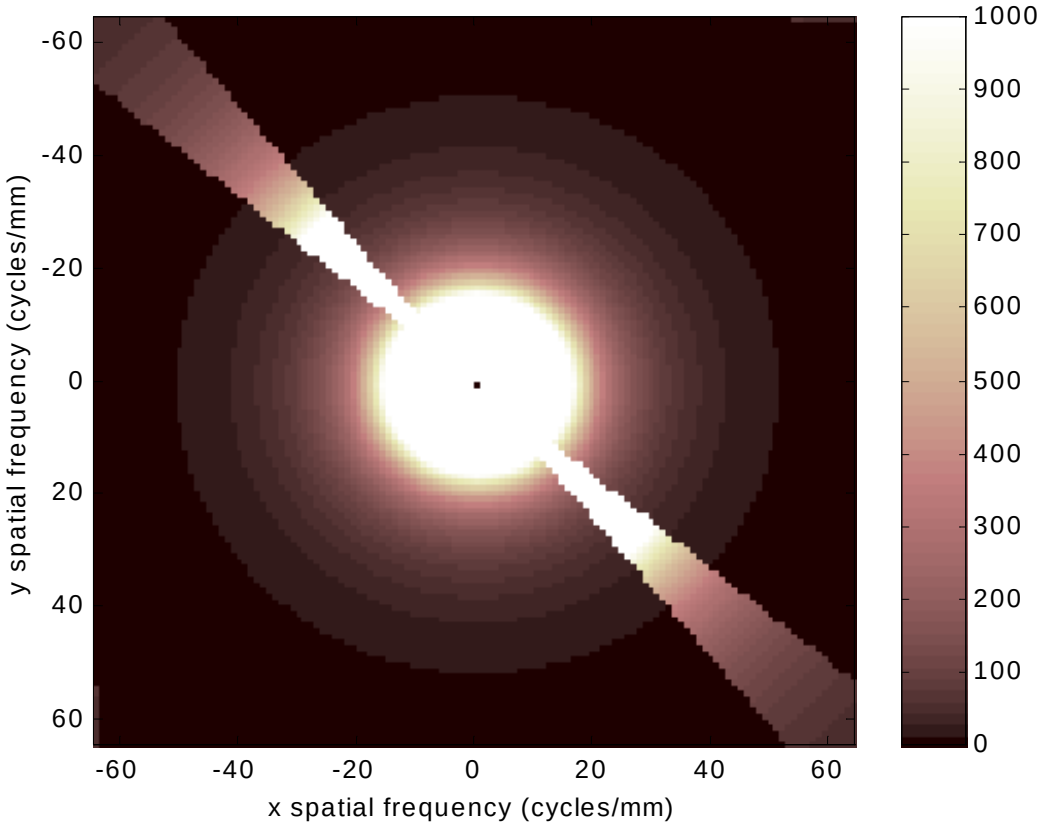


While these are positive qualitative results, further refinement with the contact modeling needs to be done before perception experimentation can begin. A quantitative perception study using one dimensional fractal profiles is described in the next chapter to relate fractal parameters to human roughness perception.

# 5 Roughness Perception of Fractal Surfaces

One of our goals in synthesizing fractal surfaces is to be able to use them to conduct roughness perception experiments. Surface profiles were generated by the fractal algorithm described in chapter 3 and were haptically rendered on a force feedback joystick. Subjects were asked to use the joystick to explore pairs of surfaces and report to the experimenter which of the surfaces they felt was rougher. Surfaces were characterized by their root mean square (RMS) amplitude and their fractal dimension. The most important factor affecting the perceived roughness of the fractal surfaces was the RMS amplitude of the surface. When comparing surfaces of fractal dimension 1.2-1.35 it was found that the fractal dimension was negatively correlated with perceived roughness.

## 5.1 Introduction

The perception of texture is an important means by which humans identify surfaces around them. In field geology, scientists use texture to help identify rocks and determine their history (e.g., the amount of weathering they have been exposed to). The work presented in this chapter is part of an effort to allow field geologists to explore remote planetary surfaces, displayed as virtual surfaces in an immersive haptic and visual display. An important component of the perceived texture of rock surfaces is their roughness, and the focus of this chapter is the display of roughness using models that produce surface profiles similar to those found in nature.

Previously in chapter 3 we identified two parameters, the amplitude coefficient and fractal dimension, that are useful for generating synthetic surfaces similar to those measured using an optical profilometer on rock surfaces. Because the RMS amplitude is commonly used in surface metrology, has a physical meaning, and can be related to the amplitude coefficient (equation 3.9 on page 30) we use it as our second parameter to char-

acterize the surfaces. In this chapter experiments to determine how human subjects relate perceived roughness to variations in these two parameters when interacting with the surfaces via a haptic display are described.

## 5.2 Previous Work

Earlier surface roughness perception experiments had subjects touch metal gratings consisting of rectangular grooves [72][73]. These studies showed that the dominant factor in determining perceived roughness was the groove width. More recent work by Lederman and Klatzky has argued for the viability of using a probe to encode vibration information to discriminate roughness [74][75]. During these experiments subjects used a probe to explore surfaces made up of a pseudo-random pattern of raised dots. It was found that the perceived roughness of the patterns when using a probe or a finger increased with increased interelement spacing until reaching a peak and then decreased [74].

A common feature of these experiments is that they use artificially constructed surfaces of predetermined heights. While the gratings are more deterministic than the spatially randomized raised dots, the dot patterns still have only two heights: the height of the dot and the flat surface it is resting on.

Other work has examined the use of stochastic methods for texture display [76][77]. In the present case, we are interested in the perceived roughness of irregular virtual surfaces whose geometric properties (e.g., peak heights and spatial intensity) match those found on rocks.

The work in this thesis used the fractal technique described in chapter 3 to simulate the surface profiles because it was found it to favorably mimic rock surface profiles when compared in terms of standard metrics from surface metrology.

## 5.3 Experimental Setup

Fractal simulated surface profiles were haptically rendered on an Immersion Impulse Engine 2000 force feedback joystick. Fourteen subjects, eleven male and three female, from ages 21 to 34, participated in the experiment. Subjects were naive to the purpose of the experiment. All subjects had at least minimal experience using haptic devices. Subjects were asked to use the joystick to explore pairs of surfaces and report to the experimenter

which one they felt was rougher, surface one or surface two. One surface was displayed at a time. Subjects controlled which surface was displayed by clicking the joystick trigger. Subjects were allowed to switch between surfaces as often as they desired and to explore surfaces as long as they desired. A computer screen displayed the subject's approximate position in the virtual world (figure 5-1). The proxy point represents the end of the user's virtual stylus used to touch the virtual surface. The fractal surface is not graphically displayed to the user so that their perception of the surface roughness is not visually influenced. A reference line through the mean value of the reference is used to indicate to the subject the approximate location of the surface.

Sixteen pairs of surfaces were given to subjects in random order. Assignment of surfaces as surface one or two was also randomized. Typically subjects spent fifteen to twenty minutes exploring surfaces, with the shortest time being approximately ten minutes and the longest being approximately thirty-five minutes.

**Figure 5-1.** Subject Interaction Screen

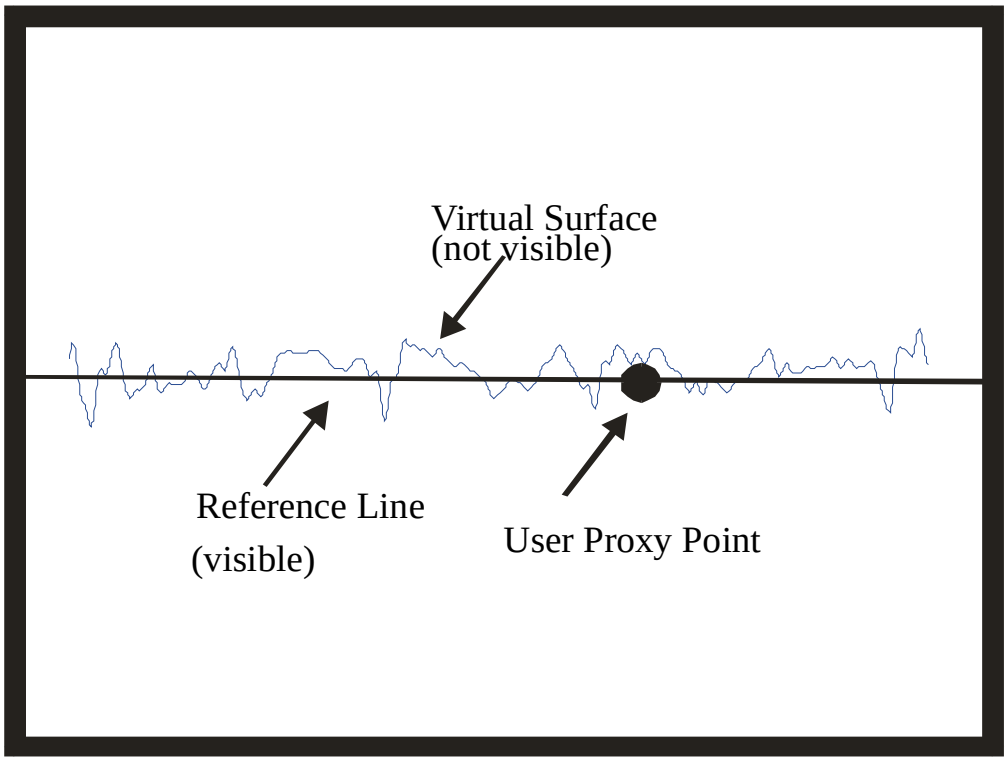


Two different reference surfaces were compared to eight surfaces to form the sixteen trial pairs. Each reference surface was compared to surfaces with a combination of

lesser, equal, and greater fractal dimension and RMS amplitude. Figure 5-2 demonstrates the surface group pairings. Reference surface one is compared against each of the surfaces of group one while reference surface two is compared against the group two surfaces.

The surfaces used in the experiment were generated in 20 mm lengths and patched together to form 80 mm lengths. Each length was offset to meet that last one so that no discontinuity between lengths could be detected. Surface profiles were resampled to a resolution of 0.1545 mm/sample, five times the encoder resolution of the joystick[1]. This reduction in memory usage allowed longer length segments to be used. Empirically this was found to be the lowest resolution that could be displayed before the feel of the synthesized profile changed noticeably. To illustrate why this happens the physical performance capabilities of the joystick need to be examined.

The joystick can display forces of up to 8.9 N with a bandwidth of 120 Hz with each axis [78]. A typical minimum user lateral exploration speed is approximately 20 mm/s. The maximum achievable spatial frequency that can be displayed at this speed is found by dividing the bandwidth by the exploration speed. For a exploration speed of 20mm/s this spatial frequency is 6 Hz. Inverting this shows that the maximum displayable spatial resolution without Nyquist considerations is 0.1667 mm/sample while laterally exploring at 20 mm/s. This is just below the synthesized profile resolution of 0.1545 mm/sample. Increasing the resolution of the sample makes does not change the feel of the surface while exploring because the it is already above the spatial resolution capable of display with the 120 Hz mechanical bandwidth of the force feedback joystick.

1. The joystick used in the experiments had an encoder resolution of .0309 mm according to the source code provided by Immersion as compared to the .0203 mm resolution listed on the current website as of October 12, 2000.

**Figure 5-2.** Surface Pairings

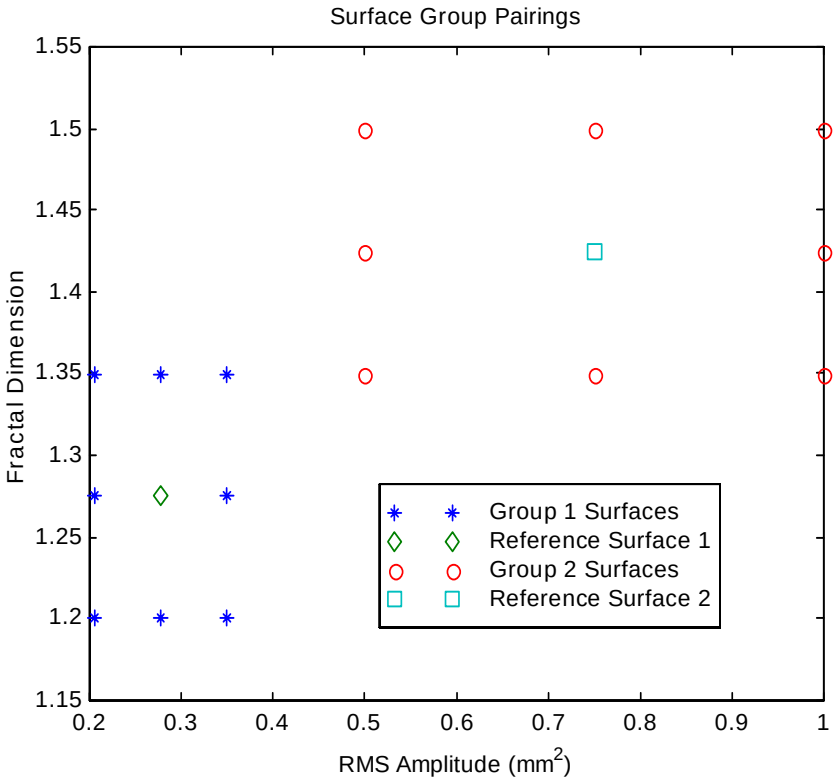


# 5.4 Contact Model

Subjects explore the virtual surfaces through the force feedback joystick. Using a dynamic model of stylus to surface contact, the forces are displayed to a user resulting from interaction with the surface profile data. Previously we had begun with an initial model similar to the Sandpaper system [79] that used tangential force feedback based on the change in heights with a vertical restoring force based on the penetration depth into the profile. In a previous project we found this model to be unsatisfactory when traversing surface profiles taken from rocks [32]. We therefore implemented a dynamic model (figure 5-3) that represents the normal and tangential forces at the stylus-surface contact and accounts for the possibility of users breaking contact and bouncing or skipping over the valleys of the surface. This model was used to display rock surfaces collected by a laser displacement sensor to planetary geologists during a NASA-Ames field experiment in February 1999 [32]. For the experiment described in this paper we used this model to haptically display the synthesized fractal profiles.

**Figure 5-3.** Model Schematic

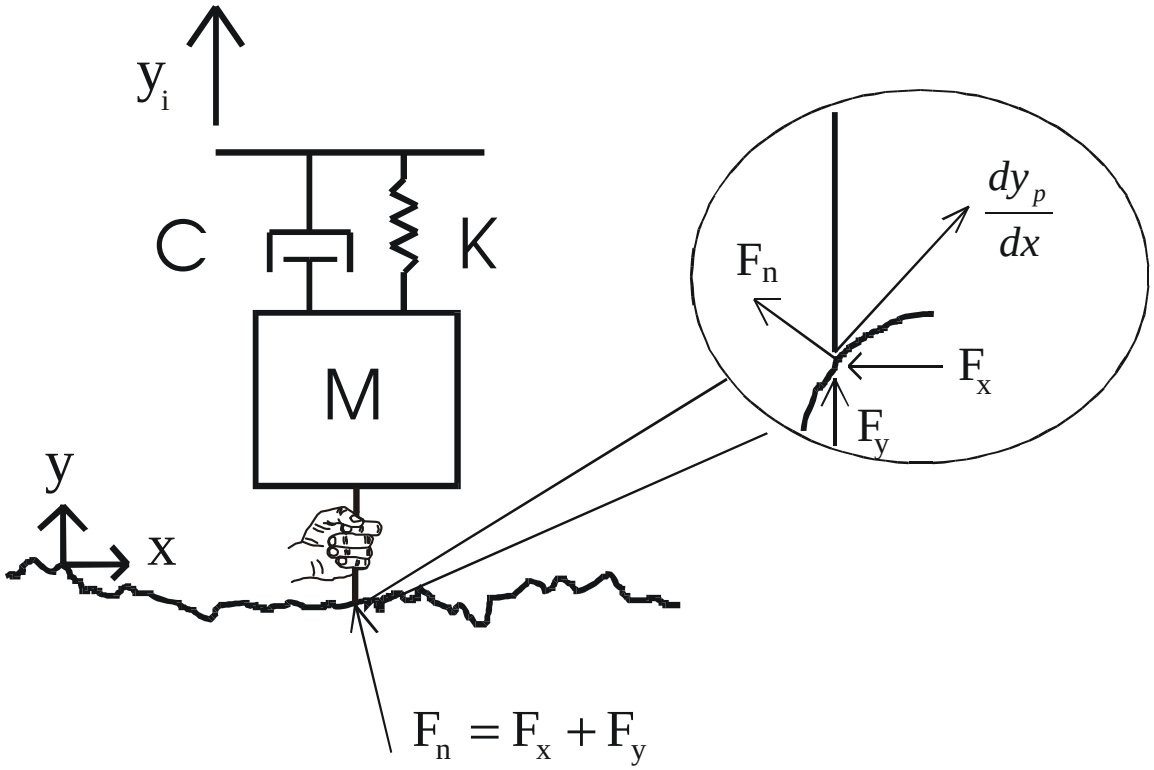


First a height profile as a function of position, $y_p(x)$, is generated by our fractal algorithm. The stylus is then modeled as a mass, spring, damper system connected to the vertical input of the user's haptic interface device, $y_i$. The horizontal position of the stylus is directly coupled to the horizontal position of the interface. While in contact with the surface the stylus dynamics are computed by

(5.1)

The contact point of the stylus against the surface is modeled as a frictionless contact point. As illustrated by the magnified portion of figure 5-3, the normal force $F_n$ is perpendicular to the tangent of the contact point. It is this reaction force that is displayed to the user. The tangent is computed by taking the derivative of the surface with respect to the x coordinate system, $dy_p/dx$. In our application this derivative is pre-computed, as we know the surface profile a priori.

The normal force is the sum of x and y component forces.

(5.2)

The y component represents the vertical reaction force. The x component represents the horizontal reaction force

$$F_x = F_y\left(\frac{dy_p}{dx}\right) \tag{5.3}$$

If the user's position $y_i$ is ever greater than the profile height $y_p$, contact is broken with the surface and contact forces are set to zero. This allows the user to bounce off and back onto the surface, especially while moving fast.

Because the subject can explore the surface freely, exact force levels displayed to the subject are dependent on how they chose to explore the surface, e.g. depth of penetration into the virtual surface, and speed of exploration.

### 5.4.1 Model Parameters

For our application the model parameters were tuned for feel to give our virtual stylus parameters of $K$=1.28 N/mm, $M$=1.85x10$^{-6}$g and $C$=4.6x10$^{-5}$ N/(mm/s). Examining the mass and damping parameters shows that these elements are much smaller relative to the spring element. It may seem that the virtual stylus is basically just a virtual spring. However when tuning the model parameters, interaction with the surface felt more realistic with the small amount of mass and damping as opposed to when these elements were set to zero. Simulations of the computed force of a model with only the spring force were compared to the complete model to investigate the parameter effects.

A fractal profile used in the subject perception experiments was selected for the model force simulations. The profile shown in figure 5-4 is 27 mm long and has a resolution of 0.1545 mm/sample.

**Figure 5-4.** Fractal Profile Used for Model Force Comparison Simulations

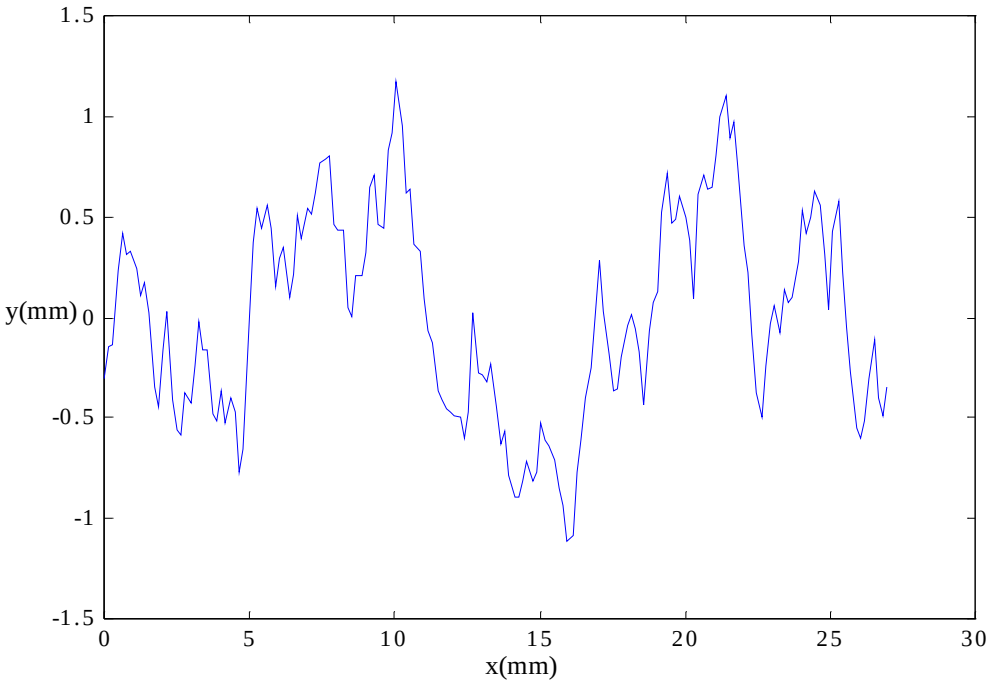


The profile of figure 5-4 was used as the input of a Matlab model of the virtual stylus. The model computed the $F_y$ reaction forces based on the computer control code. The stylus penetration depth was assumed to be at the minimum point of the profile and held constant. In practice the user sets this depth while interacting with the surface, adjusting their depth as they react to the profile. The user's lateral exploration speed was also held constant, but the value of the speed was varied during different simulations. In the first simulation a user exploration speed of 20 mm/s was set as a reasonable minimum exploration speed. In figure 5-5 the $F_y$ reaction force as a function of time is plotted out for the two conditions, the virtual stylus model force, and the spring force only. Examining the plot shows no differences between the two plots. In this case it appears that there is very little difference between modeling with mass and damping, and modeling with only the spring.

**Figure 5-5.** Force Profiles with exploration speed of 20 mm/s, M=1.85x10$^{-6}$g,

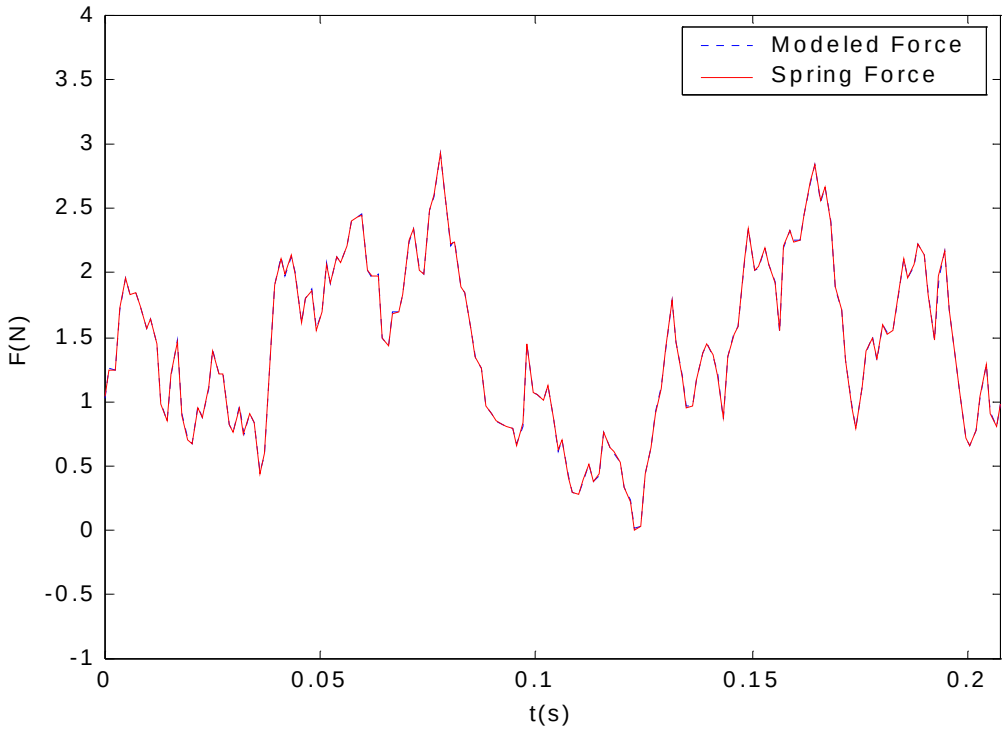


An exploration speed of 20 mm/s is quite slow. In reality most subjects explored surfaces at an estimated speed of 120 mm/s. This estimation was based on observations of subjects and some simple timing experiments. In figure 5-6 the difference between the spring only force and the modeled force is much more evident. The spring force has not changed due to the exploration speed. The modeled force has much higher and sharper force peaks at each of the profile peaks. This can be attributed to the mass term which is multiplied by the second time derivative of the profile, $M\ddot{y}_p$. The mass is constrained to the surface, so it's *y* direction accelerations are directly dependent on the lateral exploration speed.

**Figure 5-6.** Force Profiles with exploration speed of 120mm/s, M=1.85x10$^{-6}$g

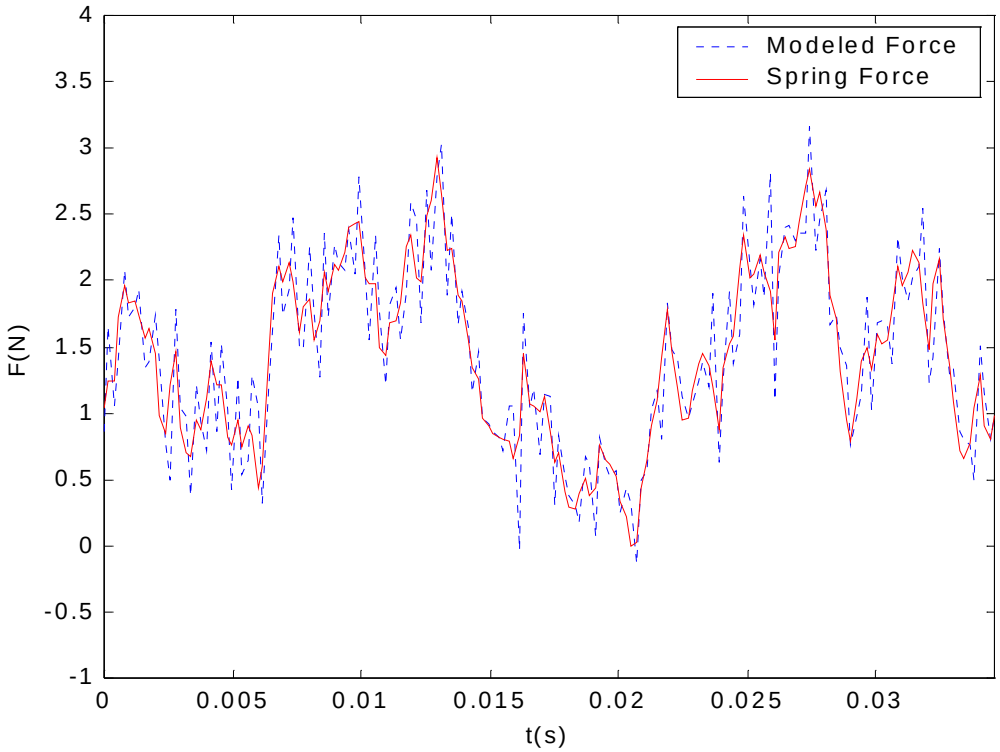


In practice it was found that although a small amount of mass improved the feel of the haptic display of the virtual stylus, very little added extra mass compromised the simulation, driving it unstable. To examine this the simulation was ran again with an exploration speed of 120 mm/s and the mass doubled to 3.71x10$^{-5}$ g. In figure 5-7 the modeled force peaks are up to 1.5 N over the spring force alone. With very little extra mass the virtual stylus model is beginning to command forces approaching the 8.9 N saturation limit of the joystick.

**Figure 5-7.** Force Profiles with exploration speed of 120mm/s, M=3.706x10$^{-5}$g

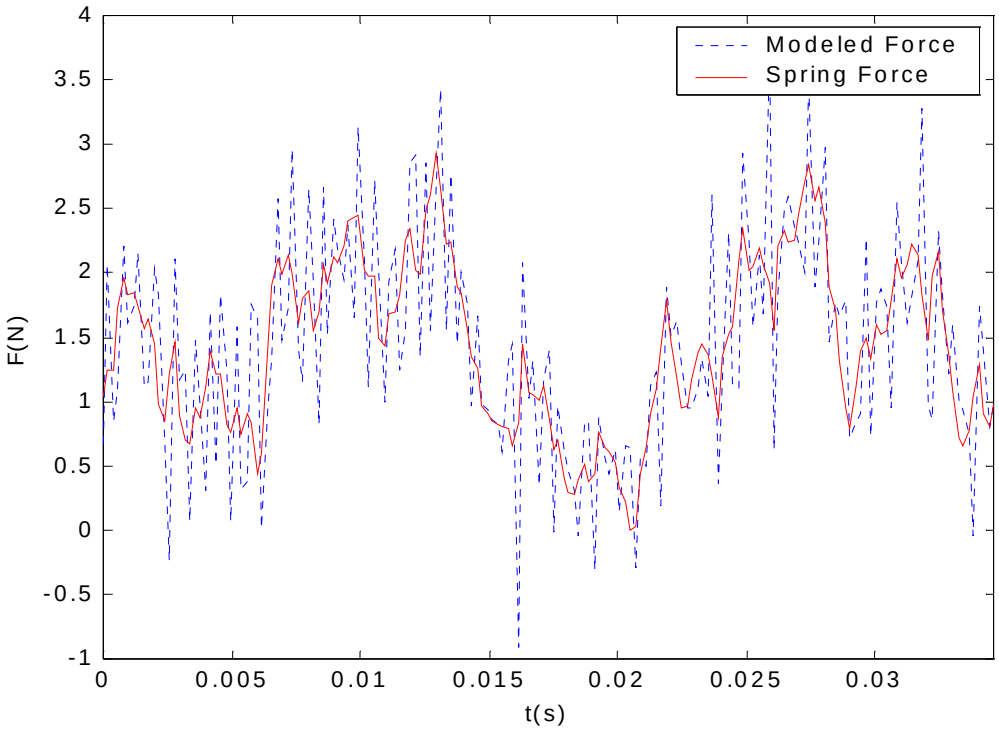


### 5.4.2 Qualitative Model Feel

It has been reported that surfaces modeled without friction feel glassy [80]. While we did not use friction in this model, during the experiment, none of the subjects commented that surface felt glassy or slippery. There is a small amount of friction inherent to the force feedback device we used. The Impulse Engine 2000 specifications report a maximum backdrive friction of 0.14 N [78]. It's possible that a combination of factors including the tangential forces displayed due to the irregularity of the surface, the backdrive friction, and device inertia eliminates any slippery feel.

Qualitatively, interactions with fractal surfaces with smaller RMS amplitudes (.2mm-.27mm) using this model feel like using a stylus to stroke sandstone, while interacting with fractal surfaces with larger RMS amplitudes (>.5mm) feels like stroking a weathered conglomerate rock or broken concrete surface.

## 5.5 Data and Analysis

Figures 5-8 and 5-9 show the percentage of subjects perceiving a surface rougher than a reference surface. Data points are plotted along the x and y axis by their fractal dimension

and RMS amplitude. The center spot labeled *ref* represents a surface (of fractal dimension 1.275, RMS amplitude 0.278mm) that was compared to other eight surfaces. For each of the eight comparison surfaces, the percentage of subjects who reported that surface as rougher than the center point surface is plotted along the z-axis. For example in figure 5-8, 71% of subjects reported that the surface of fractal dimension 1.35, RMS amplitude 0.350mm, was rougher than the reference surface. The reference surface response is set to 50%. This would represent the case of comparing the reference surface to itself, although for fatigue considerations this case was not actually presented to the subjects.

Looking at figures 5-8 and 5-9 across the RMS amplitude axis, both cases show that surfaces with a higher RMS amplitude are perceived as rougher. For all cases of different RMS amplitudes between 71.4% to 100% of subjects reported the surface with the higher amplitude to be rougher. The mean percentage of subjects reporting that a surface with a higher amplitude to be rougher was 91.7% with a standard deviation of ±8.5% for both cases.

**Figure 5-8.** Perceived Roughness, Reference surface D=1.275, RMS amplitude .278mm

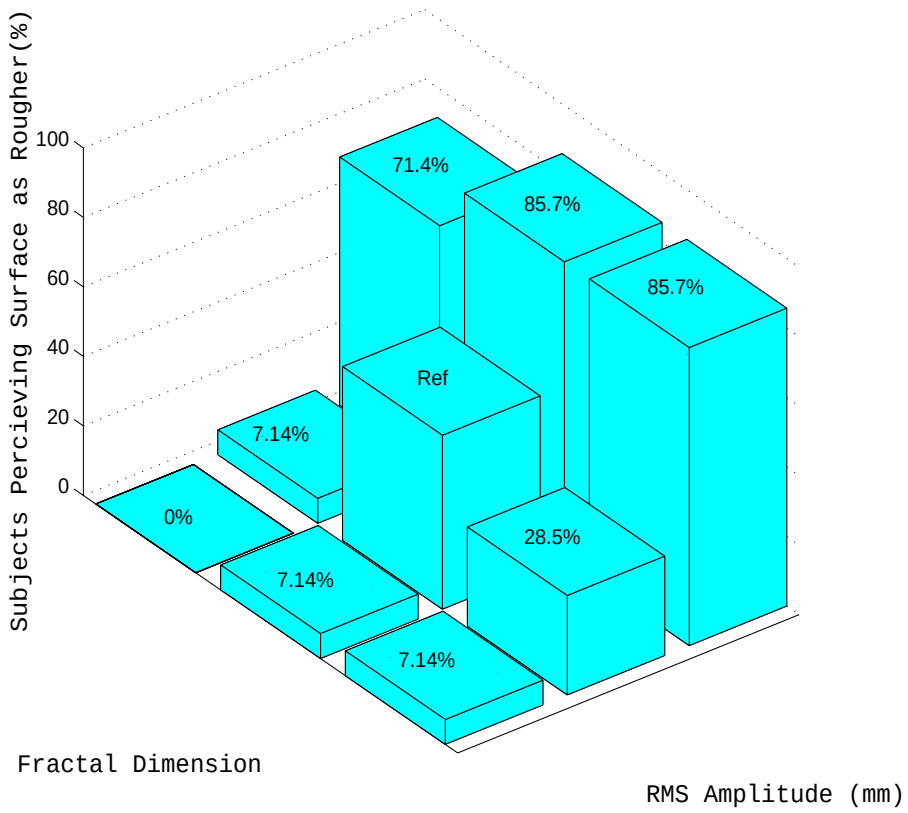

**Figure 5-9.** Perceived Roughness, Reference surface D=1.425, RMS amplitude .75mm

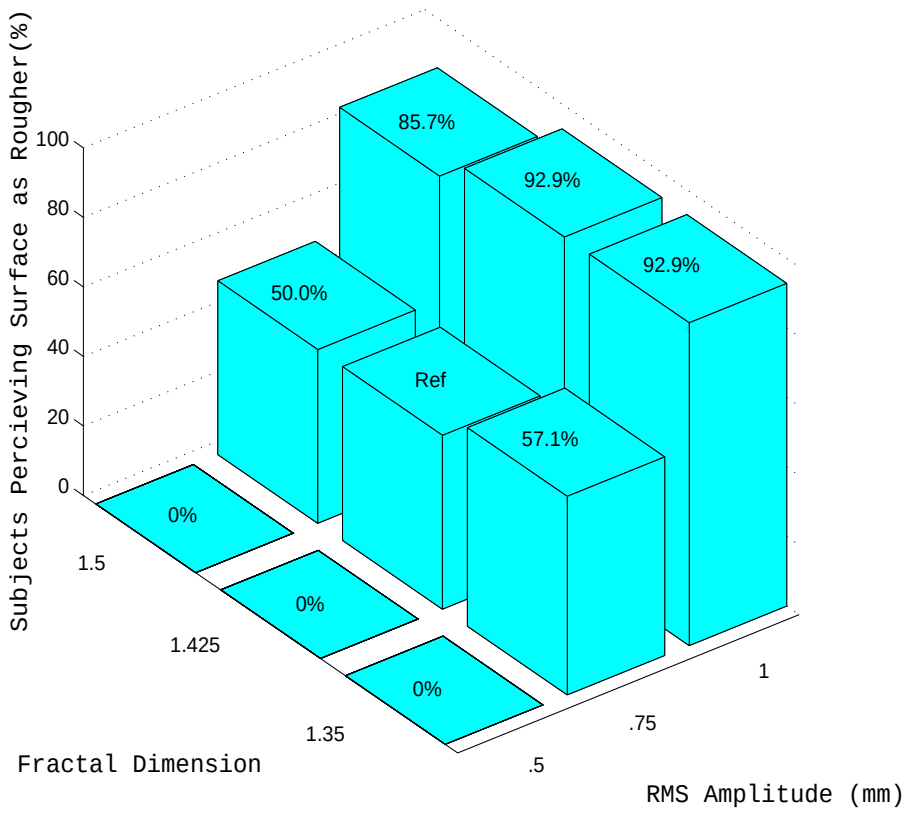


It is much more difficult to discern any trends in roughness perception due to fractal dimension by only examining the data plots. To check for the statistical significance of the dimension and amplitude parameters we performed a logistic regression analysis. A logistical regression analysis was chosen because subject responses are binary. After a subject indicates which surface they believe is more rough, the result is recorded as positive or negative depending if they chose the test surface (positive) or the reference surface (negative).

For each case we fitted the subject responses to a multiple logistic regression model of the form [81][82]

$$g(x) = \theta + \beta_1 x_1 + \beta_2 x_2 + \ldots + \beta_p x_p \tag{5.4}$$

$$P(Y = 1|x) = \frac{e^{g(x)}}{1 + e^{g(x)}}$$

using a software statistical analysis package [83]. Each coefficient $\beta_i$ of the model represents a different experimental variable: fractal dimension, RMS amplitude, or a subject variable. After computing the coefficients and their respective estimated standard errors, we performed the Wald test for logistic regression models to check for statistical significance [81]. The Wald test is conducted by first computing the univariate Wald statistic $W = \beta_i / (SE(\beta_i))$, where $SE(\beta_i)$ is the standard error of the *i*th coefficient. Next the two tailed p-value of the Wald statistic is computed from the Chi-square on one degree of freedom distribution with a significance of $\alpha = .05$. For any p-value less than .05 we consider the variable to be statistically significant.

The p-values for the coefficients are presented in tables 5-1 and 5-2. As expected for both cases the p-value of the RMS amplitude is well below 0.05, indicating that this variable is statistically significant. As the Wald statistic is positive in both cases, the likelihood of perceiving one surface rougher than the reference surface increases with increasing amplitude. For the second case of higher fractal dimensions, 1.35 to 1.5, the p-value for fractal dimension is 0.446. This indicates that this variable was not a significant factor in perceiving surface roughness when comparing surfaces of fractal dimension greater than 1.35. Interestingly in the first case when comparing surfaces of lower fractal dimension, 1.2 to 1.35, the fractal dimension parameter has a p-value of .0128 and a negative Wald statistic. With this p-value this variable does meet our test for statistical significance. This suggests that when comparing fractal surfaces with dimensions between 1.2 and 1.35, the surface with the lower fractal dimension contributes to it being perceived as rougher.

This dichotomy between the higher and lower fractal dimension cases might exist because as the fractal dimension decreases the surface becomes more coarse, enforcing the perception of roughness. The difference between two surfaces with higher fractal dimensions may not be noticeable to a person. This is supported by figure 5-9. Examining the two trials where the RMS amplitude is the same, the percentage of subjects perceiving the surface of dimension 1.5 and the surface of dimension 1.35 as more rough than the reference surface of dimension 1.425, is 50% and 57%, respectively. This indicates a random preference. Subjects reported that these two cases were difficult to distinguish.

**Table 5-1.** P-Values for Perceived Roughness when Comparing to Reference Surface 1: D=1.275, RMS Amplitude=.2781mm

| Coefficient Name | Wald Statistic | p-value |
|---|---|---|
| Fractal Dimension | -2.48803 | .0128 |
| RMS Amplitude | 4.47037 | 7.8085e-6 |
| Subject 1 | -1.027 | .3044 |
| Subject 2 | -1.027 | .3044 |
| Subject 3 | 1.027 | .3044 |
| Subject 4 | -1.5e-16 | 1 |
| Subject 5 | -.051 | .9593 |
| Subject 6 | -1.815 | .0696 |
| Subject 7 | -1.027 | .3044 |
| Subject 8 | -1.027 | .3044 |
| Subject 9 | -1.815 | .0696 |
| Subject 10 | -1.027 | .3044 |
| Subject 11 | -1.815 | .0696 |
| Subject 12 | 1.027 | .3044 |
| Subject 13 | -1.027 | .3044 |

**Table 5-2.** P-Values for Perceived Roughness when Comparing to Reference Surface 2: D=1.425, RMS Amplitude=.75mm

| Coefficient Name | Wald Statistic | p-value |
|---|---|---|
| Fractal Dimension | -.76212 | .446 |
| RMS Amplitude | 4.9217 | 8.581e-7 |
| Subject 1 | -6.63e-6 | 1 |
| Subject 2 | -1.734 | .0829 |
| Subject 3 | -1.734 | .0829 |
| Subject 4 | -2.504 | .0123 |
| Subject 5 | -.966 | .334 |
| Subject 6 | -.966 | .334 |
| Subject 7 | -.966 | .334 |
| Subject 8 | -.966 | .334 |
| Subject 9 | -.966 | .334 |
| Subject 10 | -.966 | .334 |
| Subject 11 | -6.63e-6 | 1 |
| Subject 12 | -.966 | .334 |
| Subject 13 | .719 | .4721 |

## 5.6 Conclusions

From examining both the data plots and the p-values the most important factor effecting the perceived roughness of fractal surfaces is the RMS amplitude. The logistic regression indicated that when comparing fractal surfaces with dimension 1.2-1.35, lower fractal dimension contributes to the perception of roughness. This agrees with previous work that reported roughness perception increased with increasing groove width and increasing inter-element spacing [72][73][74]. The changes in those surface parameters would have decreased the fractal dimension as well.

This effect does not hold when comparing surfaces of higher fractal dimensions - those over 1.35. For these comparisons fractal dimension was statistically insignificant. When comparing surfaces of the same RMS amplitude in the set of surfaces with fractal dimension 1.35 to 1.5, the subjects' selection were apparently random.

In any case of fractal dimension, RMS amplitude is the overriding factor in determining surface roughness perception. When comparing surfaces of different RMS amplitudes, subjects selected the surface with the higher amplitude as rougher 71.4% to 100% of the time.

# 6 Conclusions

This thesis has developed a structure suitable to study the roughness perception of natural surfaces rendered on a haptic display system using fractals. Information was provided about how surface roughness metrology is used in industry, its shortcomings, and how fractals improves upon them. Fractal theory for two dimensional anisotropic surfaces was developed. Synthesized profiles were applied to a roughness perception experiment. In this chapter a summary of the work and the contributions is made. Possible areas where future development could expand upon the work in this thesis are also discussed.

## 6.1 Summary

The most significant idea developed by this thesis was a framework to characterize the roughness of anisotropic surfaces exhibiting fractal Brownian behavior. Because fractal Brownian behavior is so common in the surface roughness of natural objects and in machined parts, the characterization can find use for a wide range of surfaces. The characterization was simple in that it only used two functional parameters per direction, the fractal dimension D, and the amplitude coefficient C. This is a vast improvement over the numerous parameters of traditional surface metrology. The characterization is both useful for measuring the roughness of surfaces and synthesizing new surfaces that exhibit realistic roughness properties. New surfaces can be synthesized based on measured parameters or be of arbitrary design.

This characterization took into account the sampling resolution of the measuring device by utilizing the Fourier sampling theorem. This was necessary as the magnitude of the power spectral density computed from a profile or surface height map shifts with changing resolution. This problem had previously occurred in fractal literature utilizing Fourier transforms to compute spectral densities to measure fractal parameters. While the fractal dimension is preserved with different sampling resolutions, the power measured decreases

with decreasing resolution. This results in different amplitude coefficients being measured for the same surface by different profiling instruments. By utilizing the Fourier sampling theorem this decrease in power was accounted for to enable the measurement of consistent amplitude coefficients for the same surface measured with different spatial resolutions.

The fractal roughness characterization was developed as an alternative framework for studying the haptic perception of rough surfaces. Instead of using artificial, deterministic surfaces for pyschophysical perception studies, fractal surfaces can be used to better reflect naturally occurring roughness. The fractal characterization of surface roughness is also a better means of describing roughness than surface metrology methods. The fractal methods give consistent results simplified to two parameters, while metrology methods give perception scientists a confusing choice of parameters and inconsistent results.

The roughness perception experiment performed utilized synthesized fractal surface profiles displayed on a haptic interface. The flexibility of a haptic replay device was used to display a large range of synthesized fractal profiles. It is much easier to simulate these profiles than to machine them. This was a serious advantage in rapidly constructing an experiment instead of manufacturing a series of test surfaces. New virtual surfaces can be generated after initial testing of the experimental conditions and integrated within a day at little cost. A new set of real surfaces would require another substantial investment of time and resources to manufacture them. Subjects used a force feedback joystick to explore virtual surface profiles and report which they thought were rougher. The most important factor affecting the perceived roughness of the fractal profiles was the RMS amplitude of the surface, although for a range of lower fractal dimensions, the fractal dimension did contribute to the perception of roughness.

## 6.2 Contributions

The main contributions of this thesis were

- Framing an anisotropic characterization of two dimensional fractal Brownian surfaces.
- Applying the Fourier sampling theorem to solve the fractal amplitude characterization problem for varying sensor resolutions.

•Using a fractal surface characterization and synthesized fractal surfaces to study roughness perception with a haptic device.

## 6.3 Future Work Suggestions

There are several possible areas to extend the work of this thesis. Certainly many more perception experiments of natural rough surfaces remain to be explored. The subjects' ability to discriminate between surfaces of similar amplitude but different fractal dimension is one such test. A study of subjects' perception of real fractal surfaces can now be done with a consistent way to characterize such surfaces. The work in this thesis done on rendering fractal surfaces on three dimensional force feedback devices such as the PHANToM was very preliminary and needs further development to explore anisotropic surface perception. Perhaps the most important idea in conducting these perception studies is that different researchers can compare their results with a consistent method of quantifying rough surfaces.

The anisotropic fractal behavior described in this thesis was only over one set of length scales. The framework could be extended for multi-fractal behavior, that is surfaces that have different fractal dimensions over different scales [46]. The type of fractal described in this thesis was limited to fractal Brownian surfaces, suitable for describing the surface roughness of rocks and machined surfaces. Ways to encode the structural information of a rock with the roughness information could be developed using a combination of fractal techniques such as iterative fractal functions with fractal Brownian functions. It may also be possible to encode this structural information using wavelets. Regardless of the technique chosen to describe roughness, fractals remain an excellent method of characterizing surface roughness.

# Bibliography


[1] J.M. Loomis, S.J. Lederman. "Chapter 31 - Tactual Perception". Handbook of Perception and Human Performance. Volume II, Cognitive Processes and Performance. Edited by K.R. Boff, L. Kaufman, J.P. Thomas. John Wiley and Sons, New York, NY. pg 31-1 - 31-40. 1986.

[2] S.M. Drucker. "Texture from Touch". Natural Computation. Edited by W. Richards. MIT Press, Cambridge MA. pp. 422-429. 1988.

[3] S.J. Lederman, R.L. Klatzky. "Hand Movements: A Window into Haptic Object Recognition". Cognitive Psychology Vol. 19, pp. 342-368. 1987.

[4] R.L. Klatzky, S.J. Lederman. "Intelligent Exploration by the Human Hand" in Dextrous Robot Hands. Edited by S.T. Venkataram. T. Iberall. Springer-Verlag, New York. pp 66-81. 1990.

[5] M.A. Costa, M.R. Cutkosky, "Interview with Professor G.J. Vermeij", http:// cdr.stanford.edu / Touch /vermeij.html, 1995.

[6] T.H. Massie, J.K. Salisbury. "The PHANToM Haptic Interface: A Device for Probing Virtual Objects". DSC Vol. 55-1, Dynamic Systems and Control: Vol. 1, ASME. pp. 295-299. 1994.

[7] G.J. Taylor. P.D. Spudis. "A teloperated robotic field geologist". Proceedings of space ’90: Engineering, construction and operations in space II. American Society of Civil Engineers. pp. 246-255. 1991.

[8] M.W. McGreevy. "The Presence of Field Geologists in Mars-Like Terrain". Presence Vol. 1, No. 4. pp. 375-402. 1992.

[9] S. Chernicoff, R. Venkatakrishnan. Geology: an introduction to phsyical geology. Worth Publishers, New York. 1995.

[10] Ersoy, Waller, "Textural Characterization of Rocks", Engineering Geology 39, 1995, pp. 123- 136.

[11] Howarth, Rowlands, "Development of an Index to Quantify Rock Texture for Qualitative Assessment of Intact Rock Properties", Geotechnical Testing Journal, Vol. 9, No. 4, Dec. 1986, pp. 169-179.

[12] H.O. Peitgen, D. Saupe. The Science of Fractal Images. Springer-Verlag, New York. 1988.

[13] S. Ganti, B. Bhushan. "Generalized Fractal Analysis and its Applications to Enigneering Surfaces". Wear, Vol. 180. 1995. pp. 17-34.

[14] Tom R. Thomas. Rough Surfaces, Second Edition. Imperial College Press, London. 1999.

[15] C.Y. Poon, B. Bhushan. "Comparison of Surface Roughness Measurements by Stylus Profiler, AFM and Non-contact Optical Profiler". Wear Vol 190. pp 89-109. 1995.

[16] J.C. Wyant, C.L. Koliopoulos, B. Bhushan, O.E. George. "An Optical Profilometer for Surface Characterization of Magnetic Media". ASLE Trans. Vol. 27, pp. 101-113. 1984

[17] B. Bhushan, J.C. Wyant, C.L. Koliopoulos. "Measurement of Surface Topography of Magnetic tapes by Mirau Interferometry". Appl. Opt. Vol. 24, pp. 1489-1497. 1985.

[18] K.J. Stout. Three Dimensional Surface Topography; Measurement, Interpretation and Applications, A Survey and Bibliography. Penton Press, London; Bristol, Pennsylvania. 1994.

[19] K.J. Stout, P.J. Sullivan. "Workshop on the Characterisation of Surfaces in 3-D". First EC Workshop on 3-D Surface Topogrpahy Measurement and Characterisation. Brussels, Belgium. September 1991.

[20] R.S. Sayles, T.R. Thomas. "Surface Topogrpahy as a non-stationary random process". Nature, London, 271, 1978. pp. 431-434.

[21] R.S. Sayles, T.R. Thomas. "The Spatial Representation of Surface Roughness by means of the Structure Function: A Practical Alternative to Correlation". Wear Vol 42, 1977. pp. 263-276.

[22] J. Feder, Fractals. Plenum, New York, 1988.

[23] H. Von Koch. "Sur une Courbe Continue sans Tanegente, obtenue par une contruction géométrique élémentaire." Arkiv för Matematik, Astronomi och Fysik. Vol 1. 1904. pp. 681-704.

[24] D.S. Ebert, F. K. Musgrave, D. Peachey, K. Peril, S. Worley. Texturing and Modeling: A Procedural Approach. Second Edition. Academic Press, San Diego. 1998

[25] S. Brown, "A Note on the Description of Surface Roughness Using Fractal Dimension". Geophysical Research Letters, Vol. 14, No. 11, November 1987. pp. 1095-1098.

[26] Y.H. Lee, J.R. Carr, D.J. Barr, C.J. Haas, "The Fractal Dimension as a Measure of the Roughness of Rock Discontinuity Profiles". International Journal of Rock Mechanics, Mineral Sciences, and Geomechanics. Vol. 27, No. 6, 1990. pp. 453-464.

[27] M.C. Shelberg, H. Moellering, N. Lam. "Measuring The Fractal of Empirical Cartographic Curves". Auto-Carto. Vol. 5, 1982. pp. 481-490.

[28] P. Longley, M. Batty. "Fractal Measurment and Line Generalization". Computers and Geosciences. Vol. 15. No. 2, 1989. pp. 167-183.

[29] S. Lovejoy. "Area-perimeter Relation for Rain and Cloud Area." Science. Vol. 216, 1982. pp. 185-187.

[30] T. Mariani, C. Fredani, C. Ascoli. "Sub-Angstrom Resolution with a Phonograph Cartridge as Bidimensional Nanodisplacement Sensor". Review of Scientific Instruments, Vol. 66, No. 11, November 1995. pp. 5337-5338.

[31] B. Kane, et al. "Force-Sensing Microprobe for Precise Stimulation of Mechanosensitive Tissues". IEEE Trans. on Biomedical Engineering, Vol. 42, No. 8, 1995. pp. 745-750.

[32] A. Okamura, M.A. Costa, M.L. Turner, C. Richard, M.R. Cutkosky. "Haptic Surface Exploration". ISER, Sydney Australia, 1999.

[33] Measurement Sensors. Omron Catalog No. GC MSEN3. Omron Electronics, Schaumburg, IL. 1998. pp. 53-72.

[34] A. Majumdar, C.L. Tien. "Fractal Characterization and Simulation of Rough Surfaces". Wear, 136, 1990. pp. 313-327.

[35] T. D. Gillespie. Fundamentals of Vehicle Dynamics. Society of Automotive Engineers. Warrendale, PA. 1992.

[36] L. Ljung. System Identification, Theory for the User. Second Edition. Prentice Hall, Upper Saddle River, NJ. 1999.

[37] J. Peklenik, M. Kubo. "A basic study of a three-dimensional assessment of the surface generated in a manufacturing process". Annals of the CIRP, vol. 16, 1967-8. pp. 257-265.

[38] M. Kubo, J. Peklenik. "An analysis of micro-generational isotropy for random surface structures". Annals of the CIRP, vol. 16, 1968. pp. 235-242.

[39] J. Wallach. "Surface topography description and measurement". Proceedings of ASME Winter Annual Meeting, Nov. 16-21, 1969. pp. 1-22.

[40] T. Tsukada, K. Sasajima. "An Assessment of Anisotropic Properties in Three-Dimensional Asperities". The Bulletin of the Japanese Society of Precision Engineering, v. 17, 1983. pp. 261-262.

[41] R.N. Bracewell. Fourier Transforms and Its Applications. Second Edition, Revised. McGraw-Hill Inc. New York. 1986

[42] D.J. Whitehouse. Handbook of Surface Metrology. Institute of Physics Publications. Bristol. 1994.

[43] D.J. Whitehouse. "The Parameter Rash - Is there a Cure?". Wear. Vol. 83. pp. 75-78. 1982.

[44] L. De Chiffre, P. Lonardo, et al. "Quantitative Characterisation [sic] of Surface Texture". Annals of the CIRP. Keynote paper, MC4021, 2001.

[45] B. Bhushan. Principles and Applications of Tribology. John Wiley. New York. 1999.

[46] J.C. Russ. Fractal Surfaces. Plenum Press. New York. 1994.

[47] A.I. Penn, M.H. Loew. "Estimating Fractal Dimension with Fractal Interpolation Function Models". IEEE Transactions on Medical Imaging, Vol. 16, No. 6, December 1997.

[48] J. Hayward, J.D. Ordford, W. B. Whalley. "Three Implementations of Fractal Analysis of Particle Outlines". Computers & Geosciences, Vol. 15, No. 2, 1989. pp. 199-207

[49] B.B. Mandelbrot. The Fractal Geometry of Nature. W.H. Freeman and Company, New York.1983.

[50] J.C. Russ. "Surface Characterization: Fractal Dimensions, Hurts Coefficients, and Frequency Transforms". Journal of Computer-Assisted Microscopy, Vol. 2, No. 3, 1990.

[51] L.F. Richardson. "The Problem of Contiguity: An Appendix of Statistics of Deadly Quarrels". General Systems Yearbook, No. 6. 1961. pp.139-187.

[52] K.C. Clarke. "Computation of the Fractal Dimension of Topographic Surfaces Using the triangular Prism Surface Area Method." Computers and Geosciences Vol. 122, No. 5, 1986. pp. 712-722.

[53] H.E. Hurst, R.P. Black. Long Term Storage: An Experimental Study. Constable, London. 1965.

[54] R.F. Voss. "Random Fractal Forgeries" in Fundamental Algorithms for Computer Graphics. Edited by R.A. Earnshaw. Springer-Verlag, Berlin, 1985. pp. 805-835.

[55] D.L. Turcotte. Fractals and Chaos in Geology and Geophysics, Second Edition. Cambridge Univeirsty Press. Cambridge, United Kingdom. 1997.

[56] C.R. Wyle, L.C. Barrett. Advanced Engineering Mathematics, Fifth Edition. McGraw-Hill Book Company. New York. 1982.

[57] V. Cizek. Discrete Fourier Transforms and Their Applications. Adam Hilger Ltd. Bristol, England. 1986.

[58] M.V. Berry, Z.V. Lewis. "On the Weierstrass-Mandlebrot Fractal Function". Proceedings of the Royal Society of London, Series A. Vol. 370. 1980. pp. 459-484.

[59] J. Lopez, G. Hansali, et al. "3D Fractal-Based Characterisation for Enigineered Surface Topography". International Journal of Machine Tools Manufacturing. Vol. 35, No. 2, 1995. pp. 211-217.

[60] A. Majumdar, B. Bhushan. "Role of Fractal Geometry in Roughness Characterization and Contact Mechanics of Surfaces". Journal of Tribology. Vol. 112. April 1990. pp. 205-216.

[61] A.S. Monin, A.M. Yaglom. Statistical Fluid Mechanics: Mechanics of Turbulence, Volume 2. The MIT Press. Cambridge, Massachusetts. 1975.

[62] V.I. Tatarskii, "Review of Scintillation Phenomena". Wave Propagation in Random Media (Scintillation). Edited by V.I. Yatarskii, A. Ishimaru, V.U. Zavorotny. SPIE Press, Bellingham, Washington. 1993

[63] R.K. Tyson. Principles of Adaptive Optics, Second Edition. Academic Press. San Diego, CA. 1998

[64] A.V. Balakrishnan. Introduction to Random Processes in Engineering. John Wiley and Sons, INC.. New York. 1995.

[65] A.M. Yaglom. Correlation Theory of Stationary and Related Random Functions Volume I: Basic Results. Springer-Verlag. New York. 1987.

[66] A.M. Yaglom. Correlation Theory of Stationary and related Random Functions, Volume II: Supplementary Notes and References. Springer-Verlag. New York. 1987.

[67] Signal Processing Toolbox User’s Guide, Version 4. The MathWorks, Inc., Natick MA. 1996. pp. 6-167.

[68] T.R. Thomas, B.G. Rosen, N. Amini, "Fractal Characterisation of the anisotropy of Rough Surfaces". Wear, 232, 1999. pp. 41-50.

[69] A. Majumdar, B. Bhushan. "Fractal Model of Elastic-Plastic Contact Between Rough Surfaces". Journal of Tribology, Vol. 113, 1991. pp. 1-11.

[70] H. J. Weaver. Theory of Discrete and Continuous Fourier Analysis. John Wiley & Sons. New York. 1989.

[71] J. S. Walker. Fourier Analysis. Oxford University Press. New York. 1988.

[72] S.J. Lederman, Klatzky. "Tactile Roughness of Grooved Surfaces: The Touching Process and effects of macro-micro surface structure." Perception and Psychophysics, 32, pp. 109-116. 1974.

[73] M.M. Taylor, S.J. Lederman. "Tactile roughness of grooved surfaces: A model and the effect of Friction." Perception and Psychophysics, 17, pp. 23-36. 1975.

[74] S.J. Lederman, Klatzky. "Feeling Through a Probe". DSC-Vol. 64, Proceedings of the ASME Dynamic Systems and Control Division, ASME 1998.

[75] Klatzky, S.J. Lederman. "Roughness Via a Rigid Probe: Effects of Exploration Speed". DSC-Vol. 67, Proceedings of the ASME Dynamic Systems and Control Division, ASME 1999.

[76] J.P. Fritz, K.E. Barner. "Stochastic Models for Haptic Texture". Proc. SPIE Int. Symp. Intelligent Systems and Advanced Manufacturing, Vol. 3901, pp. 33-44, 1990.

[77] J. Siira. "Haptic Rendering - A Stochastic Approach". Proc. 1996 IEEE Intl. Conf. Robotics and Automation, Minneapolis, Minnesota, pp. 557-562, 1996.

[78] Impulse Engine 2000 Specifications. http://www.immersion.com/impulseengine.html

[79] M. Minsky, M. Ouh-Young, O. Steele, F.P. Brooks jr., M. Behensky. "Feeling and Seeing: Issues in Force Display". Proc. Symp. Interactve 3D Graphics, pp. 235-243, 1990.

[80] D.F. Green. "Texture Sensing and Simulation Using the PHANToM: Towards Remote Sensing of Soil Properties". The Second PHANToM User's Group Workshop, MA, October 19-22, 1997.

[81] D.W. Hosmer, S. Lemeshow. Applied Logistic Regression. John Wiley & Sons. New York. 1989.

[82] S.W. Menard. Applied Logistic Regression Analysis. Sage Univeristy Papers Series: Quantitative Applications in the Social Sciences. Sage Publications. Thousand Oaks, California. 1995.

[83] G.K. Smyth. StatBox 4.0: A statistics toolbox for Matlab. Univeristy of Queensland, Brisbane. (http:www.maths.uq.edu.au/~gks/matlab/statbox.html)1999.